

Sustainability and Efficiency Improvements of Gas-Cooled High Temperature Reactors.

Proefschrift

ter verkrijging van de graad van doctor
aan de Technische Universiteit Delft,
op gezag van de Rector Magnificus prof. ir. K.C.A.M. Luyben,
voorzitter van het College voor Promoties,
in het openbaar te verdedigen op vrijdag 11 mei 2012 om 10:00 uur
door

Alain MARMIER

Ingénieur Arts et Métiers, Paris, France
Diplomingenieur, TU Karlsruhe, Karlsruhe, Germany
geboren te Montbeliard (Frankrijk).

Dit proefschrift is goedgekeurd door de promotoren:

Prof. dr. ir. T.H.J.J. van der Hagen

Prof. dr. ir. A.H.M. Verkooijen

Copromotor:

Dr. ir. J.L. Kloosterman

Samenstelling promotiecommissie:

Rector Magnificus,	Voorzitter
Prof. dr. ir. T.H.J.J. van der Hagen,	Technische Universiteit Delft, promotor
Prof. dr. ir. A.H.M. Verkooijen,	Technische Universiteit Delft, promotor
Dr. ir. J.L. Kloosterman,	Technische Universiteit Delft, copromotor
Prof. dr. R.J.M. Konings,	Technische Universiteit Delft
Prof. dr. E. Mulder,	North-West University, RSA
Prof. dr. F. Li,	Tsinghua University, CN
Dr. G.F. De Santi	JRC-Institute for Energy and Transport, NL

© 2012, Alain Marmier

All rights reserved. No part of this book may be reproduced, stored in a retrieval system, or transmitted, in any form or by any means, without prior permission from the author.

ISBN 978-90-819113-0-6

Keywords: High Temperature Reactor, pebble bed, fuel design.

Publisher

Arenea Grafimedia
Ronde Tocht 10
Postbus 2240
1507 CC ZAANDAM
The Netherlands
<http://www.araneagrafimedia.com/>

PRINTED IN THE NETHERLANDS

The research described in this thesis has been supported by the Institute for Energy and Transport of the Joint Research Center (JRC) of the European Commission.

Visiting address: Westerduinweg 3, 1755 LE Petten, The Netherlands.

Contents

1	Introduction	1
1.1	High Temperature Gas Cooled Reactor	2
1.2	HTR fuel qualification	4
1.3	Advanced fuel cycles	8
1.4	Non electrical application of HTR	11
1.5	Objective and outline of this thesis	13
2	HFR-EU1 fuel irradiation experiment.....	15
2.1	Introduction	15
2.2	Experimental	17
2.3	Nuclear Data.....	18
2.4	Power Evolution in Pebbles	20
2.5	Temperatures.....	22
2.6	Special Events	23
2.7	Fission Gas Release Measurements.....	23
2.8	Uncertainty analysis	28
2.9	Conclusions	39
3	Revisiting the concept of Wallpaper fuel	41
3.1	Introduction	41
3.2	Re-visiting “wallpaper” fuel.....	42
3.3	Method	43
3.4	Results of Full core simulations with the Monte-Carlo Method	46
3.5	Neutronic Thermal-Hydraulic and Safety Analysis	53
3.6	Investigation of fissile material cost.....	69
3.7	Thermal aspects and production process	70
3.8	Conclusion.....	74
4	Nuclear Powered Heat Pumps for Near Term Process Heat Applications	77
4.1	Introduction	77

4.2	Current Developments for Nuclear Produced Hydrogen.....	77
4.3	Reverse Brayton Cycle.....	85
4.4	Process Heat in a Large Temperature Span.....	86
4.5	Concentration of High Temperature Process Heat to a Narrow Temperature Span	90
4.6	Reverse Brayton Cycle for Combined Cooling and Desalination	95
4.7	Future Work	97
4.8	Conclusions	101
4.9	Legend.....	102
5	Conclusions and discussion.....	103
Appendix A:	Particle temperature in a Wallpaper fuel	107
A.1	Temperature profile.....	107
A.2	Average temperatures.....	108
A.3	Temperature increase vs. particle packing fraction	109
Appendix B:	Influence of particle packing fraction on fuel zone thermal conductivity	111
B.1	Introduction.....	111
B.2	Modelling.....	111
B.3	Thermal conductivity calculation	114
B.4	PBMR fuel as an example	116
	Nomenclature.....	119
	Bibliography.....	125
	List of publications	137
	Summary	139
	Samenvatting.....	143
	Acknowledgements	147
	Curriculum Vitae.....	149

1 Introduction

This thesis deals with High Temperature Reactor, a small sized nuclear reactor that targets not only electricity production but also offers the option for decentralised high temperature process heat for industrial applications.

Throughout this thesis, several key aspects of this technology (current and future fuel technology, power conversion units) were investigated and innovative concepts were developed to tackle issues such as sustainability and waste while preserving the inherent safety features of this type of reactor.

The first section introduces HTR technologies developed over 5 decades, while the remainder dwells on contributions of HTR for the sustainability of nuclear power. Sec. 1.2 focuses on different fuel cycles which are at various stages of development. Sec. 1.3 covers past fuel irradiation experiments while Sec. 1.4 focuses on different process-heat applications. The last section of this chapter provides the objectives and outline of this thesis.

With the world's population expected to grow from about 6 billion people to 10 billion in the coming decades and with an increase of living standards, the demand for energy can be expected to grow significantly [1]. To avoid using fossil fuels, while coping with this increased demand, a cost effective, reliable, safe and clean energy supply is needed. In this respect, HTR technology can be associated with the development in the world wide energy market.

16% of world-wide electricity production is generated today by means of the 439 nuclear reactors and almost one third of the European electricity production [2]. This has a positive impact on the environment as nuclear energy is a nearly carbon-free source of energy. A 1 GWe nuclear plant spares about 6-7 million tonnes of CO₂ emissions per year as well as related airborne pollutants as compared to a coal-fired plant. However, electricity remains marginal in the energy consumption mix, dominated by the transport sector. Today, petrol is the main energy carrier, but the use of synthetic fuels for transport is also gaining renewed interest, while alternative technology, such as electrically powered vehicles using batteries or fuel cell technology, are now emerging. The use of nuclear energy for the production of hydrogen or electricity for transportation opens a massive new market and emission reduction potential.

It is expected that nuclear energy will play an important role in the future energy mix [3], whether this will be limited to the replacement of existing nuclear plants or by expansion of the nuclear fleet, either to meet increasing demand for electricity or, beyond electricity generation, to serve industrial process heat applications including hydrogen production.

In order to combat climate change, the EU committed to achieve, by 2020, the “20-20-20” targets: a reduction of 20% of greenhouse emissions compared to 1990, a 20% energy savings and a 20% share of renewable energies in the total energy mix.

To this end, the Strategic Energy Technology Plan (SET Plan) was adopted by the European Union in 2008. SET-Plan is the principal decision-making support tool for European energy policy and aims, among others, at “fostering science for transforming energy technologies to achieve the 2020 Energy and Climate Change goals”.

With this respect, the SET-Plan identified a set of eight candidate technologies for low carbon energy which need to be developed and deployed. The key players in each technology are organized in “Technology Platforms”. One of them deals with nuclear energy and is called the Sustainable Nuclear Energy Technology Platform (SNETP, www.snetp.eu).

SNETP strategy rests on three “pillars”: The first one takes care of the sustainable development of nuclear power using fast reactors and the uranium-plutonium cycle. The second one deals with the safe use of second and third generation reactors which are currently operating. Nuclear cogeneration of heat and electricity in industry is the third pillar where High Temperature Reactor (HTR) technology can serve particularly well.

This thesis deals with a number of technology aspects for HTR, their analysis and improvements so as to enhance the credibility of this concept to help achieve the SET Plan targets.

1.1 High Temperature Gas Cooled Reactor

With robust safety characteristics and a high coolant temperature, the High Temperature Gas-Cooled Reactor (HTGR or HTR) is a promising design among the existing nuclear reactor concepts.

The first experimental nuclear reactors, which operated in the US in the 1940s, were moderated by graphite blocks and used air at atmospheric pressure as a coolant [4]. However, water cooled reactors offered higher power densities and were therefore developed for commercial application in the US.

In Britain, interest in gas cooling led to the construction and operation of gas-cooled reactors in the 1950s. These so-called MAGNOX reactors used metallic natural uranium fuel with a magnesium-aluminium cladding and pressurised CO₂ as a coolant. Carbon-dioxide offered better thermal properties and the potential for higher temperature operation than air. Although higher than in water-cooled reactor, the coolant outlet temperature was still limited to 415°C for technical reasons, such as possible carburization, melting of the cladding and the phase change of the metallic uranium. These limitations were taken into account for the second generation of British reactors, the Advanced Gas-Cooled Reactor (AGR): The design features uranium oxide fuel contained in a stainless-steel cladding, enabling a coolant outlet temperature of up to 675 °C and improving the efficiency to 41.5%, well above the performance of Light Water Reactors.

Moving from CO₂ to helium coolant and using an all-ceramic core precluded several issues related to CO₂ and allowed higher operating temperatures. This approach was investigated by means of test reactors in the UK with the DRAGON reactor [5], in the US with the Peach Bottom reactor [6] and in Germany with the pebble bed AVR reactor [7]. They reached criticality in 1964, 1967 and 1968, respectively.

Following these research efforts, the Fort St. Vrain reactor [8] and the Thorium High Temperature Reactor (THTR) [4], [9] were built and used as demonstration plants in the US and Germany. While the American design of General Atomic used prismatic fuel elements, the German design preferred spherical fuel (pebbles) [10].

With low uranium prices and increased public awareness for safety in the decades that followed, the next designs emphasized a small-size, modular HTR with inherent safety characteristics using the once-through ²³⁵U fuel cycle. The 200 MW_{th} HTR-MODUL design, with an helium outlet temperature of up to 700 °C using 7.8% enriched UO₂, is a good example [11].

Table 1.1 gives an overview of gas-cooled reactors that operated in the past.

Table 1.1: *Main characteristics of past gas-cooled reactors.*

Reactor	MAGNOX	AGR	DRAGON	AVR	Peach Bottom	Fort St Vrain	THTR
First pow. op.	1956	1963	1965	1966	1967	1976	1984
Country	UK/France	UK	UK	Germany	US	US	Germany
Efficiency [%]	19-34	41	-	32	35	39	40
Fuel elements	Slugs	Rods	Rods	Pebbles	Cylinders	Rods	Pebbles
Fuel loading	Nat. U	UO ₂	U-ThC	Various	U-ThC	U-ThC	U-ThO ₂
Coolant	CO ₂	CO ₂	He	He	He	He	He

High Temperature Reactors feature several important inherent and passive safety characteristics, namely:

- The high graphite inventory in the core provides significant thermal inertia thus dampening the temperature increase after typical accident scenarios. Graphite also has a high thermal conductivity, which facilitates heat transfer to the reflector, and it tolerates high temperatures.
- The strongly negative Doppler coefficient provides negative feedback, such that the reactor shuts down by itself whenever the fuel temperature is higher than normal.
- The low power density together with the high thermal inertia enables stabilization of core temperature significantly below the maximum allowable, even in case of incidents such as loss-of-coolant accident.

- The high quality of fuel elements and constituent materials – tri-isotropic (TRISO) coated particles – minimizes operational and accidental fission product release.

Together, the aforementioned aspects prevent massive release of fission products in the case of an accident, and effectively preclude core melt down.

TRISO particles are the basis of all HTR fuel design: They consist of a UO_2 (or UC) kernel, successively coated with a porous carbon buffer layer, designed to retain fission products, with an Inner Pyrolytic Carbon (IPyC) layer, a Silicon Carbide (SiC) layer and an Outer Pyrolytic Carbon layer (OPyC). TRISO particles are then mixed with graphitic powder used as a matrix and pressed to typically three different fuel geometries: pebbles, solid or annular rodlets.

Rods (“compacts”) are used in prismatic fuels: A graphite hexagonal block shows boreholes for the placement of fuel compacts or burnable poison rods and cooling channels. Several columns of stacked prismatic blocks surrounded by graphite reflectors compose the reactor core. Some blocks are dedicated to reactor control and have three larger holes for accommodating control rods and absorber spheres, which act as the reserve shutdown system. Although burnable poison is used for long term reactivity control, reactor operation has to be stopped for replacing and re-shuffling fuel blocks.

Pebbles are made of two concentric regions: An inner region of 5 cm diameter containing a mixture of TRISO particles and graphite and an outer region of pure graphite resulting in a 6 cm diameter sphere. The core of a Pebble-Bed type HTR, a moving bed in a silo type vessel, may contain several tens of thousands of pebbles that form a porous, randomly packed pebble-bed cooled by helium. Such a core includes on-line refuelling capability by removing ‘burned’ pebbles from the bottom of the core and adding fresh or insufficiently burned pebbles on the top. Since long-term reactivity can be controlled effectively in this manner, there is no need for excess reactivity or burnable poison.

1.2 HTR fuel qualification

To ensure fuel qualification, the fuel must be manufactured according to design and specifications (for instance with respect to heavy metal contamination and defective particles rate). Then the fuel must be irradiated to prove good performance under the most stringent normal operating conditions. Finally, the fuel behaviour during all postulated off-normal conditions should be assessed via post irradiation heat-up tests [12]. The objective of this section is to highlight world-wide efforts to achieve this goal.

Material Test Reactors

Material Test Reactors are used for their ability to perform accelerated irradiation tests. Furthermore, they ensure well defined conditions, similar or beyond the

operating conditions. Among others, FRJ2* in Jülich (Germany), HFR in Petten (The Netherlands), R2* in Studsvik (Sweden), BR2 in Mol (Belgium), Siloe* in Grenoble (France) were used [13]. The Dragon* reactor in Winfrith, United Kingdom [14] [5] was used, for instance, to qualify the first core loading of the AVR* reactor. (* indicate reactor that are shut-down.)

AVR (Germany)

The AVR [6] (Arbeitsgemeinschaft VersuchsReaktor) operated over 21 years in Jülich, Germany. It was used as test reactor for the different HTR fuels. Throughout the reactor lifetime 14 different fuel element designs [15] were investigated, illustrating different stages in fuel development:

The AVR first core loading was performed with (U,Th) C_2 fuels, while wallpaper fuel elements were used for the reload. Both types were hollow graphite spheres manufactured on a lathe from graphite block, then filled with particles and graphite powder, as shown in Fig. 1.1.

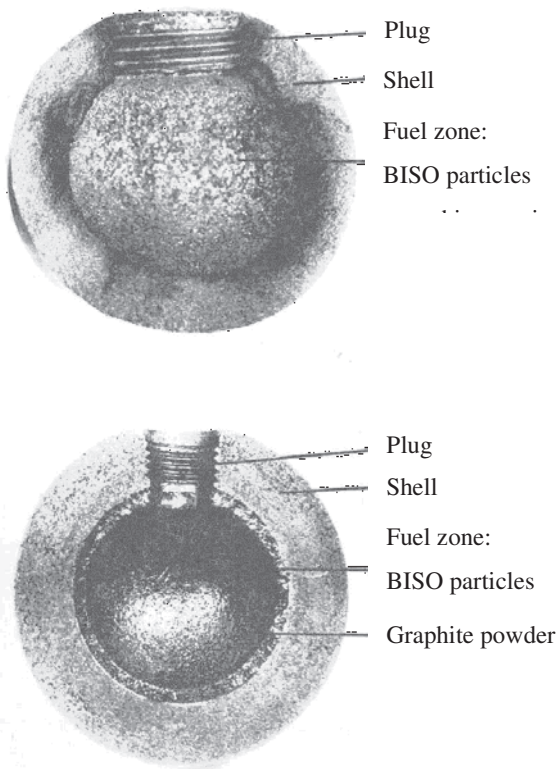


Fig. 1.1: *Lathed fuel elements used in the AVR [16].*

Following reloads were then made with fuels based on a different manufacturing process: The fuel zone was produced by semi-isostatically pressed mixtures of particles with A3-matrix material (graphite grains covered by a phenolic resin as a binder) [17]. Furthermore, the shell thickness was reduced from 10-11 mm (for lathed FE) to 5 mm (for pressed elements).

Further developments concentrated on kernel composition and coating technique: TRISO (Tri-isotropic) coatings replaced the less efficient BISO (Bi-isotropic) coatings; Carbide fuels were replaced by oxide fuels; Enrichment decreased below 20% in response to non-proliferation requirements. This technology is still in use today [18] [19].

Besides irradiation facilities, several Post Irradiation Examination (PIE) facilities have been developed for fuel testing and qualification. Among others, accident simulations were performed with the Cold Finger Apparatus (KÜFA) in Jülich. Such tests consist of fuel heat-up ramps up to 2500°C, with continuous measurement of fission products released (either with noble gas traps for gaseous FP or by condensation on the cold finger for metallic FP) [20].

After decommissioning of both AVR and THTR, this facility was shut down in 1993, [21]. In the framework of a Euratom project for HTR-technology development, an up-graded version of the KÜFA has been installed in the hot cells of the Institute for Transuranium Elements of the Joint Research Centre [22].

There are currently two HTR reactors in operation: the HTTR in Japan [23] [24] and the HTR-10 in China [25] [26]. Both are used as technology demonstrators, including fuel development.

HTTR (Japan)

The High Temperature Engineering Test Reactor (HTTR) is a 30 MWth prismatic core HTGR designed, constructed and operated by the Japan Atomic Energy Research Institute (JAERI, now JAEA). The reactor achieved initial criticality in 1998. The facility operates with core outlet temperatures as high as 950°C to support development of high temperature process heat and closed cycle gas turbine technology.

The fuel evaluations mainly focus on measurement of fission product release and degradation of the coating layers containing the fission products [27]. PIE on HTTR fuels are currently ongoing in the hot cell laboratory of the Japan Materials Testing Reactor (JMTR) [28].

Prior to use in the HTTR, Japanese fuel was investigated (for normal operating conditions) in the JMTR, using the Oarai Gas Loop No. 1 [29]. Out-of-pile ramped and isothermal-heating tests on irradiated coated fuel particles were used to determine the fuel behaviour under accidental conditions [30] [31].

Facilities of the Oak Ridge National Laboratory in the US were also used for fuel investigations [32]: Fuel compacts were irradiated in a graphite sleeve of the HRB-22 irradiation capsule in the High Flux Isotope Reactor, while performances of irradiated coated fuel particles under accident conditions were performed with the Core Conduction Cooldown Test Facility (CCCTF).

HTR-10 (China)

The HTR-10 is a 10 MWth pebble bed core HTGR designed, constructed and operated by the Institute for Nuclear Energy Technology (INET) at Tsinghua University in Beijing, China. The reactor has reached first criticality in 2000 and can operate with core outlet temperatures as high as 950°C to support the development of high temperature process heat and electricity generation technology.

Among others, the purposes of HTR-10 are to investigate technology for fuel elements and nuclear graphite development; to test the fuel elements handling system and to perform research on chemical reprocessing of thorium-containing spent fuel.

Furthermore, HTR-10 was designed for executing safety experiments and to demonstrate the inherent safety features of the Modular HTGR. For this purpose, the cooling system was designed to allow the possibility to heat fuel elements up to 1600°C.

Fuel element irradiation (including in-pile heating and Post Irradiation Examination) in the Russian MTR IVV-2M [33] [34] and Post irradiation Examination of graphite samples [35] further enhanced Chinese progress in the field of HTR fuel qualification.

Although the effects of accelerated irradiation on coated fuel are complex due to varying degrees of dependence on temperature, time, burnup and fast fluence [36], the decommissioning of European and American experimental reactors, required the use of MTRs for fuel testing in Europe and in the USA.

HFR Petten (The Netherlands)

The High Flux Reactor Petten (HFR) is a 45 MWth water cooled reactor which started operation in 1961. It offers large in-core position, capable of accommodating 6-cm diameter pebbles and was used therefore for numerous experiments related to the development of HTR technology [37] from several countries. Besides fuel element testing, the HFR is also used for irradiation of various coating materials for TRISO coated particle fuel [38] and graphite [39] [40].

Licensing requires fuel irradiations which are expensive and time consuming experiments. In most cases, several fuel elements are enclosed into one capsule, such as the HFR-EU1bis experiment [41]. The outcome of such an experiment could be jeopardized by one fuel element of lower quality. To prevent this eventuality, a non-destructive weak irradiation method was investigated [42] to determine possible particle failure prior to irradiation.

ATR (USA)

The 250 MWth Advanced Test Reactor (ATR) located at the Idaho National Laboratory (INL) [43] is the neutron source for the Advanced Gas Reactor (AGR) fuel development and qualification program [44]. The first experiment (AGR-1) was inserted in the ATR in December 2006 [45] [46] and was finished in the end of 2009. Post-irradiation examinations are planned at Oak Ridge National Laboratory [47], including safety testing with the CCCTF.

JHR (France)

The Jules Horowitz Reactor (JHR) [48], under construction, is designed for supporting existing and future nuclear reactors, including HTR.

1.3 Advanced fuel cycles

Advanced converter

Historically, the first nuclear fuels were based on natural uranium. Both Oklo [49] and CP1 [50] used natural uranium to create a sustained chain reaction. However, Oklo used light water as a moderator (when ^{235}U natural enrichment was higher), while CP-1 was an air-cooled graphite moderated reactor. In both cases they had a very thermal spectrum and heterogeneous geometries. The added value of heterogeneity has been described in [51] with a more effective neutron moderation than in the case of homogeneous reactor.

According to [52], the homogeneous core geometry of the graphite moderated gas cooled reactor requires enriched fissile material to be used. This then enables better use of the fuel [53]. However, various enrichments are feasible: One can choose Low Enriched Uranium (LEU) fuel ($< 20\%$, usually in the range of 3 to 10%), high enriched (93% ^{235}U with ^{232}Th as a fertile material) if non-proliferation rules allow, and also burn plutonium, either with ^{232}Th or with natural uranium. The objective of this section is to introduce the fuel cycle versatility of this reactor, also known as advanced converter [54].

Using online refuelling (for the pebble bed version) or more heterogeneities (for block type reactor), the concept of high temperature graphite moderated reactors offers an even greater versatility, which can be used for different fuel cycle options.

U/Pu cycle

Current reactors used for many years an open fuel cycle: fuel was enriched, burned and stored. This option is also feasible with HTR fuel and is promoted thanks to the good mechanical stability of coated particles embedded in the graphite matrix of the fuel elements. This enables final storage without reprocessing [55] due to proliferation resistance of the fuel elements. However, most of the current HTR designs accommodate LEU UO_2 fuels. After application of a head-end process to separate and crack the coated particles [56], this enables to use similar reprocessing [57] technology as designed for PWR fuels, such as the PUREX process [58], although HTR fuel is less desirable for commercial reprocessing and reuse than that from light water reactors [59].

It has been demonstrated that current water reactors could also operate with PuO_2 fuels, based on Pu actinides bred during irradiation (Light Water Reactors using LEU convert ^{238}U into ^{239}Pu). This triggered economic interest in fuel recycling.

Minor Actinide (MA) partitioning was also later promoted for the purpose of reducing spent fuel radiotoxicity. However, most MA are not recycled in a LWR. One of the most effective ways to reduce their radiotoxicity is to burn them. Although fast reactors are more efficient for this purpose, this has also been achieved in HTRs. While sharing the same technology (kernel production and safety characteristics) of LEU UO_2 fuelled HTR, the burn-up achieved with Pu and MA fuels is then much larger than with UO_2 fuel. This requires further research and development, such as it is currently ongoing in certain American [60] and European projects [61].

One of the key issues of Pu fuel is related to proliferation resistance. If coated particle fuel design acts already as a barrier against proliferation, this is, in the case of uranium-based fuel, further enhanced by the presence of ^{238}Pu . Although in limited amounts (^{239}Pu is produced with a single neutron capture from ^{238}U , while ^{238}Pu requires transmutation of ^{235}U to ^{236}U , then to ^{237}Np and finally into ^{238}Pu), ^{238}Pu displays high decay heat as well as alpha and neutron emission.

Furthermore, HTR could also be used to reduce the legacy of the cold war, by incinerating military grade Pu. As part of the Deep Burn project General Atomic Company (San Diego) and the Russian Atomic Ministry (MINATOM, Moscow) cooperate with the aim of burning weapon-Pu in an GT-MHR [62] [63]. The use of Th, as a fertile material, in combination with weapon grade Pu has been investigated [64] [66]. The main purposes were to limit MA breeding, while improving sustainability. Indeed, with a higher conversion ratio than light water reactors, they better convert fissile ^{233}U from ^{232}Th . A conversion ratio above unity was even achieved in combination with Th-blanket [65].

Thorium cycle

In a similar way as oil, the limited amount of natural ^{235}U led to speculations on the date when the demand will exceed economically retrievable resources. Therefore, the use of thorium as a substitute for naturally occurring fissile uranium and bred plutonium, has triggered worldwide interest, due to its large natural abundance and more even global distribution.

Thorium has been extensively investigated. [67] [68] [69] are key references for the use of thorium, its fuel cycle, and its potential benefits and challenges.

The technology leap from the currently prevailing U-Pu fuel cycle to a Th-U fuel cycle is hindered by the nature of thorium, which is not available as fissile material: ^{232}Th needs to capture a neutron and to decay for several days in order to produce fissile ^{233}U .

If the conversion of uranium to plutonium has already been achieved as a by-product of current reactors, breeding (when one fissile atom, disintegrated by fission, is replaced by at least one new fissile atom, bred from fertile material) of plutonium requires fast spectrum and therefore raises challenges on the moderator and coolant as well as on the in-core fissile mass required.

Thorium, however, displays a more favourable fission to capture ratio at lower neutron energy, making it suitable for thermal neutron reactors. This therefore opens the use of thorium to a wider range of reactor technologies including the HTR [70].

The conversion ratio of current water reactors is too low to ensure breeding. In current LWRs, thorium can indeed be used as a fertile material, but not to the extent that this would strongly improve resource sustainability, whereas it raises fuel production problems. There are, nonetheless, investigations to transform LWRs into thorium breeders as their conversion ratio can be improved by lowering the moderator to fuel ratio [71] [72].

Heavy water is also an option for raising the conversion ratio, as in CANDU reactors [73], the ‘A Thorium Breeder Reactor’ (ATBR) [74], or the Reduced-Moderation Water Reactor (RMWR) [75].

Molten Salt Reactors, developed at ORNL in the 1960’s [76], are still being considered among the most promising concepts by GIF [77]. The concept was also considered as thorium breeder at industrial scale [78] [79].

It is important to note that graphite moderated reactors provide very good neutron economy: due to its low absorption cross-section, graphite is a very good moderator. This feature contributed to reach conversion ratio above unity in HTRs [65] and explains why graphite moderated reactors still investigated as thorium breeders [80].

The viability of a thorium breeder concept is conditioned by the closure of the fuel cycle. For this purpose, the PUREX process has been adapted to thorium based fuel (and renamed THOREX process) [81], with the particular challenge of thorium stability, which hinders fuel dissolution in classical nitric acid [82].

Furthermore, all of the above mentioned concepts should also comply with safety requirements. In case of uranium fuelled reactors, the design of safe reactors is eased by the ^{238}U absorption cross-section broadening, which leads to a negative fuel temperature coefficient of reactivity. This characteristic is preserved, as ^{232}Th also shows resonance regions in the absorption cross-section [83], but its effect is decreased, as the resonance integral of ^{232}Th is about three times smaller than that of ^{238}U [84].

In case of water reactors, safety performances are also maintained by their negative void coefficient, while heat conduction and convection should ensure that decay heat is removed in both MSR and HTR in case of accidents.

THTR

For this reason, the only commercial reactor designed to accommodate thorium fuels, is a graphite moderated reactor: The Thorium High Temperature Reactor (THTR) [85]. The thorium fuel cycle was chosen for this design using highly enriched (93%) ^{235}U and ^{232}Th as the fertile material for breeding fissile ^{233}U . The high number of neutrons produced per neutron absorbed (η) for ^{233}U in the thermal energy spectrum [86] of an HTR is the incentive behind this choice. The concept of

this 750 MW thermal reactor was first suggested in the 1960's. Because of difficulties in licensing, the construction was spread from 1971 to 1983 [87]. It operated accordingly to predictions [88], although it only gathered 423 days of full power operation between 1983 and 1988 [89].

This reactor was fuelled with high-enriched uranium-thorium fuel and, therefore, was not designed to achieve conversion ratio above unity.

One of the key lessons learned with the THTR concerns control rods. As shown in Fig. 1.2. for operation, the rods had to be pushed into the pebble bed. Although they found their way when required (on three occasions, tests were conducted to ensure they fulfilled their objective), they broke 8000 pebbles out of 675000 contained in-core.

The THTR was not designed for fuel testing and qualification. That took place either in the AVR or Material Test Reactors (MTR).

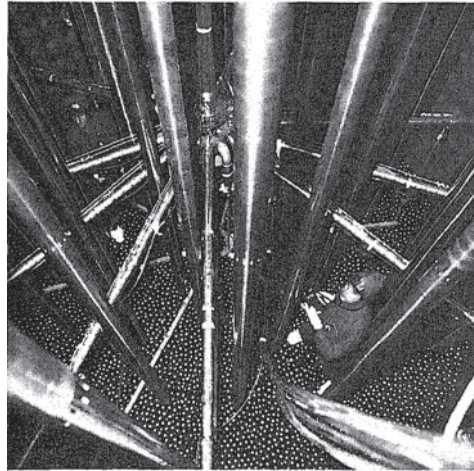


Fig. 1.2: View of the THTR pebble bed, during loading, showing the core rods, carousel switch and loading tubes.

1.4 Non electrical application of HTR

Besides robust safety characteristics and versatile fuel cycle options, the High Temperature Gas-Cooled Reactor has a high coolant temperature facilitating high power conversion efficiency and a variety of process heat applications.

Because of its limited reactor power (to maintain its full safety features), HTRs tend to be less economic than LWRs for electricity generation. HTRs, on the other hand, build on economy of replication (in-series production of identical machines) and have so far unmatched process heat generation capabilities. High coolant temperatures give access to a large existing new energy market in already existing industrial applications. This section will briefly introduce possible uses of HTR.

Among others, hydrogen is a promising application of HTR: produced mainly by steam methane reforming of natural gas with high temperature steam, it is increasingly used today for upgrading heavy crude oil and is required in large quantities in fertilizer plants [90]. The current market for hydrogen is 40 million metric tons/year (2005), worth about \$135 billion/year and growing about 10% per year [91]. Chapter 4 of this thesis deals with electricity and hydrogen production

based on different types of High Temperature Reactors. Therefore the different hydrogen production pathways are presented there and not within this introduction.

There are inherent issues related to the use of hydrogen: among others one may consider its flammability and permeation (safety) and need for infrastructures (economy) if considering a distributed hydrogen economy. To avoid the latter, research on the production of synthetic hydrocarbon fuels is under way [92].

1.4.1 Synthetic fuels

One possible strategy for reducing dependence on imported oil is to utilize alternate carbon sources like coal or biomass for the production of synthetic liquid fuels. The production of liquid fuels is energy intensive with massive requirements for high-temperature heat. High-temperature reactors can provide this heat and the required hydrogen by splitting water.

For the Coal-To-Liquid method, the first step is the production of carbon dioxide by partial combustion of carbon feedstock in oxygen. The hydrogen is then used in the reverse water gas shift reaction to react with carbon dioxide to produce carbon monoxide and water. By further adding hydrogen, the carbon monoxide can be converted to liquid fuels via the Fischer-Tropsch catalytic synthesis process: $n\text{CO} + (2n + 1) \text{H}_2 \rightarrow \text{C}_n\text{H}_{2n+2} + n\text{H}_2\text{O}$. The end product can then be cracked, isomerised and refined into e.g. jet fuel [93].

If this method can also be applied to biomass, direct production of ethanol and biodiesel might be more efficient. With the use of nuclear energy to provide heat, electricity, and hydrogen for the processing of biomass-to-liquid fuels, the liquid fuel production per unit of biomass is dramatically increased, and the available biomass could meet U.S. liquid fuel requirements. The conversion options and the energy requirements of the process facilities are described in [94]

The large scale industrial maturity of these processes is not yet achieved. As a bridging technology, process heat from nuclear reactors can be used to maximize recovery of crude oil, for instance from tar sands.

1.4.2 Oil sands

Extraction of bitumen from the deeper deposits utilises the commercially dominant Steam Assisted Gravity Drainage (SAGD) technique. This process injects high pressure steam into multiple wellheads, heating the underground oil sand reservoir and fluidising bitumen into horizontal collection pipes that have been drilled along the base of the reservoir. High pressure steam for the SAGD process is currently produced from natural gas fired boilers that are designed to work with recycled, chemically treated water from the oil separation process. Some high pressure steam is also produced by gas fired combustion turbine cogeneration units where the requirement for both power and steam exists. It is debatable whether the use of a

clean prime fossil fuel (natural gas) for extraction of another, less clean fuel (oil) makes sense.

10 GWth nuclear powered heat would support current oil sands exploitation while eliminating about 20 million tonnes per year of CO₂ emissions. This would also preserve approx. 25% of Canada's natural gas reserves that would have been consumed for steam production [95].

1.4.3 Desalination

Desalination consists in removing dissolved salts from sea water. Several systems have been developed so far, including multiple effect evaporation/distillation and membrane processes. If the membrane processes require energy mostly as pressure to force sea water through the membranes, the use of pre-heated sea water improves efficiency. With this respect, the condenser of any water cooled reactor is a suitable energy source. Evaporation processes, however, require heat of higher temperature (~300°C) to successfully evaporate water.

Desalination is already a nuclear power application: Japan and Kazakhstan have demonstrated the feasibility and accumulated over 150 reactor-years of experience [96], while economy of different reactor and different water production systems is investigated in [97].

1.5 Objective and outline of this thesis

For a given technology, operating a nuclear reactor at higher temperature and enabling a higher fuel burn-up is favourable with respect to efficiency and resource use. These goals impose constraints on the system component and safety related materials, where the fuel is of special importance since it acts as a gas tight containment in a HTR. Therefore, a first objective of this thesis (HFR-EU experiments) is to study and qualify fuels under stringent irradiation conditions.

Temperature is a direct threat to particle integrity: it contributes to different stresses in the particle layers and to the build-up of gaseous fission products in the buffer. Two options were therefore investigated to alleviate this constraint while maintaining important targets such as a high outlet temperature for process heat applications:

1) The development of innovative fuels (such as variations around the wallpaper concept):

- enables a decrease of particle temperature.
- enables enhanced neutronics: fuel burn-up can be significantly increased, stressing the need for high burn-up resistant particles.

2) The coupling of heat pumps to a nuclear reactor:

- enables the production of large quantities of high temperature process heat with high efficiency while operating the core (and thus the fuel) with acceptably low temperature constraints,
- eases the use of less ambitious (or even proven) technologies such as CO₂ gas cycles (for the coolant), steam generators of highly efficient coal-fired plants and several other heat sources like the different Gen IV reactors.

In the current safety versus economy discussion, this thesis contributes to the development of High Temperature Reactors by:

1. Investigating the behaviour under irradiation (i.e. integrity at high temperature up to elevated burn-ups) of fuel currently developed,
2. Preserving the fuel integrity with innovative fuel designs and/or power conversion units while improving the fuel cycle and/or the overall plant efficiency,
3. Improving neutronic behaviour of the reactor by changes in fuel design that also reduce the particle failure fraction.
4. Based on the above, improving economics with lower fuel consumption and waste production,
5. Diversifying the application fields of this type of reactor (i.e. process heat at higher temperature and/or in larger quantity), while preserving or enhancing the reactor safety,
6. Improving both safety and economics when starting HTR deployment with a “low-tech fast-track” approach (combining an already operating reactor with a power conversion cycle capable of producing the required high temperatures gas).

2 HFR-EU1 fuel irradiation experiment

2.1 Introduction

Like for most nuclear energy sources, the feasibility and performance of the fuel is a key issue for future improvements and requires experimental verification in view of fuel qualification and licensing. For the specific case of High Temperature Reactors, the required test string comprises high temperature irradiation to high burn-ups with fission gas release measurements, followed by post-irradiation examinations and post-irradiation heat-up tests which simulate accidental temperature evolution and record possible fission product release.

The European Commission's Joint Research Centre possesses the complete High Temperature Reactor (HTR) fuel qualification string required for licensing, including quality control, irradiation testing, Post Irradiation Examination (PIE) and safety testing. In the summer of 2002 the Institute of Energy of the European Commission (JRC-IE) proposed the HFR-EU1 irradiation experiment in the High Flux Reactor (HFR) at Petten to the European High Temperature Reactor Technology Network (HTR-TN) as a means to measure Release over Birth ratios during irradiation and to provide high burn-up HTR fuel pebbles for safety testing (KÜFA) at the Institute for Transuranium Elements of the European Commission (JRC-ITU). KÜFA tests [22] verify the fission product retention of irradiated pebbles beyond 1600°C under simulated accident conditions.

The HFR-EU1 experiment was followed by HTR-TN and was technically integrated into the Euratom projects HTR-F/F1 and RAPHAEL [98], [99]. These projects focus on the innovation potential of past and current HTR fuel technology based on Tri-Isotropic (TRISO) coated fuel particle design. Major partners in the consortium for these projects are CEA, AREVA NP, NRG, FZJ, JRC and BNFL.

As with earlier experiments, the objective of HFR-EU1 is to explore the potential for high performance and high burn-up of the existing German Arbeitsgemeinschaft Versuchsreaktor (AVR) fuel pebbles and newly produced fuel from the Institute of Nuclear and New Energy Technology (INET). During extensive irradiation tests, both at and above nominal power plant conditions in the 1980's and 1990's, not a single coated particle of German 'near-to-production' fuel elements with Low-Enriched Uranium (LEU) TRISO coated particles failed in the sense of irreversibly increased fission gas release [100], [101], [102]. Irradiating this fuel under defined conditions to high burn-ups and testing it afterwards in thermal ramp tests to simulate cooling accidents is a requirement for the licensing of new fuel and provides a better understanding of fission product release and failure mechanisms, should coating failure occur.

HFR-EU1 was dedicated to a particularly high burn-up, while an extremely high temperature test for steady-states conditions (approx. 1250°C fuel central temperature with somewhat lower burn-up) was tested in another irradiation test,

HFR-EU1bis [41], performed between 2004 and 2005. With two independent capsules containing the fuel elements in HFR-EU1, this experiment was more complex in terms of design and operation than HFR-EU1bis which had accommodated five pebbles in a single sample-holder. Moreover, HFR-EU1 was connected to a new gas handling facility that enabled continuous instead of batchwise fission gas release analysis. HFR-EU1 was initially designed to accommodate lower power densities (lower neutron flux, thus lower fission power and acceleration factor) than HFR-EU1bis, with an initially estimated 22 calendar months in position H2 (Fig. 2.1). However, the HFR conversion from High-Enriched Uranium (HEU) to LEU, which finished only a few months before the start of the experiment, required two position changes leading to significant power variations. So far, HFR-EU1 has completed 12 reactor cycles, approx. 28 Effective Full Power Days (EFPD) each, in core positions H2 (3 cycles), H4 (3 cycles) and F2 (6 cycles). Fig. 2.1 displays the successive moves of HFR-EU1 in the HFR.

Table 2.1: Nominal characteristics of INET and AVR GLE-4 particles and pebbles.

Coated Particle	INET	AVR
Particle batch	V000802	HT 384-393
Kernel composition	UO ₂	UO ₂
Kernel diameter [μm]	490.3	502
Enrichment [²³⁵ U wt.%]	17.08	16.76
Thickness of coatings [μm]:		
buffer	97.7	92
inner PyC	42	40
SiC	37.8	35
outer PyC	40.8	40
Particle diameter [μm]	926.9	916
Pebble		
Heavy metal loading [g/pebble]	5.02	6.0
²³⁵ U content [g/pebble]	0.858	1.00 ± 1 %
Number of coated particles per pebble	8500	9560
Volume packing fraction [%]	5.0	6.2
Free uranium fraction [U/U _{tot}]	2.3E-7	7.8E-6
Matrix graphite grade	A3-3	A3-3
Matrix density [kg/m ³]	1760	1750
Temperature at final heat treatment [°C]	1900	1900

The irradiated pebbles are 60 mm in diameter with LEU-TRISO coated particles. German pebbles were of type AVR GLE-4, produced as batch AVR 21-2 in October 1987. They were manufactured by HOBEG [103]. The two Chinese pebbles were produced by INET for the operation of the HTR-10 test reactor. Table 2.1 lists the key characteristics of both pebble types.

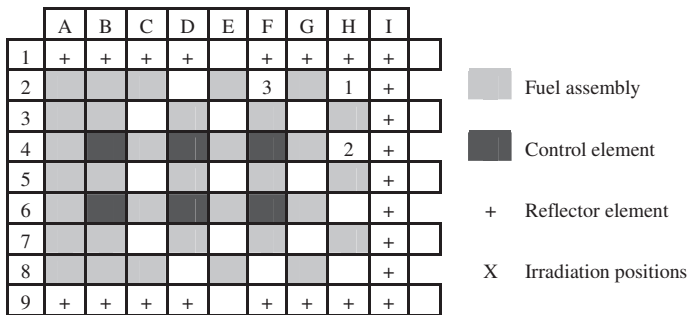
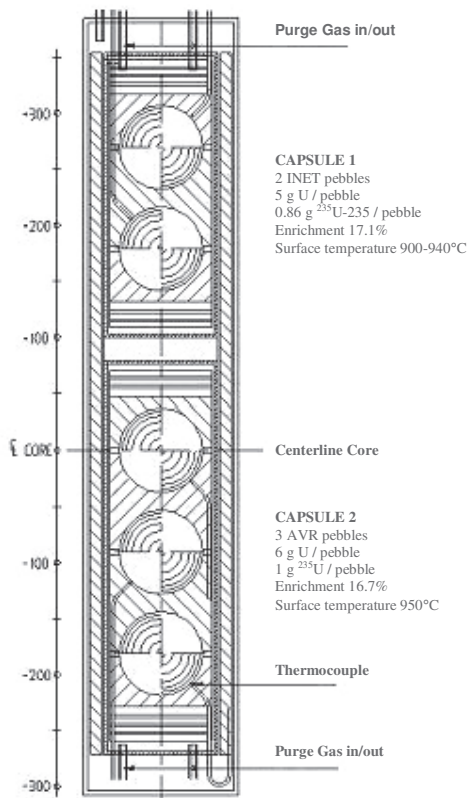


Fig. 2.1: Standard HFR core configuration showing HFR-EU1 in core positions H2, H4 and F2.

2.2 Experimental

The design of HFR-EU1 is based on previous experience of HTR fuel irradiations within the European Union, namely HFR-EU1bis, HFR-K5, HFR-K6 and SiC Balls [41], [104], [37], [105]. The five pebbles and six mini samples (10 coated particles each, packed in graphite powder and contained in a niobium tube) were tested in a standard reusable REFA-172 rig, slightly larger than a “Full Size HTR Fuel Element Rig” (REFA-170), which is a standard device in the HFR Petten. This change was required in order to accommodate the two different capsules and gas lines. A schematic drawing is shown in Fig. 2.2. The sample holders (1st containment) consist of AISI 321 capsules containing several graphite cups (SGL R6650) holding the pebbles in place. The REFA-172 rig forms the second containment. The upper sample holder (INET fuel) is equipped with 14 thermocouples, while the lower one (AVR fuel) has 20.



Thermocouples are of type N made by Thermocoax with Inconel 600 sheaths. Nuclear instrumentation includes 12 neutron fluence detector sets, 4 self-powered neutron detectors and 4 gamma-scan wires. The heat generated in the pebble by fission and photons dissipates mainly radially through the materials by conduction and through the gas gaps by conduction/radiation to the outside containment, which is cooled by primary cooling water. It was possible to control the temperature of the fuel surface by adjusting the He/Ne blend in both the first and second containments. This temperature adjustment was required to compensate for changes of time and fluence dependent operating parameters such as fuel depletion (burn-up), dimensional changes of specimen assembly (graphite shrinkage, typical turn-around dose $10\text{--}15\text{E}+25\text{ m}^{-2}$, typical shrinkage at turn-around approx. -2% at $470\text{--}500^\circ\text{C}$), changes in thermal conductivity and thermal expansion, changes in nuclear characteristics from cycle to cycle and movements of reactor control rods.

The first and second containments were continuously purged with a constant gas flow during the whole irradiation, which facilitated temperature adjustment and gas sampling. This set-up with a higher gas pressure in the second containment enabled permanent integrity surveillance of the first containment using pressure alarm units.

Cycle-by-cycle turning of the experiment, by 180° , flattens neutron fluence and radial burn-up gradients across pebbles.

The experiment was designed such that, despite the decrease in power with time, the desired surface temperature could be kept as constant as possible in all pebbles over the entire irradiation. This was achieved by sizing the gas gaps between graphite cups and first containment tube and first and second containment tubes such that a suitably adjusted He/Ne blend enabled the required pebble temperatures to be obtained.

Like HFR-K3, HFR-EU1bis was conducted with constant central temperature. While this approach imposes stringent conditions on the particles (with average particle temperature rising during the irradiation), the conduct of the experiment is challenging: Surface temperature is tuned to accommodate for power density variations. Furthermore, uncertainties in thermal conductivity data (in the order of 10%) also influence the temperature profile across the pebble. For this reasons, HFR-EU1 was conducted with constant surface temperature, although fuel depletion continuously lowers the particles temperature during the experiment.

2.3 Nuclear Data

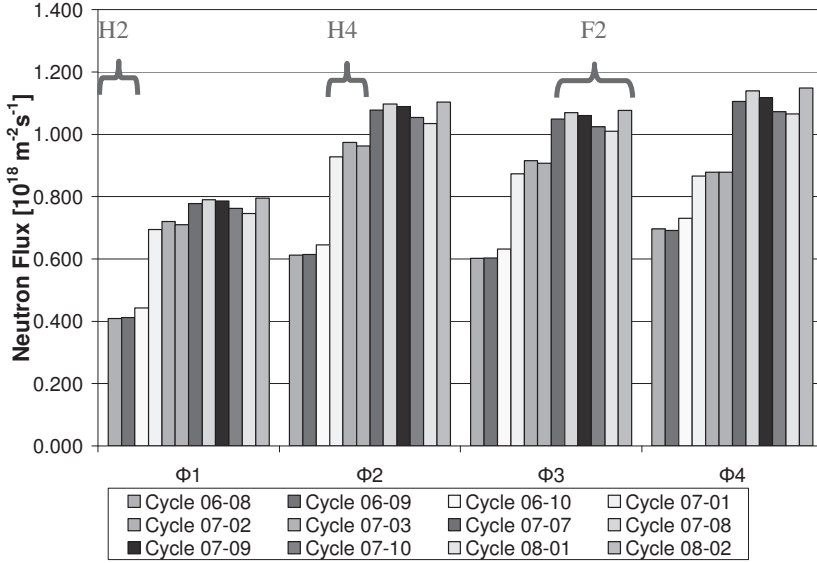
The 4-group neutron fluxes, thermal and fast fluences are listed in Table 2.2 for the 12 reactor cycles performed until being placed on hold on 24 February 2008. The position changes led to significant flux variations. A shortened reactor cycle 2006-08 was responsible for the lower fluence received during this cycle, whereas fluence fluctuations in position F2 are due to neighbouring experiments, cf. Fig. 2.3.

According to these post-cycle calculations, the currently attained thermal and fast fluences would be $2.73\text{E}+25 \text{ m}^{-2}$ and $3.68\text{E}+25 \text{ m}^{-2}$, respectively, accumulated during 332.8 EFPD. The values and axial profiles for fluence and spectrum will be verified during PIE through the analysis of neutron detector sets and gamma scan wires, and by burn-up measurement of the pebbles.

If the uncertainty of these calculations are not provided by the HFR post-cycle reports, numerous studies, including those used the pre-determination of the neutronic behaviour of the fuel experiment, were performed to ensure the quality of the values provided. Furthermore, neutronics of the experiment will be rescaled after End Of Irradiation (EOI) and measurement of the achieved burn-up.

Table 2.2: Comparison of fluxes and fluences from HFR post-cycle computations.

Reactor cycle	EFPD	$\Phi_1^{(1)}$	$\Phi_2^{(1)}$	$\Phi_3^{(1)}$	$\Phi_4^{(1)}$	Fluence $\Phi_4^{(1)}$	Fluence $E > 0.1 \text{ MeV}$
	[days]	Cycle Averaged [$10^{18} \text{ m}^{-2} \text{ s}^{-1}$]				[10^{24} m^{-2}]	
2006-08	24.2	0.409	0.612	0.602	0.697	1.46	1.63
2006-09	26.9	0.412	0.615	0.603	0.691	1.60	1.82
2006-10	28.6	0.443	0.645	0.632	0.730	1.80	3.05
2007-01	27.9	0.695	0.927	0.873	0.866	2.09	3.05
2007-02	28.9	0.720	0.974	0.915	0.878	2.19	3.30
2007-03	27.9	0.710	0.963	0.907	0.878	2.11	3.14
2007-07	27.5	0.778	1.078	1.049	1.106	2.62	3.39
2007-08	28.7	0.790	1.097	1.069	1.139	2.83	3.61
2007-09	28.0	0.786	1.089	1.060	1.118	2.70	3.49
2007-10	27.8	0.762	1.054	1.024	1.072	2.58	3.36
2008-01	27.8	0.746	1.035	1.010	1.066	2.56	3.29
2008-02	28.8	0.795	1.103	1.077	1.149	2.85	3.63
total	332.8					27.39	36.74
Variations H2 cycles	15.2%	7.67%	5.12%	4.75%	5.34%	19.0%	46.7%
Variations H4 cycles	3.67%	3.47%	4.83%	4.59%	1.37%	4.88%	7.51%
Variations F2 cycles	4.52%	6.16%	6.17%	6.22%	7.22%	10.4%	9.39%
Variations 12 cycles	16.2%	48.6%	44.5%	44.1%	39.9%	48.8%	55.2%



¹⁾Energy groups with boundaries: 14.918E+6; 1.353E+6; 0.0674E+6; 0.683; 0 eV

Fig. 2.3: Comparison of neutron fluxes per reactor cycle from HFR post-cycle computations.

2.4 Power Evolution in Pebbles

Pre-irradiation neutronic calculations had determined the heat from fission and photons in the pebbles, which decreases during irradiation (cf. Table 2.3). These calculations [106], performed with OCTOPUS [107] (coupling of MCNP43C [108] and FISPACT-2001 [109]), yielded the power density and burn-up evolutions plotted in Fig. 2.4.

The calculation scheme is as follow:

- 1- A HFR model is used to determine, with MCNP43C, unperturbed spectra tallied at the surface of the five pebbles fuel zone, for each irradiation position.
- 2- OCTOPUS performs iterations where:
 - 2a- MCNP43C uses the unperturbed spectra to determined perturbed spectra tallied on the kernels volume.
 - 2b- FISPACT-2001 uses the perturbed spectra to age the fuel.

The output of this calculation is, for each individual pebble, the evolution of the fuel atomic density vs. irradiation time. This enables to determine fission rates, while fission yields from the Joint Evaluated Fission and Fusion File (JEFF-3.1) were used

for the birth rate determination of the measured volatile fission product of Kr and Xe. Variations of slope in Fig. 2.4 are a consequence of position changes.

Table 2.3: Pre-calculated power evolution in pebbles.

Reactor cycle	Pebble Power (fissions + photons)[W]				
	INET/1 (top)	INET/2	AVR/1	AVR/2	AVR/3 (bottom)
1	810	1031	1642	1669	1546
2	803	1021	1617	1643	1523
3	788	1001	1567	1590	1479
4	892	1181	1810	1887	1691
5	875	1155	1754	1826	1640
6	857	1126	1696	1763	1587
7	1393	2083	3364	3521	3182
8	1343	1959	3130	3274	2971
9	1295	1844	2908	3039	2772
10	1252	1746	2713	2833	2598
11	1211	1656	2531	2640	2435
12	1174	1576	2372	2471	2292

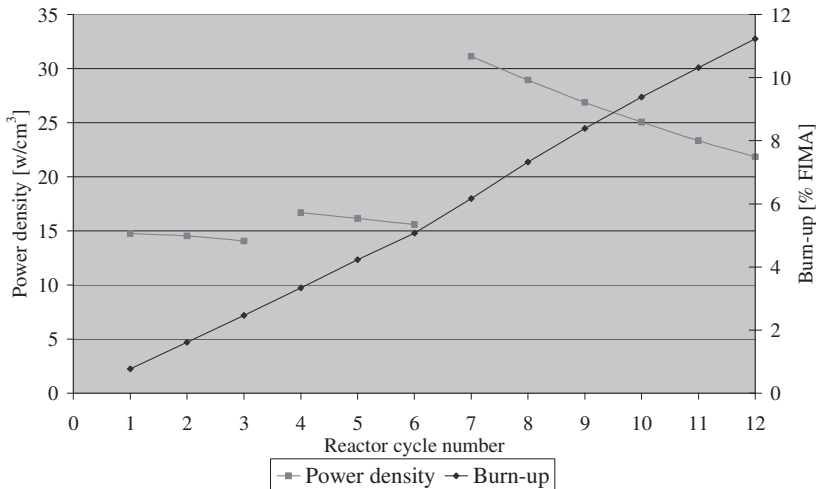


Fig. 2.4: Pre-calculated power density (fission + photons) and burn-up evolution with irradiation for pebble in maximum flux position (AVR/2).

2.5 Temperatures

Temperatures measured in the sample holder were stored in the standard HFR data acquisition system. Fig. 2.5 shows the average temperatures during the 12 irradiation cycles without correction for thermal drift and neutron induced de-calibration of thermocouples.

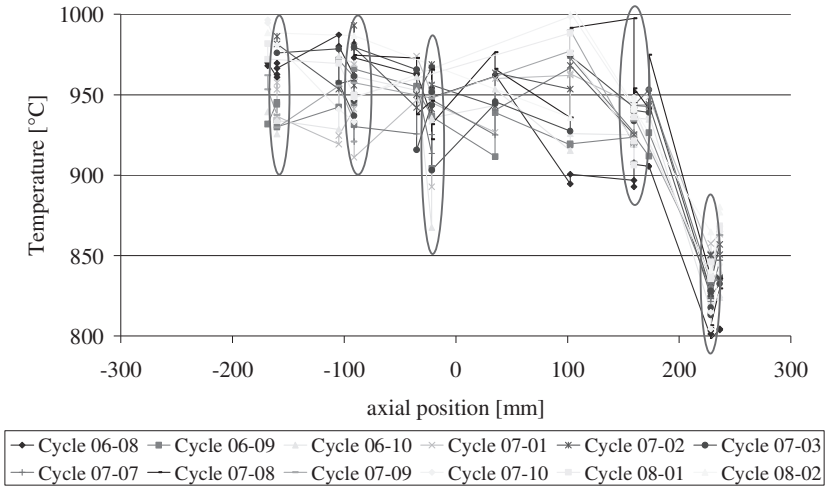


Fig. 2.5: Average temperatures measured in the irradiation rig for all 12 irradiation cycles. Ellipsoids mark pebble positions.

Thirty-four thermocouples were built into the experiment. They were supplied by Thermocoax and were of type N (Nicrosil/Nisil wires, MgO insulator, Inconel 600 sheath) with an outer diameter of 1.05 mm. After 12 irradiation cycles, 4 out of the 14 INET and 16 of the 20 AVR thermocouples provided physically impossible or unreliable signals. Several mechanisms are suspected to have been at work, such as exposure to high temperature and neutron flux for extended periods of time, carburization of the sheath, bending (required for the AVR capsule), contact problems in connectors, vibrations in the experiment, and movement of thermocouples due to thermal expansion.

While thermocouple redundancy is for the time being the only way to circumvent these reliability problems, JRC-IE has started to investigate new thermocouples for high temperature irradiation tests.

2.6 Special Events

After a two weeks period at low temperature, for graphite drying, the temperatures were raised to their initial set-points (i.e. 900/950 °C for INET and AVR capsules, respectively). During the design process, pebble powers were predicted by means of neutronic calculations. Thermal-mechanical calculations then sized the graphite sample holder to accommodate the power distribution and to flatten the temperature gradient along the capsules. However, an 80°C temperature gradient was noticed along the INET capsule, hinting at a more significant axial power gradient than anticipated by design computations. Consequently, the initial target of irradiating both Chinese pebbles at 900°C was no longer feasible. The solution was to raise the INET capsule temperature set point by 40 °C, such that the top pebble was irradiated at 860°C, while the second was held at 940°C from the beginning of the third irradiation cycle.

Conversion of the HFR to LEU fuel in 2006 had distorted the previous flux situation, and it turned out that the position originally intended for HFR-EU1 was quite strongly affected by a loss of flux and thus pebble power. As the result of these phenomena (increase in temperature set-point, conversion of HEU to LEU and fuel depletion) very little temperature adjustment margin was left after the first three reactor cycles. In a first move, the experiment was transferred from position H2 to H4 with a higher flux for another three reactor cycles. The next three reactor cycles had to be skipped to finalize detailed computations for finding a permanent position for the experiment and to update and approve safety documents.

This permanent solution was found in position F2, where target temperatures could be maintained even without fission power. The computational method applied had been qualified in the “HFR-EU1bis benchmark” exercise [106].

Massive thermocouple loss was observed during the irradiation. In particular, in the AVR capsule, 16 out of the 20 thermocouples installed were malfunctioning. This led to the loss of the approved minimum operating instrumentation (1 thermocouple per pebble, out of 4 installed). Since February 24th 2008, the experiment is on standby to investigate available options for safe continuation of the test.

2.7 Fission Gas Release Measurements

HFR-EU1 was conducted using a newly built gas handling station, the so-called “Sweep Loop Facility” (SLF). This installation provides all containments with variable gas blends for temperature control and enables permanent surveillance of containment integrity, as well as gas sampling for fission gas release measurements by gamma spectrometry with the associated alarm functions. Gas sampling was generally performed once per week per capsule. The SLF was operated from a PLC controlled command cabinet, which also contained a number of alarm functions,

such as the automatic cut-off of all gas lines to and from the irradiation rig in case of excessive radioactivity release.

Temperature was adjusted by mixing He and Ne, while keeping the total gas flow rate constant, typically 50 ml/min. For gas sampling, the gas flows from the first containments were routed through a detachable grab sample with a volume of 100 cm³. This grab sample was then removed from the glove box and placed on a multi-channel gamma spectrometer calibrated for the measurement of five different isotopes, namely ^{85m}Kr, ⁸⁷Kr, ⁸⁸Kr, ¹³³Xe and ¹³⁵Xe. Several measurements were made of each sample and the counts were corrected for decay to determine the specific isotope concentration in the purge gas at the moment of gas sampling. The statistical error of this measurement ranged from 4 to 15%. Together with the known gas flow, pressure and temperature, the fission gas release rate R from the two capsules could be determined and related to the birth rate B from neutronic calculations, thus yielding the characteristic R/B value, which is considered a good health indicator of coated particle fuel.

The burn-up shown Fig. 2.6 and Fig. 2.7 are the one pre-calculated for the experiment (capsule averaged). Subsequent adjustments will be made once the burn-up measurements of the pebbles and the analyses of gamma scan wires and fluence detectors are available.

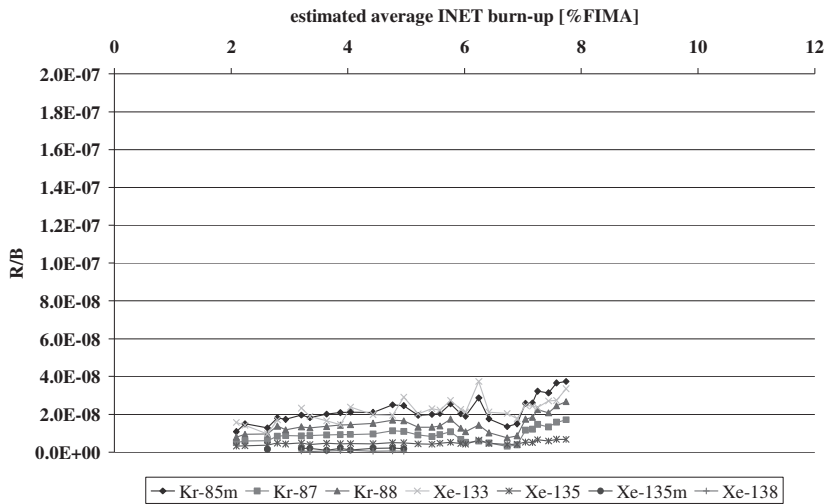


Fig. 2.6: Preliminary R/B vs. burn-up for INET pebbles.

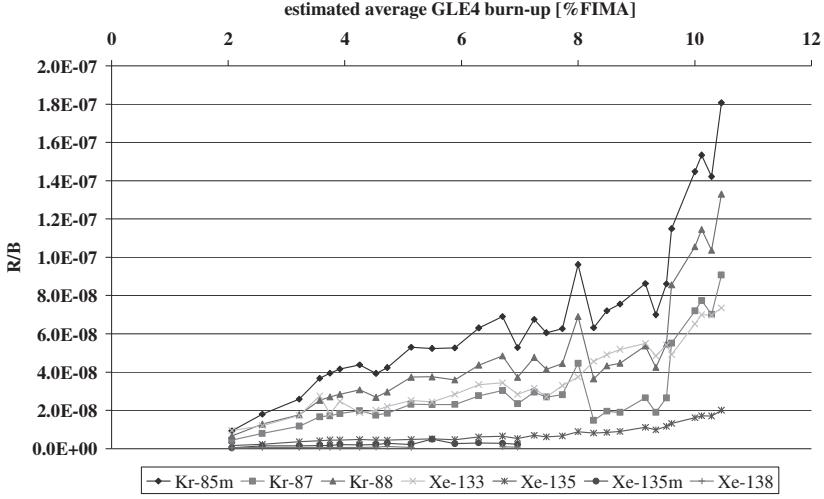


Fig. 2.7: Preliminary R/B vs. burn-up for AVR pebbles.

After 12 irradiation cycles, an R/B of approx. $4E-8$ and $1.8E-7$ was measured for INET and AVR fuel, respectively, which is at least two orders of magnitude lower than the R/B corresponding to a theoretical full fission gas release of a single particle in the capsules (approx. $1.7E-4$ and $2.8E-4$ for INET and AVR capsule, respectively).

In the earlier experiments HFR-K5 and HFR-K6, R/B values of $5E-7$ were measured on fresh fuel. More recently, HFR-EU1bis [41] produced higher R/B values of approx. $4E-6$. This may be interpreted either as an increased release from the used graphite cups (fission products from thorium and uranium impurities) or as a fractional release of one or more particles affected by manufacturing defect.

This suggests that, in HFR-EU1, no complete particle failure has so far been detected. Instead, the measured fission gas release probably originates again from uranium and thorium impurities in the matrix graphite of the pebbles and in the graphite cups used to hold the pebbles in place.

A similar method to that for HFR-EU1bis [41] was employed for the gas measurement analysis: The quality of the R/B measurement (steady-state R/B) was verified by checking that there was little or no temperature dependence on fission gas transport during the measurement, i.e. the gas sample was taken at stable temperature. In [100] we find the following expression for R/B :

$$\frac{R}{B} = 3\sqrt{\frac{D'}{\lambda}}$$

with:

R : Fission gas release rate

$$D' = D'_0 \exp\left[-\frac{Q}{RT}\right]$$

B: Fission gas birth rate
D': apparent fission gas diffusivity (temperature dependent)

$$\lambda = \frac{\ln 2}{T_{1/2}}$$

T_{1/2}: half life of concerned isotope

At constant temperature T, we can then derive:

$$\ln \frac{R}{B} = \text{const.} + n \ln \frac{1}{\lambda} = \text{const.} - n \ln \lambda$$

Consequently, when plotting the individual $\ln R/B$ values from a given measurement against $\ln \lambda$, the result should be a straight line with the negative inclination n . This method was applied to each gas sample: For each capsule and with the two different isotope groups (with ^{85m}Kr , ^{87}Kr and ^{88}Kr for the Kr group and only ^{133}Xe and ^{135}Xe for the Xe group). Besides the five scanned isotopes, two more Xe isotopes were counted, with higher statistical errors.

According to [100], the Booth model leads to $n = 0.5$ for bare kernels and heavy metal contamination of graphite grains. However, in case of coated particles, experimentations have shown a range of n values having approximate limits of 0.1 and 0.5: Coatings affect more long lived isotopes than short lived ones.

Fig. 2.8 and Fig. 2.9 display the evolution of the slope for each capsule and groups versus burn-up. In most cases the slope was above the theoretical value of 0.5. Since the Booth model applies only to the diffusive release of fission products from kernels and matrix graphite grains and since the release is not measured right after the diffusion process, the interpretation of the inclination is rather ambitious. Furthermore, one should not forget the initial idea of this investigation: Assume that measurements are performed in steady temperature conditions.

The few measurements which did not produce a straight line were omitted. Of the scanned isotopes, Kr isotopes were generally consistent. Only a few dubious results were obtained and could be traced back either to the use of a defective sampling vessel or to insufficient purging of the grab sample. These data were scrapped.

Statistics on these slopes have been performed also for Xe isotopes and HFR-EU1bis and are available in Table 2.4. This makes quite obvious the gain in stability in the HFR-EU1 irradiation compared to HFR-EU1bis: Irradiation conditions (mainly temperature) and release (HFR-EU1bis having most probably initial broken particles) are more constant in HFR-EU1.

Table 2.4: Average and variance of slope for HFR-EU1 and HFR-EU1bis capsules.

	Averaged slope	σ
HFR-EU1 INET - Kr	0.625	4.40%
HFR-EU1 INET - Xe	0.548	7.93%
HFR-EU1 AVR - Kr	0.607	5.13%
HFR-EU1 AVR - Xe	0.579	8.02%
HFR-EU1bis - Kr	0.319	10.91%
HFR-EU1bis - Xe	0.218	12.36%

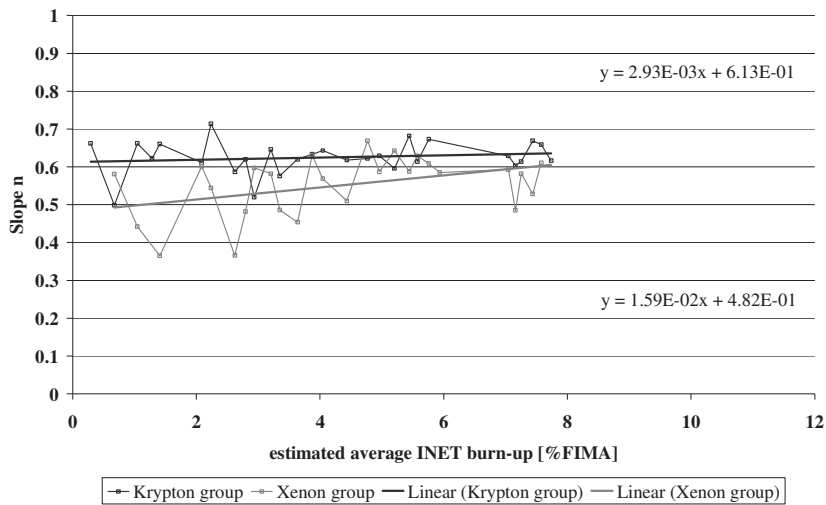


Fig. 2.8: Slope n vs. burn-up for INET pebbles.

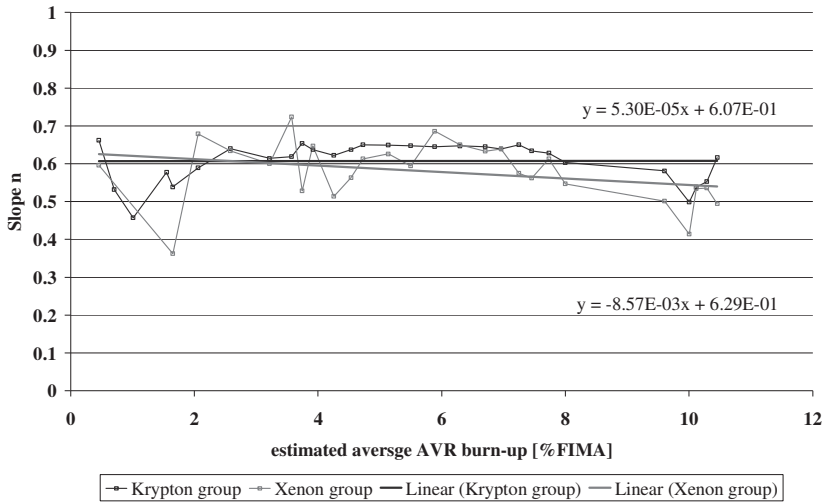


Fig. 2.9: Slope n vs. burn-up for AVR pebbles.

2.8 Uncertainty analysis

Although such low release over birth ratios suggest absence of broken particles, the following analysis aims at better understanding of the announced values. In this chapter, only R/B ratios of the last measurements (i.e. at 327.9 EFPD for INET and 328.9 EFPD for AVR capsules) are analysed: 1- Failure of particle is more likely to occur at high burn-up. 2- High fluences also correspond to the highest R/Bs measured.

Uncertainty is a parameter characterizing the range of values within which the quantity can be said to lie within a specified level of confidence. In this study, R/B uncertainties are investigated.

Accuracy is a measure of the agreement of a particular measurement with the true or accepted value of the parameter. For this experiment, the true burn-ups will be measured after EOI. Accuracy here is then the difference between the simulated burn-ups by neutronic tools and the true value to be determined later. Due to the correlation between burn-ups and fission rates (and thus birth rates), the same accounts for birth rates.

Precision is the closeness of agreement between independent measurements of a quantity under the same conditions. It is a measure of how well a measurement can be made without reference to a theoretical or true value. Since the neutronic tools used in this study are based on the Monte-Carlo method, the different codes provide precisions for the parameters sampled, such as fission and birth rates.

Error is the difference between a measurement and the true value of the quantity being measured. It then refers to gas activity being measured by γ -spectrometry. Error has two components: 1- A systematic error tend to shift all measurement in a constant way. 2- A random error which varies in an unpredictable way in the course of a number of measurements. The systematic error is then due to the calibration of the γ -spectrometer, while the random error is linked to the shape of the spectrum and the Gaussian fitting.

2.8.1 Neutronic tool validation

The applied computational method (NRG's OCTOPUS [106], combination of MCNP4C3 [108] and the FISPACT-2001 [109] used for pre-calculation of birth rates) had been qualified in the "HFR-EU1bis benchmark" exercise [110].

To conduct the uncertainty analysis, simulations were performed with MCB [111] in replacement of OCTOPUS for the depletion calculations. The use of a different code requires validation. For this purpose, an attempt was made to reproduce NRG results based on the same unperturbed flux. The comparison of the two sets of results shows the following:

Variations on the perturbed flux: Table 2.5 displays variations on the perturbed flux determined by MCB (in comparison with OCTOPUS ones) for the five fresh fuel elements (i.e. in irradiation position H2 of the HFR). MCB tends to calculate a lower thermal perturbed flux by up to 2%. This can be partly explained by the precision of the two calculations.

Table 2.5: *Variations of perturbed fluxes for the five pebbles in H2.*

Fuel elements	INET1	INET2	AVR1	AVR2	AVR3
Fast	5.92%	5.71%	5.86%	5.76%	4.87%
High Epi-Thermal	0.03%	-0.57%	0.06%	0.10%	-0.05%
Low Epi-Thermal	-2.94%	-2.17%	-2.10%	-2.74%	-2.84%
Thermal	-0.82%	-1.03%	-1.96%	-1.56%	-1.28%
Total	0.13%	0.03%	-0.07%	-0.08%	-0.19%

Variations on the fission rates: Although with a lower perturbed thermal flux, MCB shows higher fission rates at the beginning of irradiation (BOI). This can be explained by higher thermal neutron absorption (for fission purpose). This also explains why MCB fission rates decrease faster than those of OCTOPUS, leading to values that are up to 12% lower than those predicted by OCTOPUS, as shown in Fig. 2.10.

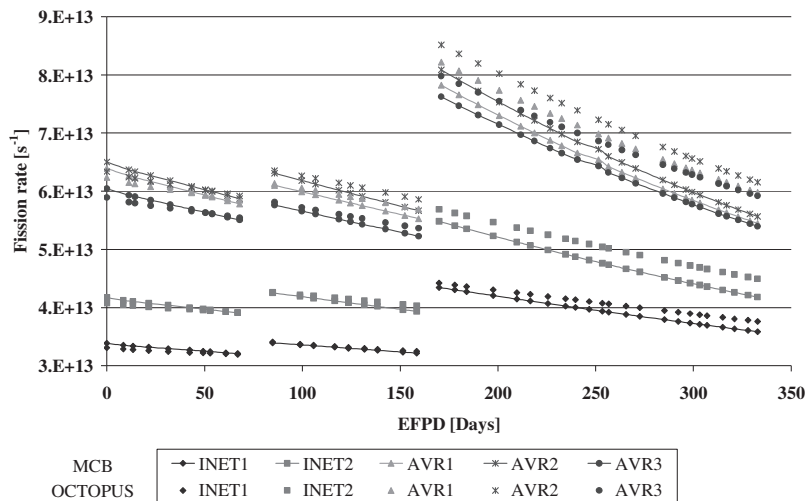


Fig. 2.10: Comparison of OCTOPUS and MCB fission rate estimates.

Variations on the burn-ups: MCB enables fuel burn-up determination. Fig. 2.11 displays burn-ups determined with OCTOPUS and MCB. The results of both codes remain consistent, although MCB tends to decrease burn-ups by 3%.

The good correlation between burn-up and fission rates is noticeable when comparing MCB to OCTOPUS: MCB higher fission rates lead to a faster increase in burn-ups and vice-versa.

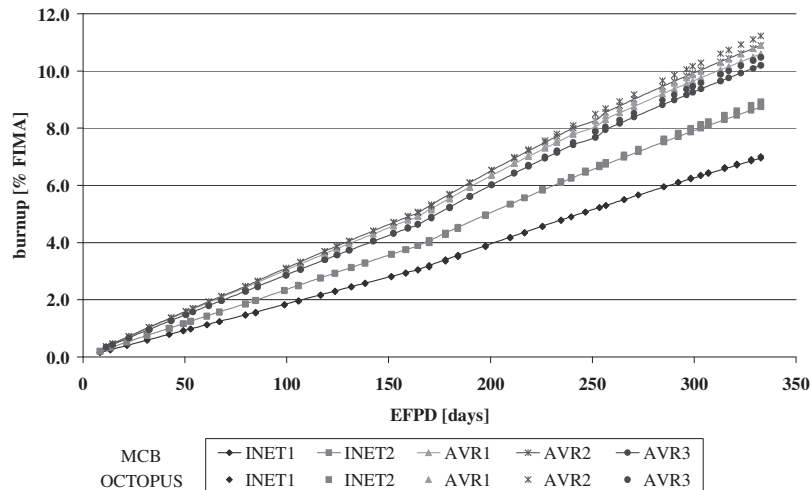


Fig. 2.11: Comparison of OCTOPUS and MCB burn-up estimates.

Variations on the birth rates: For Kr isotopes, MCB over-estimates (by 7-9%) at BOI and under-estimates (by 17-31%) after 333 EFPD in comparison with OCTOPUS. If ^{133}Xe is over-estimated by 8% at BOI, this discrepancy drops with burn-up. Initially underestimated by 11-12%, ^{135}Xe birth rate drops to 24-27% after 333 EFPD. The use of MCB causes a similar trend for all isotopes considered: namely lower values of birth rates compared to those calculated with OCTOPUS. Once corrected, this trend slightly raises R/B values.

One can however notice that the trends are different for each isotope. The variations on fission rates affect all isotopes the same way. The different trends are a result of updated fission yields used with MCB in comparison to OCTOPUS ones.

At EOI, discrepancies between MCB and OCTOPUS simulations reach at worst 31% on the birth rates of certain fission products and less than 3% on burn-ups. If this seems surprising at first, one should remember that burn-ups are integrated over the irradiation lifetime: At BOI, MCB fission rates are higher than OCTOPUS ones, leading to steeper burn-ups increase for MCB than OCTOPUS. At EOI, MCB fission rates are up to 12% lower than OCTOPUS ones. Burn-ups increase is then lower for MCB than OCTOPUS, compensating the burn-up gain accumulated in the early phase of the irradiation.

The discrepancies have an impact on R/B ratios, but not a significant one (less than an order of magnitude). Therefore, the conclusion that no particle failed throughout the irradiation of HFR-EU1 fuel experiment remains valid.

This also qualifies MCB as sufficient for the update of pre-calculated parameters, such as birth rates and burn-ups.

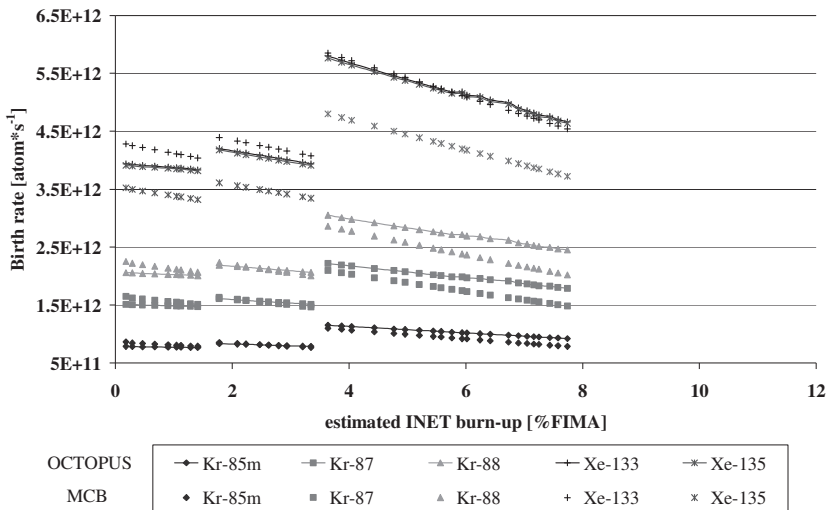


Fig. 2.12: Comparison of birth rates estimates for INET pebbles.

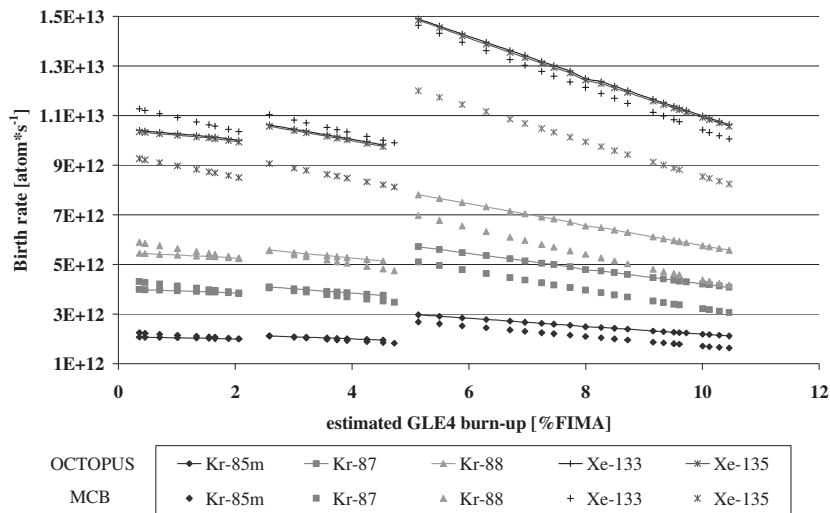


Fig. 2.13: Comparison of birth rates estimates for AVR pebbles.

2.8.2 Impact of irradiation history on the calculation of birth rates and burn-ups

Chapter 2.7 showed release measurements (and the associated uncertainty) as well as Release over Birth vs. Burn-up graphs. Both birth rates and burn-ups are based on pre-calculated values. Therefore, they do not account for flux variations over the irradiation lifetime.

Table 2.6: Comparison of pre and post-irradiation-calculated data.

Pebble	INET1	INET2	AVR1	AVR2	AVR3
EFPD [Days]	327.9	327.9	328.9	328.9	328.9
	Fission rates [fiss/s]				
Pre-Calculations	2.89E+13	3.67E+13	5.89E+13	6.00E+13	5.54E+13
Post-Calculations	4.29E+13	4.98E+13	6.35E+13	6.49E+13	6.32E+13
	Burn-ups [% FIMA]				
Pre-Calculations	6.85%	8.62%	10.49%	10.79%	10.09%
Post-Calculations	8.43%	10.48%	12.41%	12.72%	11.96%

In predictive simulations (or pre-calculations), the unperturbed fluxes applied on the matrix zones are fixed per irradiation position. Taking into account information from HFR post-cycle computations, such as those displayed in Table 2.2, one can

improve the prediction of cumulated thermal fluence (hence the post-calculations): The cycle durations and neutron flux (Influenced by the core loadings) suggest a real thermal fluence of $27.4\text{E}+24 \text{ m}^{-2}$, significantly larger than the initially assumed $21.8\text{E}+24 \text{ m}^{-2}$. Since these information were successfully used in [110] for the neutronic determination of HFR-EU1bis burn-ups, when compared with experimental results, one can safely assume this leads to higher accuracy on fission rates and burn-ups, as shown in Table 2.6.

It should be noted that a 26% increase in thermal fluence leads to a 23% burn-up increase for the least burned pebble and to only an 18 % for the most burned one.

The increase in thermal fluence can only be achieved by means of higher thermal flux. For fresh fuel, this obviously raises fission rates. However, this also increases depletion (as illustrated by higher burn-ups) and would lead, once very high burn-up is achieved, to lower fission rates. Table 2.6 shows that, although burn-ups are significantly raised, fission rates remain higher for post-calculation than for pre-calculation.

Higher fission rates (and birth rates) lead to lower R/B values. This trend is further accentuated by the increase in burn-ups. Therefore, the R/Bs announced in chapter 2.7 remain high estimates through this update of birth-rates and burn-ups.

2.8.3 Uncertainty of the release

Due to the measurements:

Gas samples are analysed by γ -spectrometry. The reports contain, for each sample tested, the activity measured of fission products found as well as a random error due to the shape of the spectra for the energy peak considered. This random error varies from 4 to 15% depending on the isotope considered and the measurement analysed.

The calibration of the γ -detector should also be taken into consideration. The system was tested with a source of known activity (and same geometry than the gas samples, filled with a low density foam) at different energy peaks to establish the efficiency of the detector. This analysis has shown that the detector tend to overestimate by 2.5% to 5.8% (depending on the energy considered) the release measured.

The overall error on the release is the contribution of both systematic and random errors and therefore depends on the isotope considered and the measurement performed: At 327.9 EFPD for INET and 328.9 EFPD for AVR capsules, the random error of γ -spectrometry reaches 4% for $^{85\text{m}}\text{Kr}$ (i.e. the release ranges in an interval of $\pm 4\%$ around the measured value). Since the $^{85\text{m}}\text{Kr}$ peak, taken into account for the γ -spectrometry, has an energy of 151 keV, the calibration of the detector tends to decrease systematically the release measured by an other 2.4 to 3.8%. Therefore, the overall error on the release varies from -7.7% to +1.5%.

Due to the origin of the activity:

As explained previously, graphite (both matrix and sample holder) contamination may lead to a significant production of fission products. According to [112], there are three possible contributions to fission product release from HTR fuels: broken particles, graphite natural contamination (of fuel matrix and experiment sample holder) and enriched uranium contained in the particle OPyC layers (contamination during the manufacturing process). This study focuses only on the natural graphite contamination: Low release over birth ratios suggest no particle failures, while enriched uranium contamination of particle layers gives only a very low contribution due to low diffusion of Kr and Xe isotopes in PyC and the isotopes' relatively short half-lives.

The same neutronic method as that developed for post-irradiation calculation was applied for the determination of graphite natural contamination influence: As in [112], a graphite contamination of 50 wppb of natural uranium and of 250 wppb of thorium was assumed for the matrix. This contamination is similar to the expected contamination of SGL 6650 graphite used as sample holder (100 wppb U_{nat} and Th) [113]. The five fuel zones were then "irradiated" and fission rates were volume-weighted to determine the capsule fission rates as displayed on Fig. 2.14.

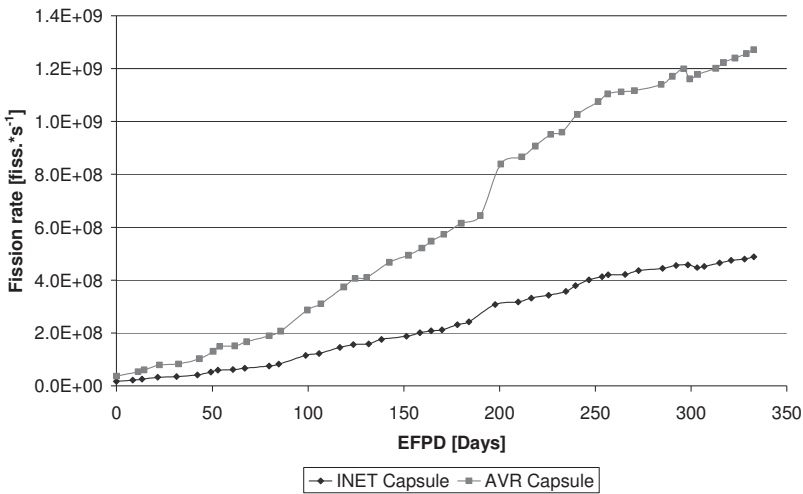


Fig. 2.14: Fission rate of assumed contamination in HFR-EU1 experiment.

Fig. 2.15 shows the ratio of contamination fission rate over one particle fission rate. This makes it clear that, at the end of irradiation (EOI), contamination accounts for more than 11% of one particle fission rate: Fission gas release must be higher than this value before one may conclude that there is complete particle failure.

Note the steep increase in fission rates over the irradiation, confirming the breeding of fissile material from fertile one. However, one should bear in mind that, even at EOI, graphite contamination accounts for only $6.5\text{E-}6$ of the total fission rate for the INET capsule and $7.5\text{E-}6$ for the AVR one. With such low values, this does not influence **fuel** Release over Birth ratios. However, since the resulting fission gases are very mobile (no containment), this production could explain the release measured.

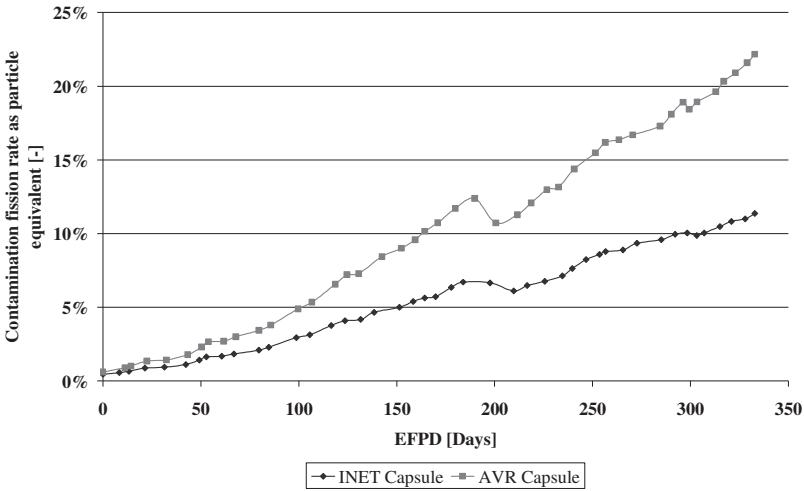


Fig. 2.15: Fission rate ratio of contamination over one particle in HFR-EU1.

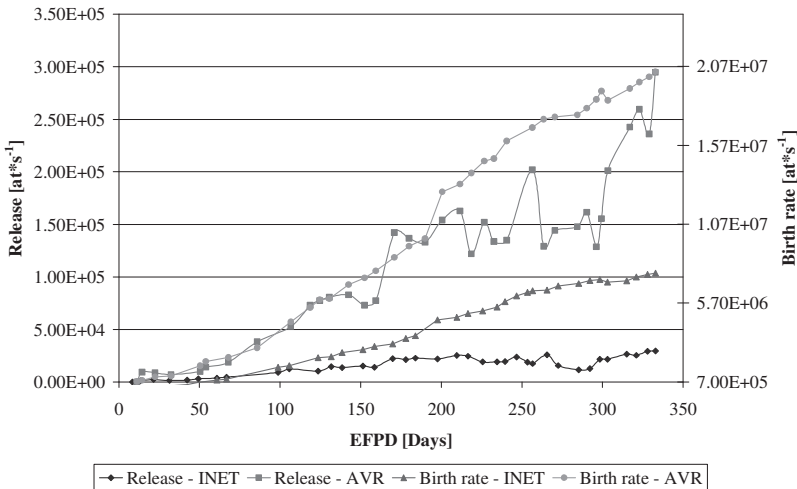


Fig. 2.16: ^{85m}Kr release and contamination induced birth rate vs. EFPD.

With fission yields from JEFF-3.1 database, birth rates from contamination of different fission product isotopes are computed. Fig. 2.16 shows the good correlation between release measured and contamination-induced birth rate for the ^{85m}Kr isotope. This graph also shows that, for the AVR capsule, both release and birth rate increase at the same rate. However, the release rate is somewhat decreased for the INET capsule. This is probably due to its lower temperature and thus slower diffusion process.

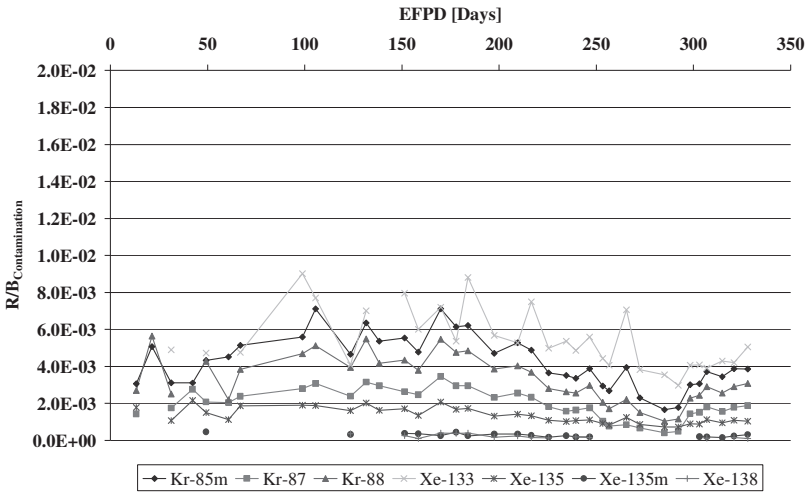


Fig. 2.17: Contamination Release over Birth vs. EFPD for INET capsule.

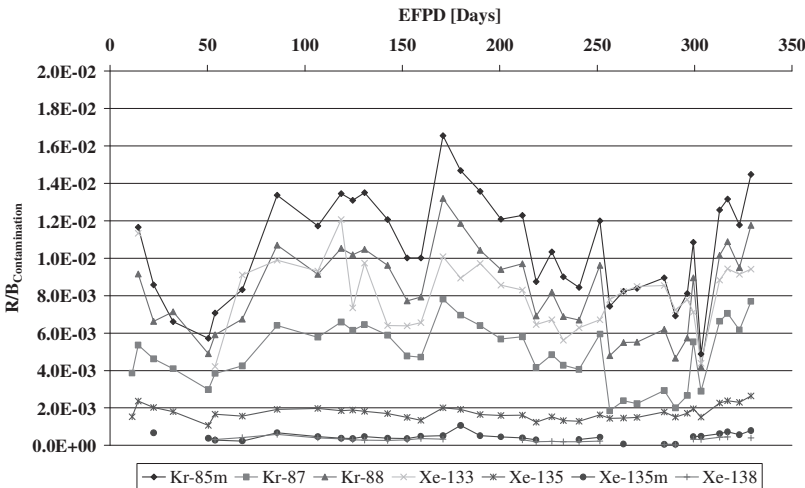


Fig. 2.18: Contamination Release over Birth vs. EFPD for AVR capsule.

This method enables the Release over Birth vs. EFPD graphs **for contamination** to be determined. Fig. 2.17 and Fig. 2.18 display these curves for the different fission products monitored and for the two capsules.

Relationship between capsules: The first observation concerns the trends: Contamination induced R/B curves remain quite flat over time, which indicates a steady diffusion process. This is consistent with the irradiation goal of constant temperatures (and thus diffusion) throughout the irradiation.

Temperatures also explain the higher R/B value in the AVR capsule: The three AVR pebbles were set at a surface temperature of 950°C, while INET pebbles reached only 860°C and 940°C. This affects the diffusion process and the release over birth ratios, leading to higher R/B values for AVR pebbles vs. INET ones.

Relationship between isotopes: If one can clearly see the good correlation between the different isotopes, with similar curve shapes, there is also a good correlation between R/B amplitudes and the isotope half-lives. Longer half-life leads to less decay during the diffusion process, higher release and therefore higher R/B ratios.

Overall, graphite contamination R/Bs in the range of 6E-3 to 1.4E-2 corroborate previous observations [114]. This further suggests that part (if not all) of the release measured is a result of graphite contamination. This requires confirmation by graphite chemical analysis. This may lead to a chronic radioactivity release from HTRs. An action to limit this release is to improve graphite purity.

2.8.4 Discussion on uncertainty

Releases: Due to the error of γ -spectrometry, the release ranges in an interval of -7.7% to +1.5% for ^{85m}Kr at the sampling time considered (i.e. at 327.9 EFPD for INET and 328.9 EFPD for AVR capsules). However, the origin of this release is still unclear: It can be attributed either to the fuel or to the graphite contamination (matrix and sample holder). Since pebbles account for approx. 50% of the capsules' graphite content, pebble release varies between 46.15% (half of 92.3% of the release measured, halving due to pebble/capsule volume ratio) and 101.5% (release measured + 1.5% error on the measurement) of the measured release.

Table 2.7 shows release measured for both capsules and the limits estimated according to the method developed previously.

Table 2.7: Release measurements and estimates.

Release [at/s]	Measured		Low estimate		High estimate	
	INET	AVR	INET	AVR	INET	AVR
^{85m} Kr	29387	294782	13562	136042	29828	299203
⁸⁷ Kr	25366	277810	11706	128209	25746	281977
⁸⁸ Kr	54009	554299	24925	255809	54819	562614
¹³³ Xe	152659	739530	70452	341293	154949	750623
¹³⁵ Xe	25173	165451	11617	76345	25550	167933
^{135m} Xe	2514	16263	1160	7506	2551	16507
¹³⁸ Xe	2336	25944	1078	11973	2371	26333

Birth rates and burn-ups: The precision of these two parameters is mostly due to the number of neutrons sampled with the Monte-Carlo method. This can be improved by simply investing in CPU time. For this study, as with the OCTOPUS calculations, 10^7 neutrons were sampled, leading to a 3σ -precision of 0.6% on the fresh fuel fission rates (precision on the burn-ups is not available with MCB).

Improving accuracy requires, however, some understanding of the phenomena to be modelled. By updating the perturbed flux according to the irradiation history, such as performed in [110], accuracy should be improved. Assuming the values with updated fluence as true value, Table 2.8 displays the accuracy ranges of birth rates and burn-ups. For birth rates, the 3σ -precision was also included.

Table 2.8: Comparison of pre and post-irradiation birth rates and burn-ups.

Capsule Calculation	INET		AVR	
	Pre (-3σ)	Post ($+3\sigma$)	Pre (-3σ)	Post ($+3\sigma$)
Birth rates [at/s]				
^{85m} Kr	7.80E+11	1.04E+12	1.62E+12	1.98E+12
⁸⁷ Kr	1.48E+12	1.96E+12	3.04E+12	3.69E+12
⁸⁸ Kr	2.01E+12	2.67E+12	4.14E+12	5.01E+12
¹³³ Xe	4.51E+12	6.22E+12	9.99E+12	1.29E+13
¹³⁵ Xe	3.70E+12	5.10E+12	8.20E+12	1.06E+13
^{135m} Xe	8.98E+11	1.25E+12	2.03E+12	2.66E+12
¹³⁸ Xe	4.17E+12	5.70E+12	9.08E+12	1.16E+13
Burn-ups [% FIMA]				
Burn-ups	7.7	9.5	10.5	12.4

Based on data from Table 2.7 and Table 2.8, uncertainty on ^{85m}Kr R/B vs. burn-up graphs is displayed in Fig. 2.19 and Fig. 2.20.

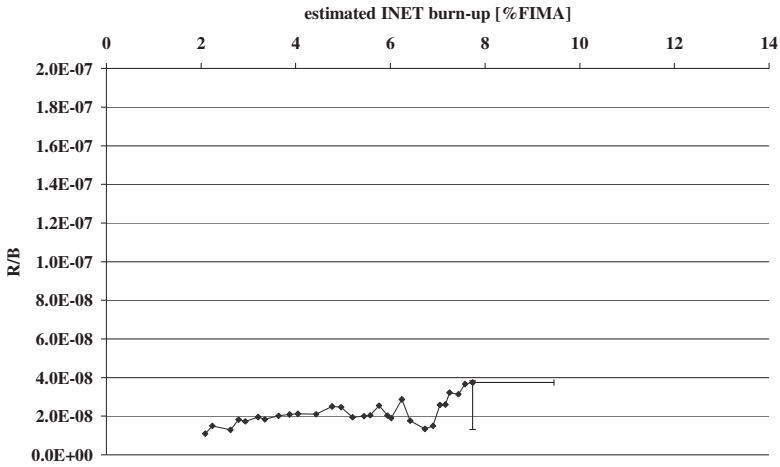


Fig. 2.19: Uncertainty of ^{85m}Kr Release over Birth vs. burn-up for INET capsule.

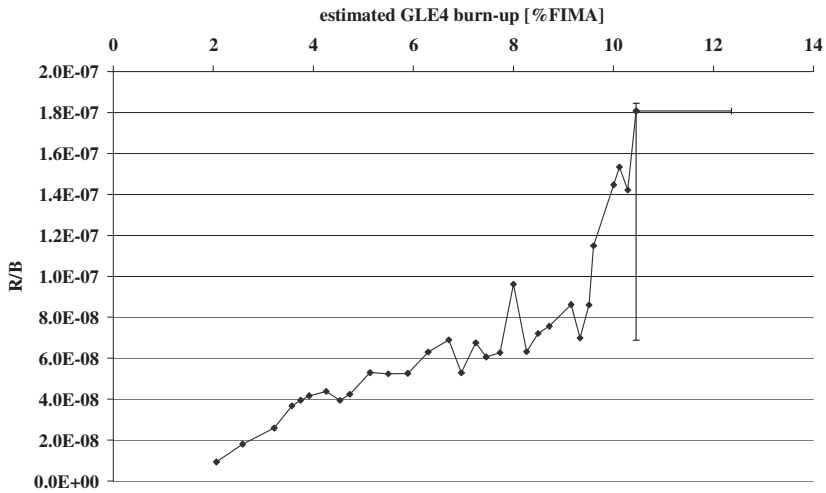


Fig. 2.20: Uncertainty of ^{85m}Kr Release over Birth vs. burn-up for AVR capsule.

2.9 Conclusions

After the completion of HFR-EU1bis in 2005, HFR-EU1 investigates higher burn-up tolerance of existing German pebbles and of newly produced Chinese fuel. The

aims of this fuel irradiation were twofold: 1- investigate fuel behaviour under irradiation condition, 2- provide high burn-up fuels for KÜFA tests, both aspects being required for the qualification of HTR fuels.

The investigation of fuel behaviour under irradiation condition was achieved by means of Release over Births vs. Burn-ups curves. Such curves display the retention capacity of the coated particles, which acts, in HTR, as primary containment. In other words, a flat curve suggests a steady diffusion process across the particles' coatings while a step-wise increase indicates particles' failure.

Curves however displayed increases, while remaining consistent with previous experiments (during which no failure of 'near-to-production' particles have been monitored). The assumption that the release measured might arise from graphite contamination has therefore been investigated and confirmed.

In addition, burn-ups were (unlike previous experiments) estimated by neutronic simulations. Therefore, the neutronic modelling of the experiment has been further investigated:

1- By comparison with NRG results, a different code has been qualified for the determination of birth rates and burn-ups.

2- With this new tool, the neutronic parameters have been updated, taking into account information from the experiment history.

These indicated that the cumulated thermal fluence should be raised from $21.8\text{E}+24 \text{ m}^{-2}$ (initially assumed) to $27.4\text{E}+24 \text{ m}^{-2}$, significantly impacting estimated burn-ups: The 26% increase in thermal fluence lead to a consistent 18 % to 23% burn-up increase for the most and least burned pebbles, respectively.

These burn-up increases, also coupled to birth rates increases, lowered the R/B values and flattened R/B vs. Burn-up curves.

Based on the investigations conducted, uncertainties on the release, the birth-rates and burn-ups were determined and displayed on R/B vs. Burn-up curves. These uncertainties do not change the outcomes of the experiment: 12 irradiation cycles, for approx. 333 EFPD, have been completed with low fission product release. R/B of approx. $4\text{E}-8$ and $1.8\text{E}-7$ for INET and AVR fuels respectively indicate that no particle failure occurred.

On hold since 24 February 2008 due to massive thermocouple failure, the continuation of the experiment is subject to a safety demonstration with less than the initially approved instrumentation.

After finalization of the irradiation test, extensive PIE is planned (at NRG Petten [115] and JRC-ITU in Karlsruhe) including KÜFA tests [22].

3 Revisiting the concept of Wallpaper fuel

The content of this chapter has been published in two papers. The first one [116] serves as feasibility study of wallpaper fuels, while [117] shows the fuel cycle investigations and the particle failure probabilities.

3.1 Introduction

Invented by Professor Dr. Rudolf Schulten [7] in the 1950s and developed in Germany in the 1970s, High Temperature Reactors feature several important inherent and passive safety characteristics, namely:

- The high graphite inventory in the core provides significant thermal inertia. Graphite also has a high thermal conductivity, which facilitates the transfer of heat to the reflector, and it can withstand high temperatures.
- The strongly negative power reactivity coefficient gives a negative feedback, such that the reactor shuts down by itself in overpower accidental conditions.
- The high quality of fuel elements – tri-isotropic (TRISO) coated particles – minimizes operational and accidental fission gas release. The selected materials exhibit good mechanical resistance and fission product retention capability at high temperatures.
- The low power density in combination with high thermal inertia and passive decay heat removal capability enables keeping the core temperature within safe boundaries, even in case of accidents such as loss-of-coolant accident.
- Together, the aforementioned aspects prevent massive release of fission products in the case of an accident. Specifically, core melt downs are excluded by natural phenomena.

Together, the aforementioned aspects prevent massive release of fission products in the case of a loss of coolant incident.

Other key features beneficial to the HTR are its high outlet temperature, suitable for process heat production [99] and high thermal efficiency, and its versatile fuel cycles (good fuel use by high burn-up, waste reduction through MA management, suitability for Th-U fuel cycle) [61]. The abovementioned aspects make HTR suitable for advanced applications, in compliance with the Generation IV International Forum objectives.

Since this reactor design has been investigated over at least three decades, the concept is mature and generates international interest: China and South Africa (up to 2009) are heavily involved in the development of their own HTR technology. In both cases, the fuel is based on a homogeneous distribution of coated particles

within a fuel pebble. This homogenizes power distribution, leading to a radial temperature gradient across the fuel sphere. Particles placed in its centre have the highest temperature. Reducing the temperatures of TRISO particles would further enhance their integrity as the first barrier against fission product release.

Already in the 1970s [118], attempts were made to reduce the peak fuel temperature by so-called “wallpaper fuel”, in which the fuel is arranged in a spherical shell within a pebble. At that time, the production process was not sufficiently mature and had caused unacceptable damage to the (less performing) BISO particles: Under irradiation conditions in the DRAGON reactor, the severe shrinkage of carbon (coke) - used as a synthetic resin to bind particles - tore off the outer PyC layer of particles. For this reason, this fundamentally promising concept has been discarded [7]. As particle and pebble production processes have improved since the 1970s, this issue is expected to be resolved.

This chapter further exploits the “wallpaper concept”, not only with a view to temperature reduction but also for enhanced neutronic performance through improvement of the neutron economy, allowing reduction of enrichment needs and fissile material inventories, and possibly achieving higher burn-up. Parameters optimized in the analyses were the particle packing fraction and the density of the central fuel-free graphite. The use of graphite with higher density (2.1 g/cm^3) was investigated, as this design change improves neutron economy as well as thermal inertia of the reactor, impacting the peak temperature in the event of a depressurized loss-of-coolant accident (DLOCA).

3.2 Re-visiting “wallpaper” fuel

A wallpaper fuel was originally developed by Teuchert [118] in the 1970s so as to lower particle temperatures. By placing particles in a spherical shell, closer to the surface of the pebble, as shown in Fig. 3.1, avoids positioning fuel particles in the central part of the pebble, where the temperature is highest. This lowers both peak and average temperatures of fuel particles, consequently decreasing the probability of failure and fission gas release.

Since the particle packing fraction of a PBMR pebble is relatively low compared to HTTR compacts [119] (9.34% vs. 30% for the compacts), condensing them within a layered fuel zone is thought feasible and would create a central fuel-free zone. Assuming a 30% packing fraction applied to a pebble, the maximum radius of this central fuel free zone can be estimated at approx. 2.21 cm.

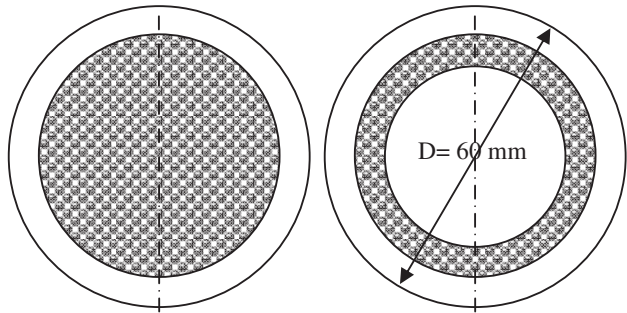


Fig. 3.1: Classic and “wallpaper design” of HTR pebbles.

3.3 Method

3.3.1 Design specifications of the different pebbles investigated

In addition to the modification brought about by the wallpaper fuel, increasing the density of the central fuel free zone offers the possibility of obtaining an even more thermalized neutron flux. In PBMR pebbles, the matrix graphite density (1.75 g/cm^3) is limited by other constraints imposed on the material - it is supposed to fix particles, remove their power and also exhibit good isotropy. The latter characteristic is important and has to be maintained in order to avoid temperature gradient-induced stress formations in the pebble during its lifetime. Alleviating the thermal issue (power peaking) allows graphite with a higher density, for instance up to 2.1 g/cm^3 , to be considered, as described in [120]. Finally, since modifications suggested so far (fuel-free central zone, higher graphite density) are intended to improve the neutronics of the reactor, it would also be possible to decrease fuel enrichment as a means of compensation, i.e. design a wallpaper pebble with reduced enrichment. This would have beneficial impacts on fuel manufacturing costs with lower fissile material requirements. Table 3.1 presents the characteristics of the four pebbles compared throughout this study and depicted in Fig. 3.2.

Table 3.1: Characteristics of the four pebble types investigated.

Fuel type	PBMR	Wallpaper Variant 1	Wallpaper Variant 2	Wallpaper Variant 3
Number of particles	15000	15000	15000	15000
Enrichment [^{235}U wt.%]	9.6%	9.6%	9.6%	< 9.6%
Graphite density [g/cm^3]	1.75	1.75	2.1	2.1
Particle packing fraction	9.34%	30%	30%	30%
Dis. Burn-up [MWd/kg]	90	90	> 90	90

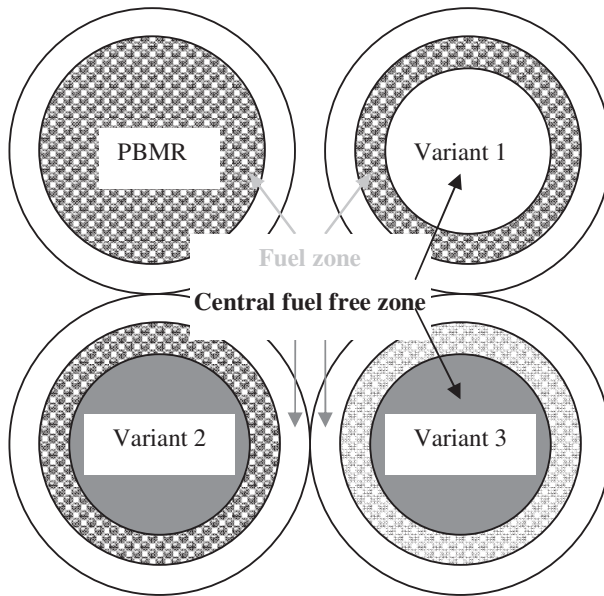


Fig. 3.2: Sketch of the four pebbles investigated.

3.3.2 Description of computational tools

Besides a reduction in temperature, modifications also have a significant impact on core neutronics: For this reason, the four pebbles specified in Fig. 3.2 were compared in full core simulations to determine the effects of fuel modifications on reactivity, spent fuel composition and the safety features of the reactor. Comparison between the PBMR pebble and variant 1 allow conclusions to be drawn regarding the impact of creation of the fuel free zone, between variant 1 and 2 regarding the increase of graphite density and between variant 2 and 3 concerning the influence of fuel enrichment.

The core model of the MCNP/MCB simulations – used for first estimate of neutron multiplication and spent fuel composition – was significantly simplified. Only the pebble bed, composed of fresh fuel, surrounded by pure graphite reflectors was modelled. MCB [111] is a general-purpose Monte Carlo Continuous-Energy Burn-up code used to calculate evolution of nuclide density over time with burn-up or decay.

The code integrates MCNP, version 4C, [108] which is used to calculate neutron transport, and a novel Transmutation Trajectory Analysis code (TTA), which is used for calculating density evolution, including formation and analysis of the transmutation chain. Thus, it includes eigenvalue calculations, as well as neutron transport calculations in fixed source mode or k-code mode to obtain the reaction rates and energy deposition that are necessary for calculating burn-up. MCB is

compatible with MCNP and preserves its structure: Complete burn-up calculations can be made in one single run, involving minor modifications to an MCNP input file.

The PANTHERMIX [121] code system, developed at NRG, performs core physics analyses of HTRs. Based on the WIMS [122] lattice code (Serco Assurance, UK), the 3-D steady-state and transient core physics code PANTHER [123] (British Energy, UK) and the 2-D R-Z HTR thermal hydraulics code THERMIX-DIREKT [124] (Research Centre FZJ Jülich, Germany), PANTHERMIX enables, among others, core characterization during steady-state operation (determination of the equilibrium core of a continuous reload pebble bed reactor) and transients (De/Pressurized Loss of Forced Cooling Accidents). The core model used throughout this study corresponds to the PBMR 400MW as defined in the “OECD 400MW benchmark” [125]. The use of wallpaper fuels required only minor code modifications, such as material database generation and temperature gradient across the fuel elements.

The optimisation of HTR fuel designs can be achieved by evaluating the failure fraction of TRISO coated fuel particles. For this purpose, a stress analysis code called CRYSTAL (Code foR analYsis of STress in coAted particLes) [126] [127] was developed at TU-Delft. This code describes the mechanical behaviour of TRISO particles during irradiation and aims at calculating the failure probability of coated particle fuel. CRYSTAL is a one-dimensional analytical and multi-layer model that takes into account the visco-elastic behaviour of the coating layers and the surrounding graphite during irradiation. The main source of stress in all layers is due to the pressure build-up from the gaseous fission products in the buffer layer. Moreover, the Pyrocarbon layers exhibit irradiation-induced dimensional changes and creep (in the radial and tangential directions). Finally, the model allows simulating thermal expansion of all layers.

The required inputs for CRYSTAL (known as pebble histories) are provided by a neutronic, fuel depletion and thermal-hydraulics code system, in our case PANTHERMIX. PANTHERMIX delivers the fuel temperature, fast neutron flux, burn-up and power density profiles. This set of parameters describing pebble characteristics over its in-core lifetime corresponds to one history. Once all equilibrium profiles have been calculated for normal operating conditions in a given reactor core, the TRISO particle failure fraction can be calculated. CRYSTAL can also evaluate the effect of varying the fuel kernel size and the thicknesses of the various coating layers surrounding the fuel kernel, the actinide density in the fuel kernel, the concentration of TRISO fuel particles in a pebble, and the pebble flow velocity in the reactor core.

The use of CRYSTAL with PANTHERMIX for our purposes required interfacing. This allowed improvement of accuracy and versatility of the code. Steady-states parameters could then be supplied for several radial zones, which enabled the sampling of different pebble routes through the core.

3.3.3 Description of the approach

Several modifications to core neutronics are expected, due to different phenomena:

- HTRs, with stochastic particle distribution within pebbles and pebbles within the core, are presented as heterogeneous. By packing particles in a thinner fuel layer, lumping of the fuel is enhanced, which decreases resonance absorption. In other words, raising the particle packing fraction within a smaller fuel zone increases the Dancoff factor. This should raise the neutron resonance escape probability, also contributing to reactivity increase.
- Graphite density increase tends to modify the moderator-to-fuel ratio. This impacts the neutron spectrum: A spectral shift towards thermal energy is expected.

To understand the different phenomena, the neutron multiplication factor was dissociated with MCNP in the five factor-formula (Leakage probability is usually also dissociated in fast and thermal ones. But since the code discards neutrons reaching reactor boundaries without taking into account their energy, a global leakage probability is directly available). This requires neutron absorption rates to be volume averaged over the core structural materials and fuel volumes. For the fuel, fission and neutron production rates are also required. These reaction rates were calculated for the different energy groups (boundaries of $0 - 0.625 - 6.74\text{E}4 - 1.35\text{E}6 - 1.96\text{E}7$ eV for the thermal to fast groups respectively), setting the thermal energy limit (required for the calculation of η , f , ϵ and p) to 0.625 eV.

This innovative study, when performed with MCNP, was enabled by the code input structure, where elements were defined once and then duplicated. This limits the number of tallies to two per material.

3.4 Results of Full core simulations with the Monte-Carlo Method

3.4.1 Criticality and the six factor formula

The effective neutron multiplication factor can be defined as the product of the six following parameters [54]:

- η is the reproduction factor,
- f represents the thermal utilization of the reactor,
- ϵ is the fast fission factor,
- p stands for the resonance escape probability,
- p_{FNL} and p_{TNL} are the probabilities that a fast/thermal neutron will not leak out of the system.

Table 3.2 displays the results of the MCNP simulations for the determination of the five factors and associated standard deviations.

Table 3.2: Six factor formula and criticality calculated in MCNP.

Fuel type	PBMR	Variant 1	Variant 2	Variant 3	Stand.dev.
Enrichment [²³⁵ U wt.%]	9.6%	9.6%	9.6%	9.0%	-
η	1.9749	1.9748	1.9749	1.9693	< 0.24%
f	0.8694	0.8699	0.8716	0.8676	< 0.02%
ϵ	1.1008	1.1009	1.0958	1.0911	< 0.12%
p	0.7417	0.7460	0.7545	0.7566	< 0.11%
P_{NL}	0.9336	0.9337	0.9358	0.9350	< 0.03%
k_{eff} tally	1.309	1.317	1.332	1.319	< 0.33%
k_{eff} track length	1.309	1.318	1.332	1.319	< 0.062%

By means of MCNP calculation, $P_{NL} = P_{FNL} \cdot P_{TNL}$ is directly available, while η , f, ϵ and p require tallies and multipliers.

The first observation is the good correlation between the neutron multiplication factor determined by the six factor formula (k_{eff} tally) and the corresponding MCNP value (k_{eff} track length). This, coupled with the high precision of the calculation, provides high confidence in the six factor values and enables the following interpretations to be made. From Table 3.2, we observe that the increase in k_{eff} (from 1.309 to 1.332) is about 1750 pcm. This is due to the mutual interplay of several effects:

- η is impacted by the enrichment decrease, which obviously decreases neutron production per absorption in the fuel. However, the changes are small and within the standard deviation of our Monte Carlo calculations.
- f denotes the competition between neutron absorption in the fuel and other materials. The value is increased by the creation of the fuel free zone (heterogeneities) and the higher graphite density (moderation increase), while a fuel enrichment drop reduces f (related to the predominant impact of fuel absorption on f).
- ϵ is raised slightly by the creation of a fuel free zone, leading to a higher average neutron energy in the fuel zone. Likewise, it falls with higher graphite density or lower enrichment (cf. Table 3.5).
- p is increased throughout these comparisons due to heterogeneities (from the creation of a fuel free zone and its density increase) and a decrease in enrichment. This can be linked to the decrease of parasitic capture in ²³⁵U, which is not fully offset by an increase of parasitic capture in ²³⁸U in the region above 0.625 eV (cf. Table 3.5).
- Variations of P_{NL} are related to the fast neutron flux, which is the main cause of leakage (cf. Table 3.4).

Several phenomena account for the effects displayed here:

3.4.2 Heterogeneities

Heterogeneity (separation of moderator and fuel) improves neutron economy in the reactor [51]. Due to heterogeneity between fuel and moderator zones, there is a higher probability for a neutron to be moderated before entering a second fuel zone, where it has a higher probability of producing fission (i.e. the probability for neutron capture in the resonance region of ^{238}U decreases).

Owing to the wallpaper design of the fuel pebble, neutron economy in the reactor is improved, which also results in higher neutron multiplication. Heterogeneity reduces the neutron capture probability p and neutrons are therefore further moderated (cf. ϵ in Table 3.2).

3.4.3 Moderator/Fuel ratio

According to [54] the ratio of moderator volume to fuel volume in a fuel cell characterizes the effectiveness of neutron moderation in the core. This is true for homogenized lattice cells. For heterogeneous fuel cells, account also has to be taken of the spatial distribution, as shown by the comparison between PBMR fuel and variant 1 in Table 3.3.

Table 3.3: *Effect of moderator/fuel ratio and heterogeneities on neutron multiplication.*

Fuel type	PBMR	Variant 1	Variant 2	Variant 3
k_{eff} at 0s [-]	1.309	1.318	1.331	1.319
σ	0.058%	0.060%	0.060%	0.062%
Frac. of $^{12}\text{C}/^{235}\text{U}$ in fuel [-]	1.79E+02	1.79E+02	1.98E+02	2.11E+02

Pebbles are deliberately designed to be under-moderated: Due to fuel depletion, neutrons have more collisions before being absorbed (moderation increases), somehow compensating for fission product poisoning. By raising the fuel free zone graphite density (by 20%), the moderator-to-fuel mass ratio in a fuel cell is also raised (by 11%), improving neutron multiplication (cf. comparison between variants 1 and 2 in Table 3.3).

3.4.4 Neutron spectrum modification

As a result of geometry and materials modifications, the neutron spectrum also changes. Table 3.4 displays the neutron flux in TRISO particles averaged over the core.

Note a decrease of flux in the energy range of 0.625 - 6.74E4 eV which, together with higher p values, indicates enhanced down-scattering of neutrons in graphite to energies below pronounced ^{238}U resonances.

Table 3.4: Neutron fluxes for the pebble design variants.

Fuel type	PBMR	Variant 1	Variant 2	Variant 3
Energy group	Averaged neutron flux on kernels [$/\text{cm}^2/\text{s}$]			
Thermal	5.767E+13	5.773E+13	5.785E+13	6.180E+13
Lower epithermal	5.799E+13	5.784E+13	5.472E+13	5.549E+13
Higher epithermal	2.271E+13	2.265E+13	2.116E+13	2.139E+13
Fast	8.081E+12	8.166E+12	7.649E+12	7.730E+12
Total	1.464E+14	1.464E+14	1.414E+14	1.464E+14

To further demonstrate the spectral shift to thermal energy, Table 3.5 presents energy dependent reaction rates and the Averaged Neutron Energy (ANE) calculated by MCNP.

Table 3.5: UO_2 reaction rates and average neutron energy.

Fuel type	PBMR	Variant 1	Variant 2	Variant 3
Energy group	Fission rate UO_2 [fis./particle/s]			
Thermal	1.85E+09	1.85E+09	1.86E+09	1.87E+09
Lower epithermal	1.75E+08	1.75E+08	1.67E+08	1.60E+08
Higher epithermal	4.53E+06	4.52E+06	4.23E+06	4.02E+06
Fast	6.83E+08	6.91E+08	6.47E+08	6.49E+08
Total	2.04E+09	2.04E+09	2.04E+09	2.04E+09
Energy group	Capture rate UO_2 [abs./particle/s]			
Thermal	4.32E+08	4.33E+08	4.34E+08	4.43E+08
Lower epithermal	7.04E+08	6.83E+08	6.55E+08	6.63E+08
Higher epithermal	5.00E+06	4.99E+06	4.66E+06	4.69E+06
Fast	7.97E+05	8.06E+05	7.55E+05	7.61E+05
Total	1.14E+09	1.12E+09	1.09E+09	1.11E+09
ANE [MeV]	1.85E-04	1.85E-04	1.73E-04	1.64E-04

As expected, p is influenced by the decrease in the resonance capture cross-section, while ϵ follows the trend of the averaged neutron energy. Both are increased by the creation of the fuel-free zone, and decrease when graphite density is raised. The use of denser graphite means even more thermalised spectrum than in variant 1, which decreases ^{238}U capture rate and MA build-up even further. Finally, a drop in enrichment reduces the probability of neutron absorption leading to fission of ^{235}U (η). With a constant power density, and thus fission rate, this change raises all parts of the spectrum, but with a higher impact on the thermal one. This thermal shift confirms the higher moderation achieved by neutrons, although this is also accompanied by a higher ^{238}U capture rate, which leads to higher MA build-up.

3.4.5 Dancoff factor

Besides the neutron spectrum, heterogeneity also influences the Dancoff factors. The switch from PBMR to wallpaper fuel requires a modification of geometry, i.e. particles are packed more densely in a shell layer. This increases the probability of a neutron to jump from one kernel to another without interactions in-between with the moderator. The Dancoff factor is actually the sum of two separate factors [128]:

- The intra-pebble Dancoff factor is calculated as the infinite medium Dancoff factor corrected for the probability that neutrons may leak from the fuel zone of a pebble to the moderator shell without interaction.
- The inter-pebble Dancoff factor takes into account the probability that these escaping neutrons may enter a fuel kernel in another pebble, either a neighbouring one or one that is further away.

Since the diameter of the central fuel-free zone is of the order of magnitude of one neutron mean free path in graphite, the use of a wallpaper fuel increases the intra-pebble Dancoff factor. The same applies to the inter-pebble Dancoff factor, as the fuel zones of two adjacent pebbles are closer. The Dancoff factors, calculated with a modified version of PEBDAN [128], are available in Table 3.6:

Table 3.6: *Dancoff factor for PBMR and wallpaper fuels calculated with a modified version of PEBDAN [128].*

PBMR	Variant 1	Variant 2
0.420	0.589	0.590

As an increase in the Dancoff factor is related to an increase in the resonance escape probability (cf. p in Table 3.2), this leads to increased neutron multiplication. This fact is corroborated by a decrease in the lower epithermal flux, indicating higher fuel self-shielding, as seen in Table 3.4.

3.4.6 Conversion ratio

The conversion ratio for the different fuel loading was calculated by checking respectively the capture and fission rates of the fertile or fissile actinides (fertile: ^{238}U and ^{240}Pu , fissile: ^{235}U , ^{239}Pu and ^{241}Pu) as displayed in Table 3.7.

$$CR = \frac{\text{Neutron capture rates of } ^{238}\text{U} \text{ and } ^{240}\text{Pu}}{\text{Neutron absorption rates of } ^{235}\text{U}, ^{239}\text{Pu} \text{ and } ^{241}\text{Pu}}$$

The length of the fuel cycle was 915.3 days to reach the 90 MWd/kg_U with a reactor power of 400 MW_{th}.

Table 3.7: Conversion ratio for the different fuel loadings.

Fuel type	PBMR	Variant 1	Variant 2	Variant 3
CR at BOI [-]	0.288	0.280	0.272	0.280
CR at EOI [-]	0.653	0.652	0.654	0.690

This confirms the possibility to decrease MA build-up: By increasing heterogeneity, either with pebble geometry or the material modifications (comparison of PBMR fuel with variant 1 and 2), the conversion ratio drops by a few percents for fresh fuel while it remains high for the depleted ones.

This also shows (by comparing variant 2 and 3) a significant increase in conversion ratio, improving conversion capacity of HTR, also referred to as advanced converter reactors, as well as slightly enhancing sustainability of this reactor concept.

Table 3.8 displays fuel burn-up characteristics, including production/destruction rates of actinide isotopes. It can be seen that heterogeneity reduces MA build-up, while increasing ^{235}U consumption. On the contrary, a lower enrichment decreases significantly ^{235}U consumption as bred fissile isotopes also contribute to fissions. The evidence for this is a lower ^{239}Pu concentration and a higher ^{240}Pu concentration. This corroborates calculations of the conversion ratio.

Table 3.8: Fuel composition evolution through burn-up [g/TWh_{th}].

Fuel type	PBMR	Variant 1	Variant 2	Variant 3
k_{eff} at EOI [-]	0.879	0.882	0.887	0.861
σ	0.052%	0.053%	0.051%	0.056%
^{235}U cons.	3.41E+04	3.42E+04	3.43E+04	3.32E+04
^{239}Pu prod.	2.35E+03	2.25E+03	2.14E+03	2.04E+03
^{240}Pu prod.	1.83E+03	1.78E+03	1.74E+03	1.75E+03
^{241}Pu prod.	1.15E+03	1.10E+03	1.05E+03	1.03E+03
^{241}Am prod.	1.87E+01	1.77E+01	1.65E+01	1.54E+01

In fact, in variant 3 only 40.9 % of total power at the end of life is due to fission of ^{235}U , while the corresponding figure for variant 1 is 43.4%. Table 3.9 shows the distribution of fission power between isotopes leading to fissions for each fuel variant after fuel ageing.

Table 3.9: Fission power from isotopes leading to fissions.

Fuel type	PBMR	Variant 1	Variant 2	Variant 3
%FP ^{235}U [-]	42.70%	43.44%	44.35%	40.89%
%FP ^{238}U [-]	0.50%	0.52%	0.51%	0.53%
%FP ^{239}Pu [-]	40.73%	40.14%	39.45%	41.64%
%FP ^{241}Pu [-]	16.08%	15.91%	15.70%	16.94%

3.4.7 Temperature coefficient of reactivity

The Doppler effect contributes to the inherent safety of all reactors, but this assertion is even more valid for HTRs. In HTRs, a negative reactivity feedback, introduced by a broadening of neutron absorption resonances following temperature excursion, can induce a reactor to safe shut-down (simulation of the loss of coolant accident with the AVR reactor [7] and transient tests at the HTR-10 reactor [129]). The Doppler feedback can be estimated by simulating the same reactor and fuel at different temperatures and studying the resulting variations in k_{eff} .

Table 3.10 displays the effective neutron multiplication coefficient calculated in MCNP (1 σ standard deviation below 0.066%) and the fuel temperature coefficient of reactivity CT_F .

Table 3.10: Neutron multiplication vs. fuel temperature and CT_F .

Fuel type	PBMR	Variant 1	Variant 2	Variant 3
k_{eff} at 300 K	1.367	1.372	1.387	1.373
k_{eff} at 1800 K	1.287	1.295	1.311	1.297
CT_F [pcm/K]	-3.04	-2.90	-2.79	-2.82

CT was calculated with k_{eff} values corresponding to the change of fuel temperature (not density) from 300 to 1800 K using the formula from [54]:

$$CT = \frac{\Delta \rho}{\Delta T}$$

The drop in CT_F between PBMR fuel, variants 1 and 2 is caused by higher moderation: Table 3.2 displays the resonance escape probability. This reveals a decrease in neutrons available for absorption in the resonance range. The increase between variants 2 and 3 is a direct result of the increase in ^{238}U concentration (or decrease in ^{235}U enrichment). A different trend is observed when raising the graphite temperature (cf. Table 3.11).

Table 3.11: Neutron multiplication vs. graphite temperature and CT_G .

Fuel type	PBMR	Variant 1	Variant 2	Variant 3
k_{eff} at 300 K	1.320	1.327	1.343	1.334
k_{eff} at 1800 K	1.293	1.302	1.314	1.302
CT_G [pcm/K]	-1.03	-0.96	-1.11	-1.26

According to [54], the primary reactivity effect for solid moderated cores is due to the hardening of the thermal neutron spectrum with increasing temperature, as shown in Table 3.12, which modifies the thermal group constants.

Table 3.12: *Thermal flux [$/\text{cm}^2/\text{s}$] vs. graphite temperature.*

Fuel type	PBMR	Variant 1	Variant 2	Variant 3
Thermal flux at 300 K	3.62E+10	3.62E+10	3.61E+10	3.83E+10
Thermal flux at 1800 K	6.68E+10	6.68E+10	6.70E+10	7.17E+10

Table 3.10 and Table 3.11 show that fuel changes introduced in this study modify the effects of temperature on reactivity change. For Variant 2 and 3, the different effects tend to mitigate themselves. For this reason, a joint (fuel and graphite) coefficient of reactivity was calculated, as shown by Table 3.13 for BOI and Table 3.14 for EOI.

Table 3.13: *Neutron multiplication vs. graphite temperature and CT_{FG} at BOI.*

Fuel type	PBMR	Variant 1	Variant 2	Variant 3
keff at 300 K	1.378	1.382	1.399	1.387
keff at 1800 K	1.272	1.280	1.294	1.281
CT_{FG} [pcm/K]	-4.06	-3.84	-3.88	-4.01

Table 3.14: *Neutron multiplication vs. graphite temperature and CT_{FG} at EOI.*

Fuel type	PBMR	Variant 1	Variant 2	Variant 3
keff at 300 K	0.862	0.862	0.868	0.830
keff at 1800 K	0.768	0.770	0.777	0.748
CT_{FG} [pcm/K]	-9.38	-9.18	-9.01	-8.87

Reactivity effect is clearly a function of the fuel type and burn-up. For all three variants, this leads to somewhat decreased margins on decay heat removal due to a slower reactor shut-down. Variations are however small when compared to the evolution of core composition from BOI to EOI.

Furthermore, since the initial target of the wallpaper fuel was to reduce particle temperature and to achieve higher burn-up while keeping the reactor critical – effects which are not taken into account here – further investigations need to be conducted with deterministic codes such as PANTHERMIX [121].

3.5 Neutronic Thermal-Hydraulic and Safety Analysis

3.5.1 Fuel cycle studies of start-up cores with PANTHERMIX

Database generation with WIMS

Simulations performed with WIMS enable the inventory of depleted fuel to be determined. Table 3.15 presents the atomic density of ^{235}U and several transuranics (TRUs) before and after the fuel depletion process. The discharge burn-up selected for this study was 90 MWd/kg, which corresponds to the “OECD 400MW benchmark” target. The composition of the variant 3 fuel depends on its enrichment, which will be determined later, based on reactivity increase between steady-states of PBMR and variant 2 fueled cores. For this reason, the composition of variant 3 is not displayed in Table 3.15 and Table 3.16.

Table 3.15: ^{235}U and TRU atomic densities [at/m^3] at 0 and 90 MWd/kg.

Fuel type	PBMR	Variant 1	Variant 2
^{235}U BOL	1.19E+25	1.19E+25	1.19E+25
^{238}U BOL	1.11E+26	1.11E+26	1.11E+26
^{235}U EOL	3.32E+24	3.20E+24	3.01E+24
^{238}U EOL	1.04E+26	1.04E+26	1.05E+26
^{238}Pu EOL	4.36E+22	4.32E+22	4.02E+22
^{239}Pu EOL	1.02E+24	9.31E+23	8.01E+23
^{241}Pu EOL	4.69E+23	4.38E+23	3.88E+23
^{241}Am EOL	1.13E+22	9.47E+21	7.98E+21
^{242}Cm EOL	5.42E+23	5.24E+23	5.12E+23
^{244}Cm EOL	9.18E+21	9.17E+21	8.07E+21

Besides fissile isotopes, Table 3.15 also includes ^{238}Pu , ^{241}Am , ^{242}Cm and ^{244}Cm , key nuclides for the waste fuel decay heat, as well as neutron and gamma dose. Based on the figures of Table 3.15, ^{235}U consumption and TRU production (and destruction for negative values) rates can be deduced, as reported in Table 3.16.

Table 3.16: PBMR fuel integral actinide production/destruction rate in [$\text{g}/\text{TWh}_{\text{th}}$] and variations in comparison with the PBMR reference fuel for wallpaper fuels.

Fuel type	PBMR	Variant 1	Variant 2
^{235}U	-3.20E+04	1.4%	3.6%
^{238}U	-2.54E+04	-3.7%	-9.3%
^{238}Pu	1.64E+02	-0.9%	-7.6%
^{239}Pu	3.85E+03	-8.6%	-21.3%
^{241}Pu	2.06E+03	-3.4%	-5.7%
^{241}Am	1.79E+03	-6.5%	-17.2%
^{242}Cm	4.30E+01	-16.1%	-29.3%
^{244}Cm	3.54E+01	-0.2%	-12.1%

In comparison with PBMR fuel, Variant 1 displays a slight ^{235}U consumption increase, compensated by a decrease in most of the transuranics, including ^{241}Am . These trends are further pronounced when switching from variant 1 to variant 2, which corroborate the calculated decrease of the conversion ratio, as reported in [116].

Throughout the depletion process, WIMS determines the neutron multiplication in an infinite medium for individual pre-specified burn-up levels. Fig. 3.3 presents the values for the three pebbles.

Fig. 3.3 shows that reactivity burn-up swing of the wallpaper type of fuel is actually larger than for a PBMR type fuel, which is a consequence of the lower breeding potential of these fuels.

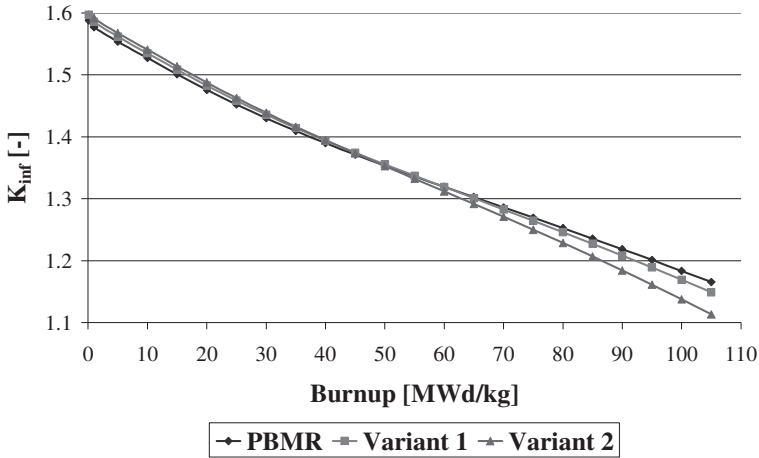


Fig. 3.3: Neutron multiplication in an infinite medium as function of burnup for the three different fuels.

Equilibrium calculations by coupling WIMS-PANTHER and THERMIX-DIREKT

Once the material database generation is completed by WIMS, the calculation procedure to determine the steady-states characteristics at equilibrium involves the following steps:

1. The core geometry is defined,
2. The core is filled with fresh fuel,
3. The material and geometry characteristics of the system corresponding to operating temperatures are calculated,
4. The code shuffles and reloads the fuel to achieve equilibrium.

The reloading/shuffling process leads to oscillations of the different parameters, such as the neutron multiplication factor, as shown in Fig. 3.4. Waiting for a correct stabilisation of the parameters would require extensive CPU time. It was therefore decided to extrapolate the equilibrium steady-states from the calculated conditions at the last three peaks of the oscillations.

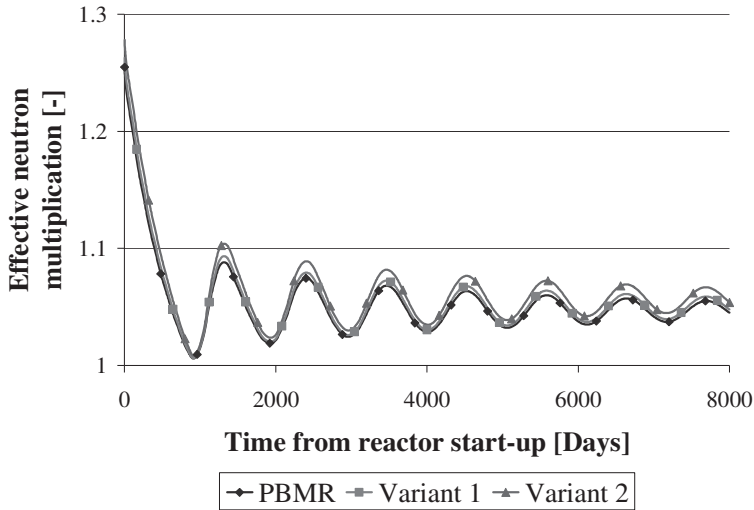


Fig. 3.4: Oscillations through the shuffling process.

Table 3.17 present characteristics of the extrapolated equilibrium core at steady-state filled with different types of fuels. When targeting the PBMR average discharge burn-up with fuel variant 1 and 2, one can notice a reactivity, up to +925 pcm in case of the high graphite density case. The average discharge burn-up is determined by the pebble discharge rate.

Table 3.17: Characteristics of the extrapolated equilibrium core at 90 MWd/kg.

Fuel type	PBMR	Variant 1	Variant 2
Max. graphite temp. [K]	1341.95	1286.43	1282.11
Average graphite temp. [K]	1041.16	1025.83	1033.41
Max. coolant temp. [K]	1267.38	1265.19	1262.91
Max. mesh power density [W/m ³]	1.30E+07	1.30E+07	1.32E+07
k_{eff} [-]	1.047	1.050	1.056
¹³⁵ Xe [at/m ³]	1.61E+20	1.58E+20	1.51E+20
N. of daily discharged pebbles [pebbles/d]	459.8	459.6	461.2
Average discharge burn-up [MWd/kg]	96.66	96.69	96.38

We note that the excess reactivity available during the approach to equilibrium could be used for MA incineration or fissile material breeding. These options were not investigated here. It was instead decided either to extend the discharge burn-up or to decrease the enrichment of the wallpaper type of fuel until k_{eff} matches that of the PBMR reference. Both options are used as compensation means to decrease the reactivity introduced by the two first fuel modifications. Results are displayed in Table 3.18, where variant 2 refers now to the extended burn-up version.

Table 3.18: *Characteristics of the extrapolated equilibrium core for modified wallpaper fuels.*

Fuel type	Variant 2	Variant 3
Enrichment [^{235}U wt. %]	9.6%	9.277%
Max. graphite temp. [K]	1281.80	1280.46
Average graphite temp. [K]	1031.47	1031.98
Max. coolant temp. [K]	1262.68	1261.67
Max. mesh power density [W/m^3]	1.33E+07	1.32E+07
k_{eff} [-]	1.047	1.047
^{135}Xe [at/m^3]	1.49E+20	1.46E+20
N. of daily discharged pebbles [pebbles/d]	438.8	461.0
Average discharge burn-up [MWd/kg]	101.3	96.42

The burn-up increase, introduced by the use of variant 2 of wallpaper fuel, is 5.01% while variant 3 displays an enrichment reduction from 9.6% to 9.277%. Both options tend to decrease the fuel cost and further improve the sustainability of the concept.

Based on the average discharge burn-up and the fuel data-base generation (WIMS output), one could retrieve the composition of the waste, as specified in Table 3.19. This indicates that higher moderation (either by geometry or material changes) leads to lower ^{235}U and TRU content in the spent fuel.

Based on the waste composition, effective destruction and production rates for the different actinides are calculated for the PBMR fuel. Table 3.20 also presents the variations in destruction/production rate of wallpaper fuels in comparison with the PBMR reference fuel.

Table 3.19: Burn-up [MWd/kg] and depleted fuel composition [at/m³].

Fuel type	PBMR	Variant 1	Variant 2	Variant 3
Burn-up	96.66	96.69	101.3	96.42
²³⁵ U BOL	1.19E+25	1.19E+25	1.19E+25	1.12E+25
²³⁸ U BOL	1.11E+26	1.11E+26	1.11E+26	1.11E+26
²³⁵ U EOL	2.95E+24	2.82E+24	2.36E+24	2.30E+24
²³⁸ U EOL	1.04E+26	1.04E+26	1.04E+26	1.05E+26
²³⁷ Np EOL	1.19E+23	1.18E+23	1.16E+23	1.07E+23
²³⁸ Pu EOL	5.32E+22	5.28E+22	5.61E+22	5.00E+22
²³⁹ Pu EOL	1.00E+24	9.11E+23	7.60E+23	7.44E+23
²⁴⁰ Pu EOL	5.52E+23	5.32E+23	5.22E+23	5.18E+23
²⁴¹ Pu EOL	4.81E+23	4.47E+23	3.93E+23	3.81E+23
²⁴¹ Am EOL	2.93E+23	2.91E+23	3.17E+23	3.02E+23
^{242m} Am EOL	1.19E+22	9.92E+21	8.30E+21	7.80E+21
²⁴³ Am EOL	2.25E+20	1.86E+20	1.52E+20	1.42E+20
²⁴² Cm EOL	4.64E+22	4.61E+22	5.02E+22	4.60E+22
²⁴³ Cm EOL	7.20E+21	6.75E+21	6.72E+21	6.31E+21
²⁴⁴ Cm EOL	1.54E+20	1.44E+20	1.48E+20	1.34E+20
²⁴⁵ Cm EOL	1.29E+22	1.30E+22	1.44E+22	1.27E+22

Table 3.20: PBMR fuel integral actinide production/destruction rate in [g/TWh_{th}] and variations in comparison with the PBMR reference fuel for wallpaper fuels.

Fuel type	PBMR	Variant 1	Variant 2	Variant 3
²³⁵ U	-3.11E+04	-0.1%	1.7%	-0.8%
²³⁸ U	-2.58E+04	-5.1%	-8.1%	-7.1%
²³⁷ Np	4.14E+02	-2.2%	-6.4%	-9.9%
²³⁸ Pu	1.84E+02	-2.3%	0.7%	-5.8%
²³⁹ Pu	3.53E+03	-10.5%	-27.6%	-25.5%
²⁴⁰ Pu	1.95E+03	-5.1%	-9.8%	-5.9%
²⁴¹ Pu	1.71E+03	-8.4%	-22.0%	-20.5%
²⁴¹ Am	4.24E+01	-2.2%	3.3%	3.3%
^{242m} Am	8.01E-01	-18.2%	-33.6%	-34.5%
²⁴³ Am	1.66E+02	-18.6%	-35.3%	-36.6%
²⁴² Cm	2.57E+01	-2.2%	3.2%	-0.6%
²⁴³ Cm	5.52E-01	-7.7%	-10.9%	-12.2%
²⁴⁴ Cm	4.64E+01	-7.8%	-8.3%	-12.6%
²⁴⁵ Cm	2.29E+00	-1.2%	6.6%	-1.3%

Conversion ratio

Due to different burn-up achieved by the fuels investigated, the comparison of Table 3.20 results with conversion ratios seen in [116] is complex. Assuming that average discharge burn-ups of PBMR, variant 1 and 3 are equal, one may conclude that:

1. the slight ^{235}U consumption decrease, compensated by a decrease in most of the minor actinides production (for variant 1 in comparison with PBMR fuel), confirms the decrease in conversion ratio reported in [116].
2. the strong reduction in ^{235}U consumption, compensated by the breeding and fission of Pu isotopes (for variant 3 in comparison with variant 1), corroborates the increase in conversion ratio reported in [116].

For the comparison of variant 2 with other fuel types, one should first consider results of Table 3.16, where production and destruction rates are produced for the same fuel burn-up. This table shows that the trends, when switching from PBMR fuel to variant 1, are more pronounced when switching from variant 1 to variant 2. This suggests that, at equal discharge burn-up, variant 2 has an even lower conversion ratio than variant 1, as reported in [116].

The main change, when comparing results of Table 3.16 and Table 3.20, concerns the relative decrease in ^{235}U consumption of variant 2 in comparison with variant 1. This can be explained by an increase of conversion ratio for variant 2 when raising the discharge burn-up. The burn-up increase (at high burn-up, when most of ^{235}U is burned) can then be considered in a similar way as the enrichment reduction, indeed increasing the conversion ratio.

Loss of Coolant Accident calculations with PANTHERMIX

One severe incident HTR could face is the Depressurized Loss of forced Cooling Accident (DLOCA) [130]. Chronology of such an incident is as follow: A break in the primary system induces depressurization. This reduces heat removal by the coolant, which initiates a core heat-up. Coupling Doppler Effect and Xenon poisoning, the reactor shuts-down by itself: Only decay heat is produced. This decay heat is removed by conduction to the Reactor Pressure Vessel (Convection, which helps cooling the core in case of a Pressurized Loss of Cooling Accident, is negligible here due to the low density of helium at atmospheric pressure). The decay heat drops, while the heat conduction and the thermal inertia of the core limit and slow down the temperature increase. After Xenon decay, the cores reach re-criticality, which then produces heat (at a lower level), contributing to the further core heat-up. The core power then keeps oscillating at very low levels that can be removed passively. The starting point for this scenario is defined by the preceding steady-state conditions. As expected, the wallpaper fuels perturb the neutron spectrum: Fig. 3.5 shows a higher maximal thermal flux when comparing wallpaper fuels-fuelled reactors to a PBMR one.

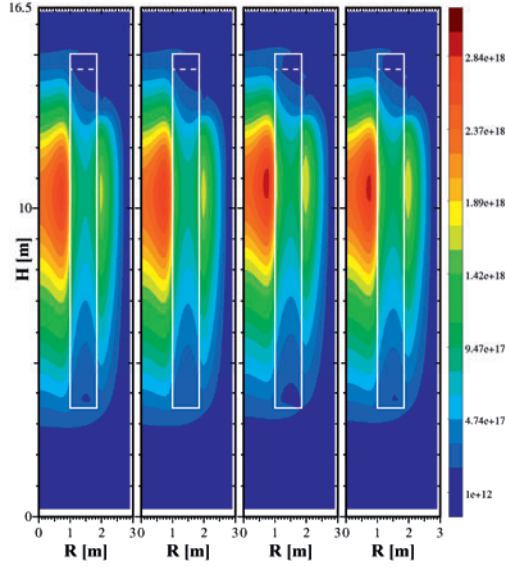


Fig. 3.5: Thermal flux [m^2/s] distribution for PBMR and variant 1 to 3 (left to right) fuelled reactor.

The flux perturbation leads to higher fission rates and thus higher power close to the central reflector, as shown in Fig. 3.6.

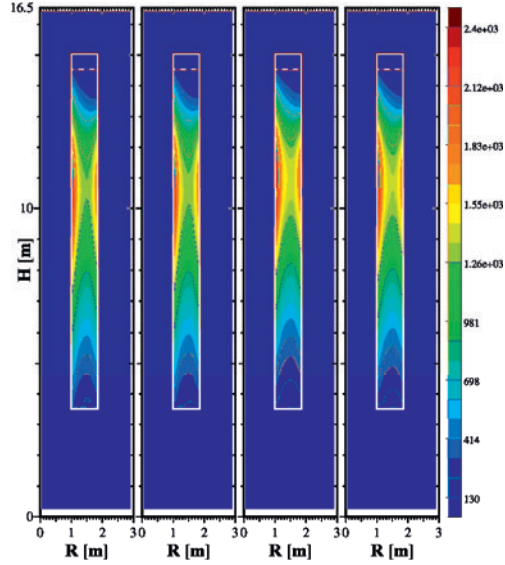


Fig. 3.6: Mesh averaged pebble power [W] distribution for PBMR and variant 1 to 3 (left to right) fuelled reactor.

This is even more obvious when considering the core section with the highest power density, as displayed in Fig. 3.7

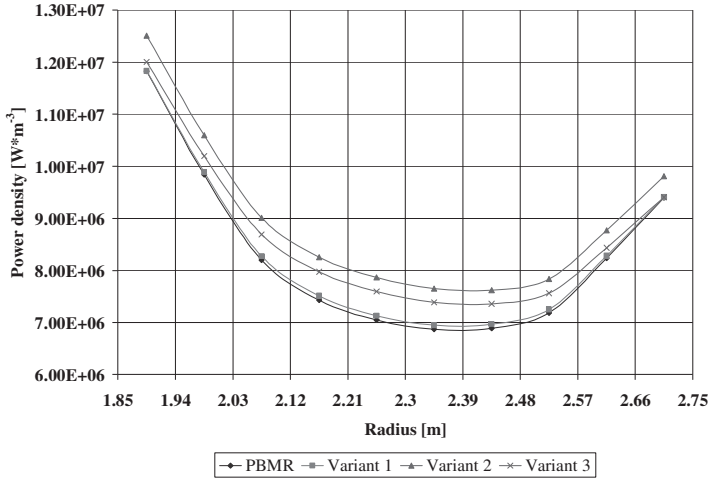


Fig. 3.7: Section with the highest mesh averaged power density.

In case of DLOCA, the heat is transferred through the pebble bed and the reflector to the outside. Since these higher powers are located at the most central part of the core, the radial temperature gradient (through the core and external reflector) leads to higher temperatures.

With identical boundary conditions, but higher temperature gradient, the temperatures of the fuel elements close to the central reflector are higher for wallpaper-fueled cores: Fig. 3.8 represents the core maximum kernel temperature through the DLOCA.

This graph shows first that this temperature does not exceed 1600°C, licensing limit for the German HTR Modul design, when fueled with PBMR pebbles and remain very close for variant 1 pebbles (1872 and 1876 K resp.). It also displays that wallpaper fuels with high FFZ graphite density present higher kernel temperature than those of the PBMR case, namely 1917 K for variant 2 and 1895 K for variant 3.

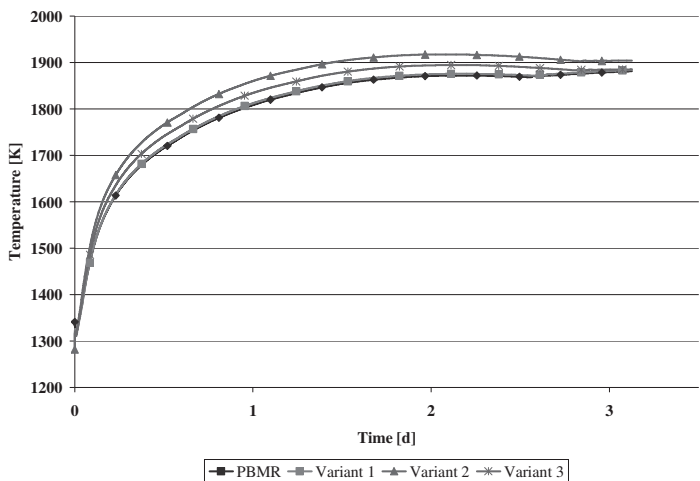


Fig. 3.8: *Maximum particle temperature [K] in case of DLOCA.*

Fig. 3.8 also shows the impact of re-criticality, as temperature increases further after reaching a first maximum. It should be noted that, even after re-criticality, PBMR kernel temperatures remain below the wallpaper ones.

The temperature evolutions during the DLOCA directly impact the neutron multiplication, as seen on Fig. 3.9. This graph clearly illustrates the impact of FFZ graphite density on temperature coefficient of reactivity.

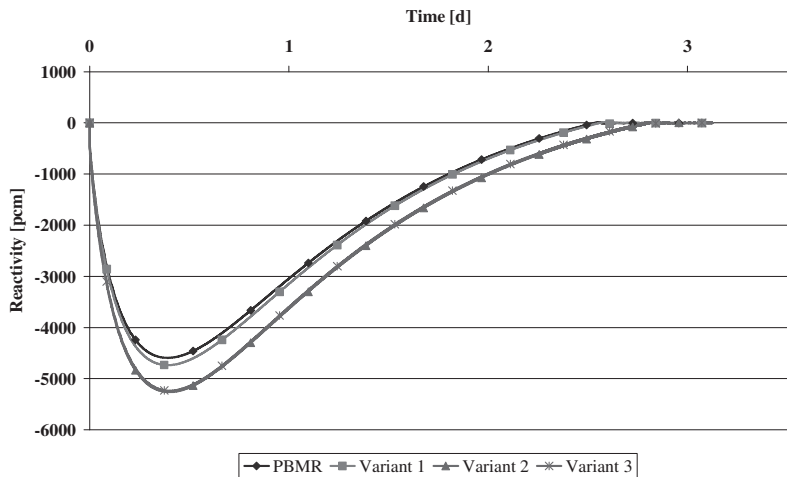


Fig. 3.9: *Reactivity [pcm] evolution through a DLOCA.*

The temperature evolutions during the DLOCA also impact the maximum power density, as seen on Fig. 3.10. Both graphs show that raising FFZ graphite density also delays re-criticality.

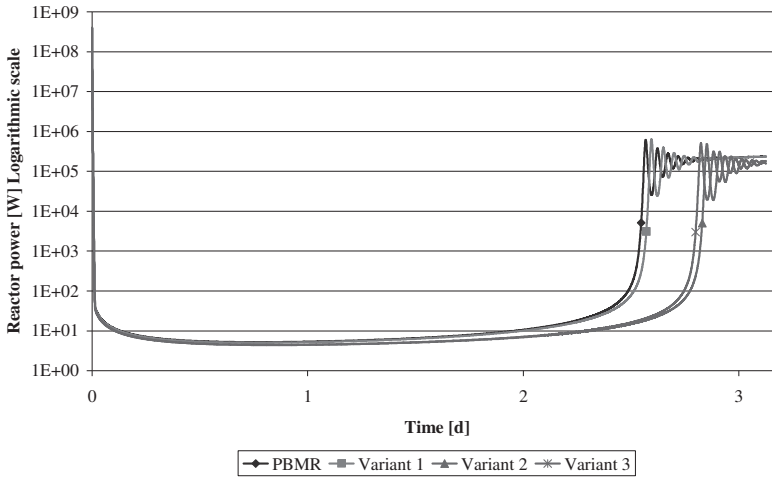


Fig. 3.10: Power [W] evolution through a DLOCA.

The fuel temperature excursion during DLOCA is well explained by the reactor power profile during steady-state operations. This leads to higher temperatures for wallpaper type of fuel in comparison with PBMR one. However, the temperature increase remains relatively low. This is the result of other aspects that tend to temper this increase:

1. Wallpaper fuels with high graphite density display a significant increase in heat capacity (from 3.02 Ws/m to 3.56 Ws/m for the FFZ), which limit temperature excursion.
2. This is especially true since reactors fuelled with wallpaper pebbles shut-down faster than PBMR-fueled one: Fig. 3.11 shows the reactor power variations, when comparing wallpaper-fueled reactors with PBMR one, after the transient start-up. Therefore, the higher temperatures, seen with high density FFZ graphite fuels, are not the result of a slower reactor shut-down.

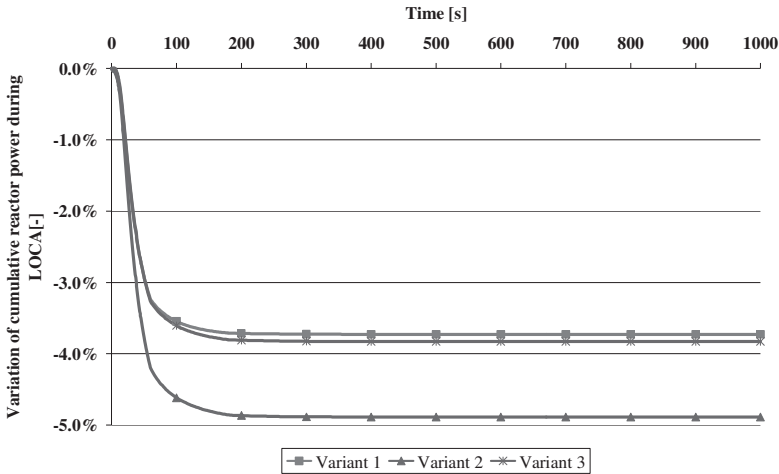


Fig. 3.11: Variations of cumulative reactor power (when fueled with wallpaper fuels) during DLOCA in comparison with PBMR fuel.

In fact one can draw a parallel between this situation and wallpaper fuels, where the power is generated closer to the shell, leading to a lower temperature gradient across the fuel. For core calculation, the use of wallpaper with higher graphite density increases the thermal neutron flux, leading to higher pebble power at the center of the core. This, in opposition to the fuel, raises the temperature gradient across the core and thus the temperature excursion in case of a DLOCA.

This can be corrected, by applying a special shuffle scheme, where fresh fuels would be located in the middle of the core, while depleted ones (with lower fission power) would be recycled close to the reflectors. As shown in [131], such a shuffle scheme would flatten the power profile across the core, significantly reducing the temperature in case of a DLOCA.

This option is particularly interesting since the retention capability of the wallpaper fuel is improved at lower temperature.

Based on, among others, temperature calculated during steady-states operations, the retention capability of this fuel can be estimated by evaluating particle failure probability.

3.5.2 Particle failure probability

Methodology

Stresses in particle coatings can be determined according to the method developed in [126] and [132] and shown in Fig. 3.12.

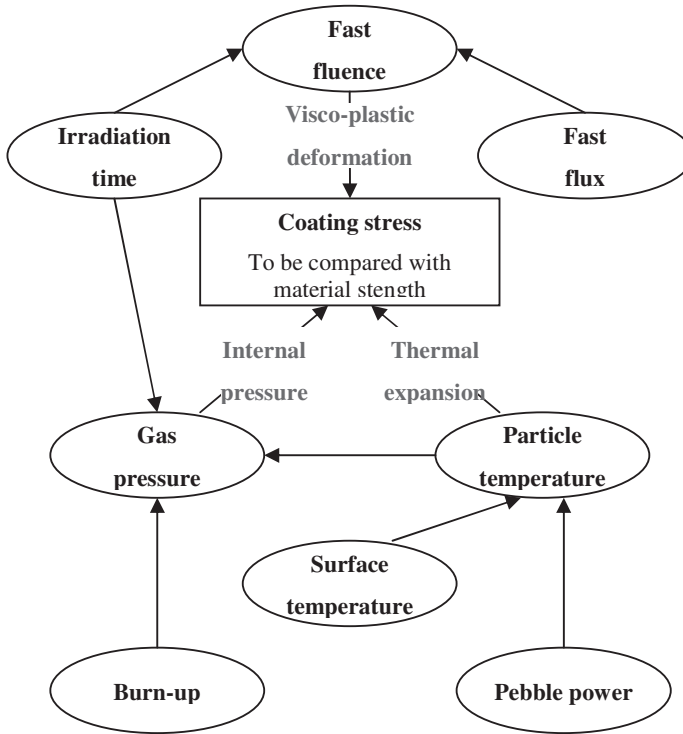


Fig. 3.12: *Stress determination in coating layers.*

Based on the reactors equilibrium conditions, the required parameters were collected for the four different fuels and for several different histories. Most of the PBMR benchmark codes follow pebbles over a fixed number of passes. PANTHERMIX works in a different way, similarly to the real reactor operation. The burn-up of discharged fuel elements is calculated, from which the future of each pebble is determined, i.e. the pebble is either recycled or disposed. Following the pebble course is not possible with this approach and histories are missing. Therefore, a procedure was developed to rebuild histories:

1. The mesh-averaged pebble power distribution, such as displayed in Fig. 3.6, is calculated for a limited number of radial and axial meshes (here, 3 radial and 66 axial meshes were selected).
2. Based on mesh average pebble power for one radial position, the burn-up increase for one pass through this radial position is determined. Examples of burn-up histories for fuel variant 1 through multiple recycling in the three radial zones are displayed in Fig. 3.13.

3. Fuels are recycled (with burn-up increment), until the discharged burn-up value is reached. A different radial position is sampled for each pass, covering all the possible combinations of positions per pass in-core.
4. Based on the different radial position for each pass, the other parameters (such as surface temperature and fast fluence) are collected.

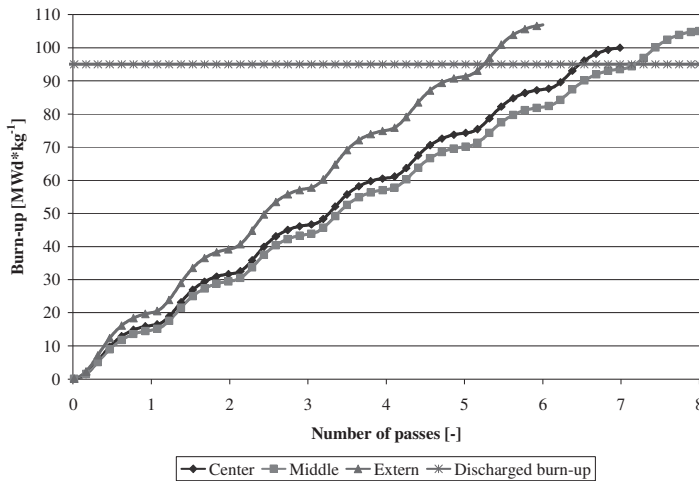


Fig. 3.13: Examples of burn-up increase through multi-pass recycling in three different radial zones for variant 1 fuel.

All possible histories (depending on the number of radial positions, the core power profile and the average number of passes through the core as shown in Table 3.21) were sampled and provided to CRYSTAL. The code then determined the particle failure fraction occurring for each history.

Table 3.21: Number of histories reconstructed.

Fuel type	PBMR	Variant 1	Variant 2	Variant 3
Number of histories	1233	1215	1821	1187

The probability that fuels pass through one radial section is proportional to the relative cross-sectional area of the section. Based on this concept, the probability for each individual history is calculated. This enables the determination of the average particle failure probability. Since CRYSTAL samples the full pebble history (pebbles are not discharged when a particle fails), the particle failure probability is calculated for the discharged fuel, and is not representative of the reactor equilibrium state.

Table 3.22 shows the comparison of results obtained with PANTHERMIX and by use of the history generator. There is a good match in general.

Table 3.22: *Comparison of PANTHERMIX and profile generator.*

	Number of Passes		Average discharge BU	
	PANTH.	Hist. Gen.	PANTH.	Hist. Gen.
PBMR	6.52	6.41	96.66	96.54
Variant 1	6.55	6.39	96.69	96.40
Variant 2	6.84	6.81	101.29	101.72
Variant 3	6.52	6.39	96.42	96.57

Simulations performed

The CRYSTAL code has been applied to the four fuel designs shown in Table 3.17 and Table 3.18. The particle failure fraction is calculated for different combinations of Fission Gas Release (FGR) and stress models. More details on these models can be found in [127]. Table 3.23 presents the different cases calculated for each design.

When the FGR column shows “100%”, the stable fission gases produced in the fuel kernel (He, Xe and Kr) are assumed to be instantaneously released into the buffer layer.

When the FGR is chosen to be “approx.”, the Booth equation has been modified for non-constant irradiation conditions and used. The latter FGR model is very fast and has proven to give results in good agreement with a more detailed FGR model [132].

When “PyC failure” is allowed (“yes” in Table 3.23), this means that the Pyrocarbon layers can fail prior to the SiC layer during irradiation. Pyrocarbon layers are also considered to be brittle, and can therefore crack if the tensile tangential stress exceeds the characteristic strength of the layer.

Finally, the effect of packing fraction also has been calculated for the last two cases (5 and 6). In the case of the wallpaper design, the thickness of the graphite matrix layer between adjacent particles is smaller, which may cause a higher stress factor on a given particle from the neighbouring particles.

Table 3.23: *CRYSTAL simulations performed.*

Case	FGR	PyC failure	Effect of packing fraction
1	100%	Yes	No
2	100%	No	No
3	Approx.	Yes	No
4	Approx.	No	No
5	100%	Yes	Yes
6	100%	No	Yes

Results and discussion

The results presented in Table 3.24 show that the failure fraction is very sensitive to the stress model: The crack-induced failure model that allows the PyC layers to fail always gives a much larger failure fraction and the different FGR models yield to results that differ by about two orders of magnitude.

Table 3.24: Failure fractions for different configurations of fuel, FGR and stress Models as calculated by CRYSTAL.

Case	PBMR	Variant 1	Variant 2	Variant 3
1	2.74E-06	2.66E-06	2.44E-06	2.66E-06
2	0	0	0	0
3	1.58E-08	1.27E-08	1.46E-08	1.30E-08
4	0	0	0	0
5	5.98E-05	2.05E-05	9.29E-06	2.49E-05
6	0	0	0	0

When the PyC failure is not allowed, in cases 2, 4, and 6, no failure among the 10^7 particles in the PBMR core is predicted. The resulting failure is therefore calculated to be lower than one particle per core, for particles within the history with the lowest weighting factor (least common history). A pebble in this least common history is always passing through the centre of the core. It has therefore the highest temperature and fluxes, which corresponds to the worst conditions regarding the fuel integrity. Although the model of PyC failure in CRYSTAL still needs to be validated, the preliminary results emphasize the role of PyC layers in the particle integrity.

For the cases when PyC failure is allowed (cases 1, 3 and 5), particle failures do occur during the simulation process. Those cases are important to understand if and which parameter (other than PyC failure) has a prevalent role in the particle failure.

The comparison of the different fuels through cases 1, 3 and 5 provides information on the impact of temperatures: For all three cases, the use of wallpaper fuels (and their lower fuel kernel temperature) decreases particle failure fraction.

The comparison of case 1 and 3 provides information on the impact of fission gas release: The Booth model tends to decrease fission products diffusion through the kernel, effectively reducing the buffer pressure and, subsequently, the particle failure fraction by two orders of magnitude. Furthermore, the FGR is also temperature dependent. Therefore the modified Booth equation gives more benefit to the colder fuels: The evolutions of particle failure fraction from cases 1 to 3 can be partially explained by a correlation with core-averaged kernel temperatures, as displayed in Table 3.17.

The comparison of case 1 and 5 gives the impact of the packing fraction variation. In case 5, all failure fractions are larger than in case 1: The thickness of the graphite

matrix layer is smaller, leading to a higher stress factor. By using this model, CRYSTAL also predicts an increase of failed particles even when the TRISO packing fraction remains low. This is the case of the PBMR fuel element with 9.34% packing fraction. This result is consistent with the conclusions given in [126]. Moreover, at higher packing fractions such as in the Wallpaper pebbles, the increase in failure fraction is also significant, although not as large as in the PBMR pebble. The lower temperature in the Wallpaper fuel zone yields a lower radial stress (used as boundary conditions), resulting in a lower true radial stress within the SiC coating for Wallpaper fuels.

Although the method reported in [126] and used in the present analysis has some limitations, the results presented in Table 3.24 tend to show that the lower temperature in the Wallpaper pebble fuel zone compensates the higher TRISO particle packing fraction. Reducing the temperature within the pebble reduces the pressure in the buffer. The same conclusion is drawn for all cases in which at least one TRISO particle is predicted to fail (cases 1, 3 and 5): The Wallpaper fuel designs always show the lowest failure fraction, as compared to the PBMR fuel element.

Between the different Wallpaper designs, variant 2 gives the lowest failure fraction in cases 1 and 5. The decrease in particle failure fraction between the reference fuel and variant 2 of wallpaper fuel ranges from 7.4% to 85%. According to the results calculated with the CRYSTAL code, the wallpaper fuel failure fractions are, in all cases, very consistent and lower than the PBMR design.

Through out this study, six scenarios were investigated, including two scenarios which are more accurate than the others (case 3, approximated Booth model, and case 5, particle packing fraction). While CRYSTAL already contributes to the understanding of failure mechanisms, this could still be improved by specifically looking at conditions during which particle failures occur and testing fuels with the approximated Booth model and effect of particle failure fraction.

3.6 Investigation of fissile material cost

Since HTR fuels uses relatively high enrichment (although still within the LEU limit of 20%), the enrichment process accounts for a significant part in the reactor operating cost. In [133], a method is developed to quantify costs related to the enrichment process (by both gaseous diffusion and centrifugation). For this investigation, three scenarios were assumed: The PBMR case (target burn-up of 96.66 MWd/kg for a ^{235}U enrichment of 9.6 wt. %), the variant 2 case (target burn-up of 101.29 MWd/kg for a ^{235}U enrichment of 9.6 wt. %) and the variant 3 case (target burn-up of 96.42 MWd/kg for a ^{235}U enrichment 9.277 wt. %). The burn-up target is used for the determination of fissile material flow required to operate a 400MWth HTR during a year. Natural uranium is used as feed material and a weight fraction of ^{235}U in the depleted stream of 0.2% is considered.

Table 3.25 summarizes key parameters and results for the comparison of enrichment costs.

Table 3.25: *Enrichment cost comparison.*

Fuel type	PBMR	Variant 2	Variant 3
Enrichment [% wt.]	9.6%	9.6%	9.277%
Burn-up [MWd/kg]	96.66	101.29	96.42
Enriched material flow [kg/y]	1511	1442	1515
Cost [kg SWU/GWd(th)]	205.72	196.32	198.06
Variations [-]	-	-4.57%	-3.72%

This comparison shows a decrease in yearly fissile material cost of 4.57% for variant 2 and 3.72% for variant 3. In addition, variant 3 requires lower enrichment than the other options, leading to a reduction of the number of enrichment stages required.

This cost investigation does not account for waste management. With a reduction of fuel material flow and TRU content reduction, as shown in Table 3.20, the cost for fuel reprocessing (if envisaged) can also be assumed to drop.

3.7 Thermal aspects and production process

3.7.1 Determination of the thermal profile through pebbles

Due to the fuel geometry and heat transfer, a temperature gradient occurs between particles placed in the centre of the pebble and those at the periphery. This gradient, which is mainly dependent on the power density, can reach up to 200 K at the beginning of life, as shown in [134].

The gradient can be determined according to the method developed in [135]: In radial coordinates, the stationary heat equations are the following:

$$\frac{1}{r^2} \frac{d}{dr} \left(r^2 \lambda \frac{dT_{CZ}}{dr} \right) = 0 \quad \text{for the central fuel free zone}$$

$$\frac{1}{r^2} \frac{d}{dr} \left(r^2 \lambda_f \frac{dT_{FZ}}{dr} \right) = - \frac{P}{\frac{4}{3} \pi (R_i^3 - R_c^3)} \quad \text{for the fuel zone}$$

$$\frac{1}{r^2} \frac{d}{dr} \left(r^2 \lambda \frac{dT_{Sh}}{dr} \right) = 0 \quad \text{for the graphite shell}$$

P is the pebble power,

T_{Sh} is the temperature in the shell,

T_{FZ} is the temperature in the fuel zone,

T_{CZ} is the temperature in the central fuel free zone,

λ represents the graphite thermal conductivity,

λ_F is the graphite thermal conductivity in the fuel zone.

Several boundary conditions need to be accounted for the temperature profile determination:

At $r = 0$, pebble center:

$$\frac{dT_{CZ}}{dr} = 0$$

At $r = R_C$, central fuel free zone radius:

$$\frac{dT_{CZ}}{dr} = \frac{dT_{FZ}}{dr} = 0 \quad \text{and} \quad T_{CZ} = T_{FZ}$$

At $r = R_i$, fuel zone radius:

$$T_{FZ} = T_{sh}$$

At $r = R_o$, pebble radius:

$$T_{sh} = T_0$$

T_0 being the gas temperature.

This leads to:

$$T_{sh}(r) = T_0 + \frac{P}{4\pi\lambda} \left\{ \frac{1}{r} - \frac{1}{R_0} \right\}$$

$$T_{FZ}(r) = T_0 + \frac{P}{4\pi\lambda} \left(\frac{1}{R_i} - \frac{1}{R_0} \right) + \frac{P}{4\pi\lambda_F (R_i^3 - R_C^3)} \left(\frac{R_i^2 - r^2}{2} + \frac{R_C^3}{R_i} - \frac{R_C^3}{r} \right)$$

$$T_{CZ}(r) = T_0 + \frac{P}{4\pi\lambda} \left(\frac{1}{R_i} - \frac{1}{R_0} \right) + \frac{P}{4\pi\lambda_F (R_i^3 - R_C^3)} \left(\frac{R_i^2 - R_C^2}{2} + \frac{R_C^3}{R_i} - \frac{R_C^3}{R_C} \right)$$

Another key parameter for determining the temperature gradient is the graphite thermal conductivity. According to the ‘‘Kania’’ model [136], graphite thermal conductivity depends on the type of graphite, its temperature, heat treatments, neutron fluence and particle packing fraction. To simplify the investigation, the following assumptions were considered:

- The graphite thermal conductivity used in this study was set to 26 W/m/K, as used in the PBMR benchmark [125].

- Since the thermal conductivity of graphite is one order of magnitude higher than that of UO_2 , particles are considered as void for the calculation of the integral thermal conductivity. Raising the particle packing fraction decreases the graphite fraction, which lowers the thermal conductivity of the layer. Particle packing fractions equal to 0% (no fuel), 8.95% and 30% are investigated; these represent the fuel free zone, the fuel zone of PBMR pebble and the fuel zone of wallpaper pebbles, respectively. For wallpaper pebble design, the packing fraction influences the thermal conductivity, but also the central fuel free zone diameter (the number of particles in the pebble is kept constant) and thus the temperature profile across the pebble.
- Finally, since the power density of pebbles changes during burn-up, several assumptions had to be made in order to determine representative temperature profiles: Surface temperature was set to reactor outlet temperature (1 000 °C), while the conservative value of 885 W was selected as the pebble power (pebble power averaged over its lifetime in the reactor).

The temperature profiles across the pebble are shown in Fig. 3.14.

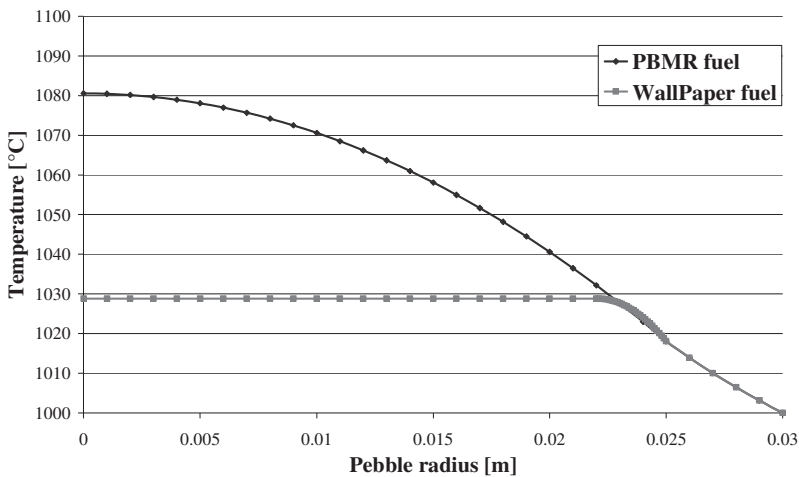


Fig. 3.14: *Temperature profile vs. pebble radius.*

In the case of conventional PBMR fuel, particle temperatures range from 1 018 to 1 081 °C through the fuel zone. For wallpaper fuel, peak temperature and also the range of temperatures in the pebble are smaller: 1 018 to 1 029 °C.

Since less particles are positioned in the inner layers of the pebble than in the outer ones, the averaged temperature of particles has to be determined by weighting using the particle volume ratio. This results in an averaged particle temperature of 1 043 °C for conventional PBMR fuel and of 1 025 °C for wallpaper design.

However, the benefits of the decrease of average and peak temperatures are accompanied by increased temperature gradients. The average temperature increase across the conventional PBMR fuel zone was calculated at 3.68 K/mm, which compares with 3.74 K/mm for the wallpaper design. This may somewhat enhance kernel migration or the amoeba effect [137], which is also responsible for particle failures.

Needless to say, the impacts of parameters (maximum and average temperature decrease and amoeba effect) have to be determined experimentally, for instance by means of release measurement under fuel irradiation and post irradiation examinations. It should be noted that temperatures and the increase in temperature within the wallpaper fuel are comparable to those undergone by particles close to the outer edge of the fuel zone of a conventional pebble (cf. Fig. 3.14). Irradiation of conventional pebbles should already provide valuable information concerning the particles' behaviour in wallpaper fuels.

3.7.2 Production Technology for “Wallpaper” fuel

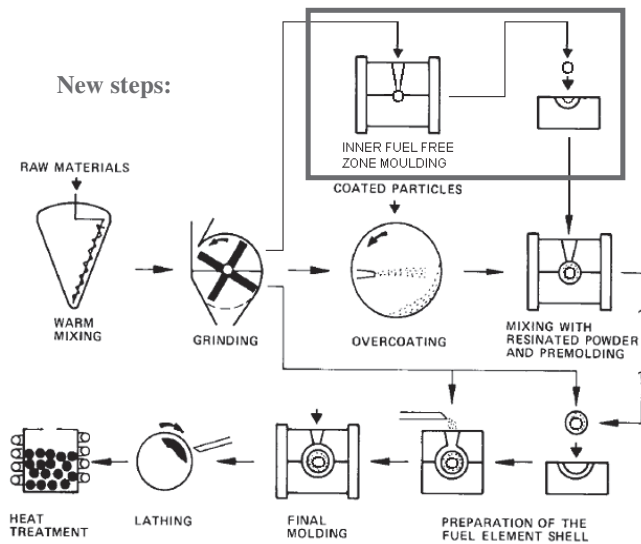


Fig. 3.15: *Modification of pebble production.*

In order to be attractive, the wallpaper fuel concept needs to have only a minor impact on the current production process [138]. Fortunately, the additional demands made of the fabrication process are modest and consist in centering different zones: this process is already used for current pebbles, where the graphite shells are moulded around the fuel zone. Since the resin, used in the 1970s to bind BISO

particles for wallpaper design, is no longer needed, the irradiation performance of this fuel is expected to be more favorable and no fabrication issues due to the modification are expected (cf. Fig. 3.15:).

3.8 Conclusion

This chapter investigates ways of optimizing the HTR concept and diversifying its fuel cycle by modifications at the fuel element level. The wallpaper fuel makes it possible to lower the temperature across the pebble. This helps to protect the coating layers and to reduce thermal stress, and the probability of coated particle failures resulting in fission product release. Wallpaper fuels are feasible, since the particle packing fraction can be raised significantly, without affecting production, up to 30%. As a result, this newly-created central fuel-free zone can be used for neutronic optimization of the core. The end result of these optimizations is an increase in neutron multiplication, increase in average burn-up, and decrease of enrichment needs and amount of spent fuel produced, leading to lower costs.

MCNP/MCB simulations have shown that the fuel change offers more versatility to the HTR concept:

- The conversion ratio can be decreased (Variant 1 and 2);
- or increased (Variant 3).
- Variant 2 also offers higher reactivity.

This is translated in:

- Neutron multiplication of the reactor increases by approx. 1750 pcm, which is also accompanied by a reduction of at least 4% on key MA production (when comparing variant 2 to PBMR case);
- Enrichment can be reduced from 9.6% to 9% while maintaining neutron multiplication above PBMR design targets (variant 3).

This has been confirmed by means of PANTHERMIX simulations, which have shown that:

- Neutron multiplication of the reactor can be increased from 1.047 for PBMR fueled core to 1.056 for variant 2 fueled core, leading to a reactivity increase of 925 pcm;
- This reactivity gain can be used to further deplete fuel: A gain of 5.1% in term of burn-up is feasible, which increases ^{235}U consumption (+1.7%) but reduces Pu and MA (-9.8% to -33.6%);
- Alternatively, enrichment can be reduced from 9.6% to 9.277% while maintaining neutron multiplication at PBMR design targets (variant 3) and reducing ^{235}U consumption (-0.8%) and TRU production (-5.9% to -34.5%).

These considerations also influence reactor economy. Fuel manufacturing costs can be reduced through lower enrichment or by achieving higher burn-up (better use of fissile material). The reactivity caused by changing the fuel allows initial enrichment to be decreased or, alternatively, higher burn-up to be achieved. Investigations shown suggest that the cost of the yearly required fissile material can be reduced by 4.6% when using variant 2 with extended burn-up and by 3.7% when reducing fuel enrichment. The fuel cycle implications might have an even greater impact on economy. Indeed, the use of wallpaper fuels considerably reduces waste.

Lastly, peak temperature during nominal operation is reduced by approx. 55 K. This reduces the thermal stresses within the coating layers as well as the internal pressures. The latter effect is particularly relevant for Pu/TRU-based fuels, as they tend to produce He, which contributes to the increase in internal pressure.

The integrity of the particles during steady-state operations, for the different fuel element, has been investigated by means of the CRYSTAL code. It is concluded that even though the higher packing fraction in the Wallpaper designs has a negative impact on the failure fraction, the lower temperature in the Wallpaper fuel zone has a more important and positive effect, leading to a reduction of the particle failure fraction up to 85% between the reference fuel and the variant 2 of Wallpaper fuel for the selected case 5. Furthermore, there is no strong difference between the different Wallpaper designs.

The safety feature of the reactor, fuelled with the different pebbles, has also been evaluated. Simulations of Depressurized Loss of Forced Cooling Accident scenario with PANTHERMIX have shown that:

- With PBMR fuel, the maximum kernel temperature does not exceed 1600°C (which was the license limit of German fuel in the HTR Modul design and is used as a reference temperature here);
- The use of wallpaper fuels changes the neutron spectrum, leading to higher power density generated closer to the central reflector;
- This results in higher particle temperatures during a DLOCA, exceeding 1600°C by up to 44K;
- This temperature increase is only slightly tempered by the higher thermal inertia (when fueled with high density graphite) and its ability to shut down faster (with all wallpaper fuels).

This can be corrected, by applying a special shuffle scheme, by locating fresh fuels in the middle of the core, while depleted pebbles (with lower fission power) could be recycled close to the reflectors. As shown in [131], such a shuffling scheme would flatten the power profile across the core, significantly reducing the temperature in case of a DLOCA.

Finally, reducing fuel temperatures and improving the burning capabilities of HTRs would enable safer and more efficient plutonium and MA management with HTR, beneficial for sustainability aspects of the concept.

Among the three concepts investigated, Wallpaper fuel with high graphite density and high enrichment is the most interesting option in steady-state conditions, as it shows the highest decreases in cost and particle failure fraction. However simulations of the different shuffling scheme (as suggested above) should ensure that the temperature of this fuel type remains within safe margin (here 1600°C was assumed as the limit) in case of DLOCA.

Furthermore, the suggested fuel designs would require irradiation testing for qualification purposes. Since the reactor design could easily accommodate such a change in fuel technology without modification of the concept, this is not part of the critical path for reactor licensing.

This study has shown that there is potential to improve HTR by means of minor modifications to the fuel. Furthermore, understanding physical phenomena makes it possible to investigate different fuel and core geometries in order to further improve neutron economy and to gear the reactor towards higher burning or breeding capabilities, thereby enhancing the sustainability of this very promising reactor concept.

4 Nuclear Powered Heat Pumps for Near Term Process Heat Applications

4.1 Introduction

The sustainability of nuclear power increases linearly with power conversion efficiency and can be further raised by co-generation of electricity and heat for various process heat applications. As an example, the Generation IV VHTR reactor concept aims at approx. 50% power conversion efficiency and, according to the prevailing opinion, a temperature close to 1000°C would be required to enable centralized hydrogen production. These high temperatures put severe constraints on materials, components and fuel and imply massive R&D requirements with uncertain outcome thus unnecessarily delaying introduction of this otherwise very attractive reactor concept.

The first objective of this chapter is to develop an alternative option to both reach the VHTR power conversion efficiency target and the capability to deliver high temperature process heat with a reactor or other heat source with lower temperature output that would be feasible in the near-term. The approach was to separate the requirement for high temperature process heat production from the nuclear part of the plant, in other words the nuclear part of the power plant would run at acceptably low temperature while the high temperature heat production would be limited to a conventional external circuit, thus avoiding nuclear constraints. Two such methods would be feasible: electric superheating to the desired temperature level or the use of heat pump (HP) technology via compression to the desired temperature level. While the heat thus generated is then delivered to a heat exchanger, some of the compression work can be recovered in a turbine, which makes this option energetically more efficient than electric heating.

The second objective of this chapter is to show how the same heat pump technology can be used for combined desalination and district cooling which corresponds to market needs in arid regions.

While classical gas-cooled reactors are proven technology, the GIF VHTR still requires a strong R&D effort. Based on already available technology, the power conversion options proposed here would introduce a near-term solution to provide nuclear produced high temperature process heat.

4.2 Current Developments for Nuclear Produced Hydrogen

So far, nuclear power is mainly used for base-load electricity production. To extend the use of nuclear power into new markets, different additional options are explored

such as cogeneration of process heat and electricity for efficiency increase and eventually massive H₂ production.

4.2.1 Power at high temperature

The Generation IV International Forum (GIF) VHTR concept for co-generation of process heat and electricity is expected to reach an overall efficiency of approx. 50% [77]. For electricity generation with gas-cooled reactors, a combined He Brayton cycle bottomed by a steam Rankine cycle seems to be the high-efficiency reference, whereas several other cycle combinations can be optimized for various co-generation applications. Fig. 4.1 shows a possible layout (left) from [139] for the co-generation of process heat and electricity. This layout is not suitable for the production of large quantity of very high temperature process heat (as required for optimised hydrogen production, see 4.2.2): The feasibility can be achieved by diverting the full helium flow across the intermediate heat exchanger (30) while reducing its temperature span. But such an option has one major drawback: The reactor inlet temperature should be raised. This requires, on one hand, to also raise the coolant flow (to ensure the correct cooling of the reactor), which then increases the pressure drops across the reactor and the heat exchanger. On the other hand, the reactor pressure vessel cannot be cooled by Helium anymore and therefore deals with much higher temperatures.

For all of the above reason, Fig. 4.1 shows an other possible layout (right). In this layout, only the highest temperatures are used for process heat application, while the rest is used in a Power Conversion Unit for electricity production.

According to [139], a 500 MW (300/900°C) reactor is coupled to a process steam generator. The whole reactor power (to which a part of the required circulator power was added) allows the production of 508 MWth reaching efficiency above unity! This at first glance surprising figure is explained by how process heat production efficiency is defined:

$$\eta_{PHP}^{High_Exergy} = \frac{Process_Heat_Power}{Reactor_Power}$$

For an ideal gas as primary coolant, high and low process heat temperatures determine the process heat quality.

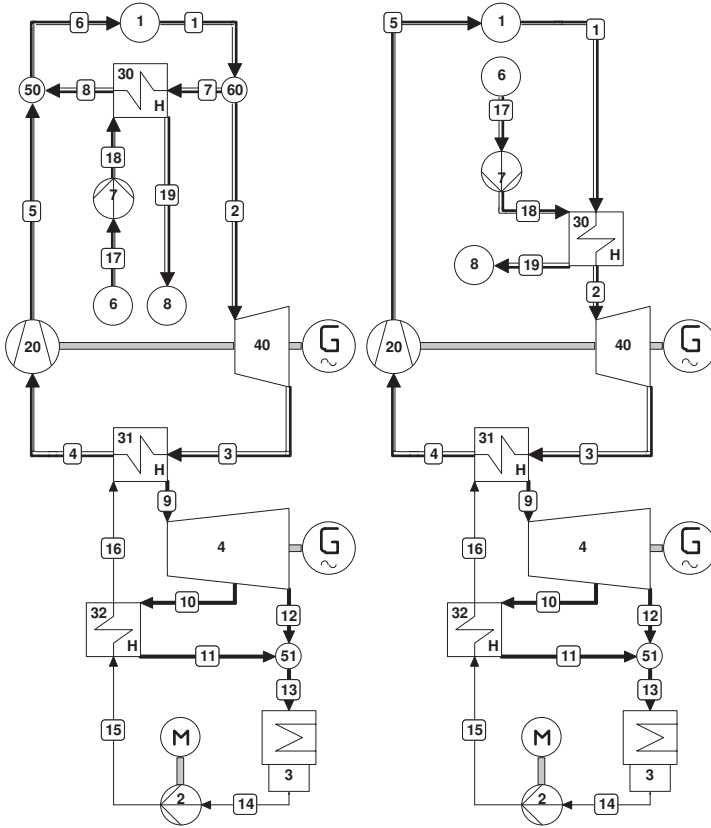


Fig. 4.1: Combined co-generation cycles for VHTR power conversion.

Efficiency of process heat production

Process heat production efficiency can be defined as:

$$\eta_{\text{HTPH LPHT}}^{\text{HPHT}} = \frac{\text{High_Temperature_Process_Heat_Power}}{\text{Reactor_Power}} = \frac{Cp_{\text{HX}} * \dot{m}_{\text{HX}} * (T_{\text{HX}}^o - T_{\text{HX}}^i)}{Cp_{\text{R}} * \dot{m}_{\text{R}} * (T_{\text{R}}^i - T_{\text{R}}^o)}$$

$$\text{Assuming } Cp_{\text{HX}} * \dot{m}_{\text{HX}} = Cp_{\text{R}} * \dot{m}_{\text{R}}, \quad \eta_{\text{HTPH LPHT}}^{\text{HPHT}} = \frac{\text{HPHT} - \text{LPHT}}{\text{ROT} - \text{RIT}} = \frac{\text{ROT} - \text{LPHT}}{\text{ROT} - \text{RIT}}$$

- with
- HPHT: High Process Heat Temperature [K] or T_{19}
 - LPHT: Low Process Heat Temperature [K] or T_{18}
 - RIT: Reactor Inlet Temperature [K] or T_5
 - ROT: Reactor Outlet Temperature [K] or T_1

To avoid taking IHX efficiency into account, LPHT and HPHT refer here to the primary coolant temperatures on the boundary of the IHX.

Based on this definition, Fig. 4.2 plots the resulting process heat production efficiency for different process heat qualities (or LPHT) with a VHTR operating between RIT (or T_3) = 400°C and HPHT (or T_{19}) = ROT (or T_1) = 1000°C.

In an ideal case, it is obvious that the fraction of reactor power, used as process heat is proportional to the useful temperature span of the delivered heat. In other words: when a thermo-chemical process can accept process heat only in a narrow temperature window, the power of the process heat is low.

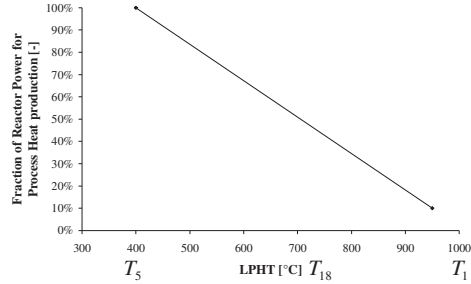


Fig. 4.2: Process heat production as reactor fraction vs. useable temperature span.

This is a major issue that temperature sensitive thermochemical reactions have to cope with. Below we will present an approach to respond to this problem.

VHTR for electricity generation

The most efficient power conversion option for a VHTR would be to couple a direct primary Brayton cycle to a bottoming secondary Rankine cycle [139]. Assuming a Rankine cycle efficiency of 50% with 600°C steam turbine inlet temperature [140], a pinch point of 15 K in the steam generator and a reactor outlet temperature of 1000°C, a VHTR might achieve an electric efficiency of 60.4% (10.4% for the Brayton and 50% for the bottoming Rankine cycle):

The code Cycle Tempo [141] was used to determine the thermal efficiency of this cycle. Based on calculations and analogies, pressure drops in pipes, reactor and heat exchangers were computed and integrated as well as turbomachinery efficiencies leading to the determination of net efficiency, see Fig. 4.3.

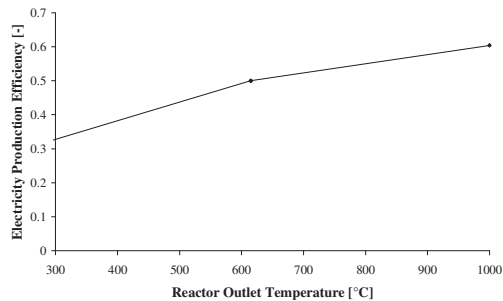


Fig. 4.3: Electricity Generation Efficiency vs. Reactor Outlet Temperature.

With a PWR efficiency of 32%, a Rankine cycle efficiency of 50% and a VHTR efficiency of 60.4% for respectively 285°C, 600°C and 1000°C reactor outlet temperature, we assume that electricity production efficiency can be approximated by two straight lines:

$$\text{if } 300^{\circ}\text{C} < \text{ROT} < 615^{\circ}\text{C} \text{ (Rankine): } \eta_{\text{Elec ROT}} = \frac{\text{ROT} - 285}{600 - 285} * (0.5 - 0.32) + 0.32$$

$$\text{if } 615^{\circ}\text{C} < \text{ROT} \text{ (Brayton + Rankine): } \eta_{\text{Elec ROT}} = \frac{\text{ROT} - 600}{1000 - 600} * (0.604 - 0.5) + 0.5$$

VHTR overall efficiency

A VHTR can be used for cogeneration of high temperature process heat and electricity. Therefore, the reactor coolant is not directly routed to the turbine but to an Intermediate Heat Exchanger that delivers the highest temperatures to the process heat application.

Under the assumption that both products (process heat and electricity) have the same commercial value, the overall energy and efficiency are then defined by:

$$P_{\text{VHTR}} = P_{\text{HTPH LPHT}}^{\text{HPHT}} + (P_R - P_{\text{HTPH LPHT}}^{\text{HPHT}}) * \eta_{\text{Elec LPHT}}$$

$$\eta_{\text{VHTR}} = \eta_{\text{HTPH LPHT}}^{\text{HPHT}} + (1 - \eta_{\text{HTPH LPHT}}^{\text{HPHT}}) * \eta_{\text{Elec LPHT}}$$

Fig. 4.4 shows the evolution of the overall efficiency as a function of low process heat temperature assuming again a heat-up span in the reactor from 400 to 1000°C. After feeding the high temperature process, the excess heat is supplied to a power conversion cycle for electricity generation. The efficiency of electricity generation is calculated from the two formulae in the section above, using LPHT instead of ROT.

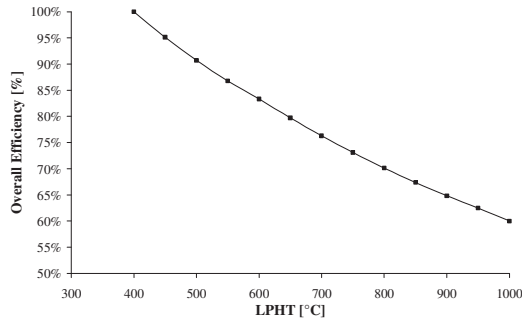


Fig. 4.4: VHTR Overall Production Efficiency vs. Low Process Heat Temperature.

Use of process heat vs. electric heating

Coupling a nuclear plant to a process heat consumer makes energetically sense only if the efficiency of process heat production is higher than the efficiency of electricity production. At the same time, this coupling makes economically sense only if the cost of process heat is lower than the cost of electric heating. It is currently impossible to assess the cost of process heat produced by a VHTR, which is why in the following we limit ourselves to efficiency aspects.

We assume that the efficiencies of the IHX and of electricity to heat conversion are unity, electricity production efficiency is 60%, RIT/ROT is 400/1000°C. If the reactor was dedicated to either pure process heat or pure electricity generation (i.e. no co-generation), the following applies:

$$\eta_{HTPH} > \eta_e \Leftrightarrow \frac{ROT - LPHT}{ROT - RIT} > \eta_e \Leftrightarrow ROT - \eta_e * (ROT - RIT) > LPHT$$

From this we may conclude that electrical heating of a process is energetically more attractive than coupling of reactor and process heat consumer, unless the low process heat temperature LPHT is below 650°C. In other words, this coupling would make energetically sense only if the process heat can be usefully delivered in a relatively large temperature window (from 1000°C to below 650°C). This conclusion is no longer true when considering co-generation of heat and electricity.

In this case (cf. Fig. 4.5), the overall efficiency is in all cases higher than pure process heat or pure electricity production. This advantage has to be traded against significant constraints on reactor design, operating conditions, increased complexity etc. Only a detailed economic and safety assessment of various symbiosis options will enable the choice between process heat use and electric heating.

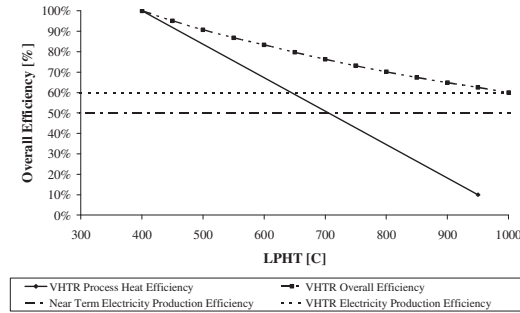


Fig. 4.5: *Process Heat Production Efficiency vs. Quality.*

4.2.2 From High Temperature to Hydrogen

There are several ways to generate H₂ based on process heat [142]. Due to its large CO₂ production and use of fossil resources, Steam Methane Reforming (SMR) is not

described here. Electrolysis can be performed at low temperature, but high temperature steam electrolysis minimizes electricity needs and improves efficiency. Thermochemical cycles couple several reactions for the dissociation of water. The most developed is the Iodine-Sulfur process. Finally, hybrid cycles such as the Westinghouse cycle are based on thermochemical reactions but including an electrolysis step.

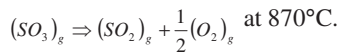
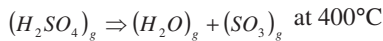
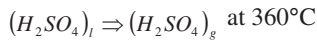
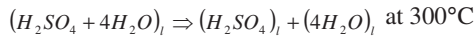
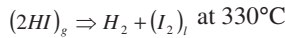
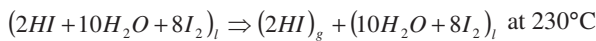
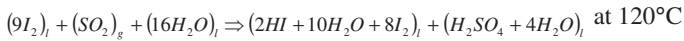
High Temperature Steam Electrolysis

Hydrogen production by High Temperature Steam Electrolysis (HTSE) was investigated in [143]. HTSE decreases electricity required by the electrolysis by raising steam temperature. Efficiency enhances with temperature. It was suggested to recuperate heat from the electrolysis products H_2 and O_2 : This heat is used for pre-heating steam between the reactor outlet temperature up to 30 K below the required 900°C.

In [144], the high temperature steam electrolysis was experimentally achieved with an efficiency of 53% at a temperature of 800°C.

Iodine-Sulfur Cycle

The Iodine-Sulfur (IS) cycle splits water using I_2 and SO_2 in a Bunsen reaction [145]. HI produced by this reaction is vaporized and decomposed into hydrogen and I_2 which is fed back into the Bunsen reaction. The sulfuric acid needs to be decomposed. It is first concentrated and evaporated and finally dissociated.



Water dissociation requires sulfur dioxide produced at high temperature. The advantage of this method is that it avoids electrolysis which requires electricity: Except sulfur trioxide decomposition, all the other reactions require heat at much lower temperature. Process optimization uses product heat recuperation thus increasing efficiency.

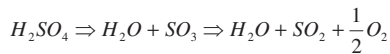
In [146], an optimized Iodine-sulphur cycle achieved a hydrogen production efficiency of 44% based on HTTR temperature of 1000°C.

Westinghouse Cycle

The Westinghouse (or hybrid) cycle is composed of four main steps [147]:

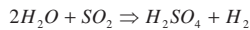
A concentrator increases the concentration of sulfuric acid by evaporation of water. This improves the efficiency of the decomposition.

Decomposition of sulfuric acid into sulfur dioxide and oxygen requires high temperature heat at 871°C.



Once sulfuric acid is split into sulfur dioxide and oxygen, a separator performs a fractional distillation to remove SO₂ from the gas phase.

Finally, the second chemical reaction producing hydrogen while reforming sulfuric acid is performed in the electrolyzer at 87°C:



The layout suggested in [147] uses heat recuperation after decomposition up to 30 K below the required decomposition temperature thus increasing process efficiency. Therefore, high temperature heat is only needed in a small temperature window around the decomposition temperature. The highest decomposition temperature leads to the most efficient process (47% at 926.8°C or 1200 K). Unlike for high temperature steam electrolysis, the efficiency has been determined based on LHV. This leads to an HHV-efficiency of 55.6% at 926.8°C.

4.2.3 Coupling Challenges

Intermediate Heat Exchanger

Several technologies are available for the IHX. Efficiency and compactness are antagonistic effects that have to be balanced which led to the development of printed circuit heat exchanger technology from Heatric [148] for HTR applications with compactness as the main objective with little compromise on efficiency. Pressures in the different channels have to be as close as possible to minimize mechanical loads. High temperature heat transfer can be achieved, but with a low temperature difference between the primary and secondary flows.

Optimized Hydrogen Production Cycles

For all three processes, high temperature heat is needed to enable and speed up reactions. In the two chemical processes, the lower temperature limit is 871°C for

sulfuric acid dissociation. There is no such limit for HTSE but all three processes improve in efficiency with increased reaction temperature. Process optimization uses product heat recuperation for the preheating of the reactants up to 30 K below the reaction temperature. The downside of this approach is that it makes the temperature window shrink in which high temperature heat must be delivered. This requires high fluid flows and large heat exchange surfaces.

Another realistic option to increase temperature between recuperator outlet and reaction might be electric heating. But due to the involved efficiency chain, a heat pump cycle might be the more efficient method.

4.3 Reverse Brayton Cycle

The principal objective of a heat pump [149] is to remove heat from a low temperature environment and to release it to a high temperature environment. This transformation requires mechanical work, which is exactly the opposite of the working process. To achieve that goal, a fluid is used as energy carrier: It undergoes transformations to be colder than the low temperature environment (to remove heat there) and then hotter than the high temperature environment (to release heat there).

If the energy gained from the cold source is considered as a loss that would otherwise be simply rejected, energy input into a heat pump is the compression work only. Both heat and compression work increase the energy in the fluid: The efficiency of this system is then higher than unity. In this study, the cold energy source cannot be considered as a loss such that efficiency is $< 100\%$, but still much higher than the working cycle efficiency.

This gas cycle is the opposite of a Brayton cycle:

- Heating at low temperature,
- Compression and superheating,
- Cooling at high temperature,
- Expansion for extra cooling.

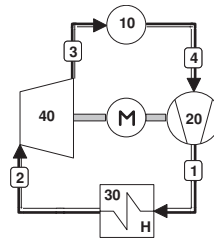


Fig. 4.6: *Reverse Brayton HP.*

In the lay-out of Fig. 4.6, the fluid remains in gaseous form. It is heated in the low temperature environment and superheated by compression. It delivers heat to the high temperature environment and is finally expanded in the turbine to recover some of the mechanical work from compression.

This method can be applied in a wide temperature range and reduced losses compared to a reverse Rankine heat pump or even electric heating. Although the compression work is much higher than for a liquid, a large part of it (around 60%) is recovered in the turbine. This enhances efficiency.

Shortcomings are:

- Poor heat transfer to and from the gaseous fluid implying high mass flows. As the sensible heats are smaller (per unit mass on a unit mass), latent heats, mass and volume flow are larger.
- The gas state, which implies non-isothermal heat exchanges.

In a reverse Brayton cycle, both mechanical power and low temperature power are transformed into high temperature power. As the goal is to maximize the contribution of the low temperature power compared to the valuable mechanical work, a reverse Brayton cycle with single compression and no recuperation (RB1CNR) is needed for the heat pump system. This implies production of process heat over a large temperature span. A reverse Brayton cycle with multiple recompression more would lead to an efficiency decrease but would provide process heat in a narrow temperature window.

4.4 Process Heat in a Large Temperature Span

4.4.1 Grid Motorized Reverse Brayton Cycle

For this cycle (either direct on Fig. 4.6 or indirect on Fig. 4.7), the reactor is considered as the lower temperature heat source. The gas from the reactor outlet is compressed to reach the required process heat temperature. Then, this gas transfers its heat to the high temperature process. It is then expanded in a turbine to cool it before returning to the reactor. During expansion, some mechanical work is recovered to power the compressor thus reducing external power needs.

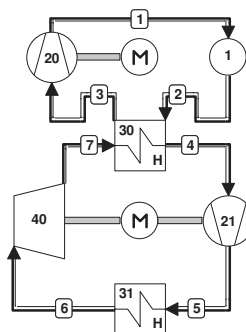


Fig. 4.7: *Indirect Reverse Brayton HP.*

In a reverse Brayton cycle, mechanical power converts low temperature heat into high temperature heat with a thermal efficiency of 1. Losses (pressure drops or turbomachinery efficiencies) only increase mechanical work required to transform the reactor power into high temperature process heat. Even if losses do not deteriorate the efficiency here, a distinction has to be made between the two power sources because mechanical power is more valuable than heat. For optimum overall efficiency, the contribution of the thermal power compared to the valuable mechanical work has to be maximized.

Prior to efficiency calculation (cf Table 4.2), conditions of Table 4.1 were selected as design point:

In this case, process heat is produced between the targeted 1000°C and 457°C, determined by the compression ratio of the cycle and the reactor inlet temperature.

Besides the high efficiency of this cycle, its simplicity implies reliability and low capital investment. Capital investment might be lower compared to a conventional power conversion unit for HTR due to the fact that the compression ratio is much lower: Here, compression is used only for superheating, thus between 850°C and 1000°C, leading to a compression ratio of only 1.257, although high temperature materials are required.

Table 4.1: *Operating Conditions of the RB1CNR Cycle.*

Medium	Line nr. on Fig. 4.7	Helium	-
Compressor Outlet Pressure	1	7	MPa
Reactor Inlet Temperature	1	400	°C
Reactor Outlet Temperature	2	850	°C
Process Heat High Temperature	5	1000	°C
Reactor Power		400	MWth

Table 4.2: *Powers and Efficiency of the RB1CNR Cycle.*

Mechanical Power	82.44	MW
Process Heat	682.44	MW
Efficiency	100%	-

4.4.2 HTR-Motorized Cycles

So far, the heat pump cycle required mechanical work and was powered from electricity taken from the grid. But the nuclear power plant can also produce this mechanical work itself in a working cycle. In case of single shaft architecture, this would save power transformation from mechanical to electrical power and back, thus increasing global efficiency. Of course, a multi-shaft architecture is still possible, and may be advantageous in transient operation.

Coupling with Reactor

For this cycle (cf Fig. 4.8), the reactor is the only power source. Helium is heated in the reactor and then split into two: one fraction generates mechanical power via a Brayton cycle with two compressors and a recuperator (B2CR). This mechanical power is then delivered to the reverse Brayton cycle to superheat the other fraction of the helium flow.

Based on the same method and software, net efficiency (cf Table 4.4) was estimated for the conditions of Table 4.3.

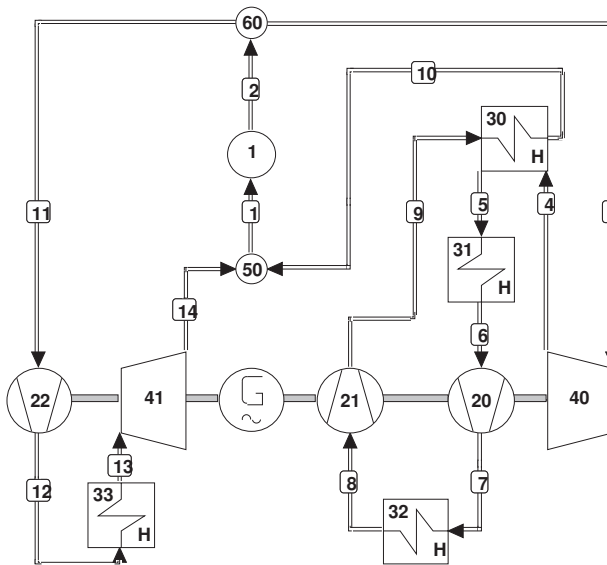


Fig. 4.8: *CC_B2CR_RB1CNR.*

Table 4.3: *CC_B2CR_RB1CNR cycle operating conditions.*

Fluid	Line nr. on Fig. 4.8	Helium	-
Compressor Outlet Pressure	14	7	MPa
Reactor Inlet Temperature	1	400	°C
Reactor Outlet Temperature	2	850	°C
Process Heat High Temperature	12	1000	°C
Heat Sink Temperature	6 or 8	50	°C
Recuperator Temperature Difference		15	°C
Reactor Power		400	MWth

Table 4.4: *Flows, production and efficiency of the CC_B2CR_RB1CNR cycle.*

Production	Electricity only	Process Heat only	Unit
Reactor Flow	171.1	171.1	kg/s
Flow Through B2CR	171.1	57.9	kg/s
Flow Through RB1CNR	0	113.2	kg/s
Electricity Produced	149.1	0	MW
Process Heat Produced	0	313.6	MW
Efficiency	37.27%	78.71%	-

In this case, process heat is produced between the targeted 1000°C and 466°C. Due to mixing with the B2CR flow and to match the reactor inlet temperature of 400°C, this value is slightly higher than in the RB1CNR case.

Reactor power can be transformed either into electricity or process heat, or both by balancing the flow between the two power conversion cycles. In case of the B2CR, both compressors have a compression ratio of 2.17. In case of the RB1CNR, it is still 1.257. For large-scale hydrogen production, the full reactor power might need to be transformed into process heat. As only 33.84% of the reactor flow (and power) is driven through the B2CR cycle, the average compression ratio for the whole installation is again lower than the one of a classic HTR.

Self-cooled Configuration

This cycle concept (cf. Fig. 4.9) uses a simplified power conversion unit for the generation of mechanical power (Brayton cycle with one compressor and no recuperator). While this power conversion cycle (B1CNR) is less efficient than more complex configurations, its heat is rejected at high temperature level that can be used e.g. for preheating the heat pump fluid. In other words, the heat pump cycle cools the power conversion cycle thus necessitating a single heat rejection only in the heat pump part. The high temperature heat exchanger (8) provides the desired process heat while the intermediate temperature heat exchanger can provide valuable heat for additional uses, e.g. a bottoming power conversion cycle.

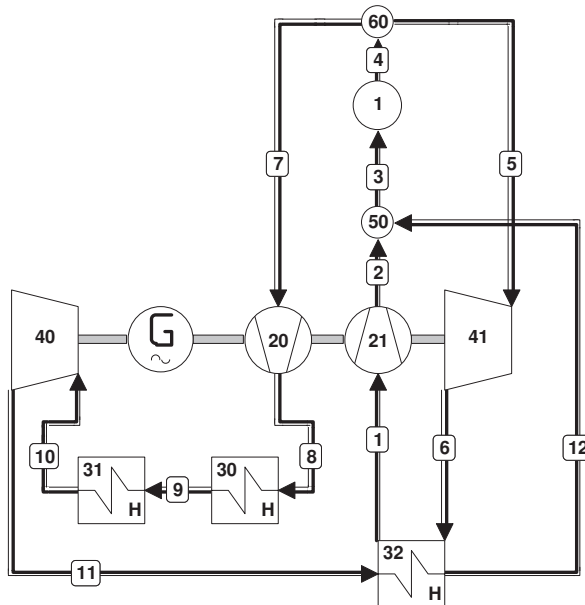


Fig. 4.9: Self-cooled CC_B1CNR_RB1CNR.

Based on the same method and software, net efficiency (cf Table 4.5) was estimated for the conditions of Table 4.1.

Table 4.5: *Flows, production and efficiency of the CC_B1CNR_RB1CNR cycle.*

Production	Heat only	Unit
Reactor Flow	171.1	kg/s
Flow Through B1CNR	86.2	kg/s
Flow Through RB1CNR	84.9	kg/s
Electricity Produced	0	MW
Process Heat Produced	400	MW
Efficiency	100%	-

In this case, process heat is produced between the targeted 1000°C and 93°C. Such a low temperature allows, by mixing with B1CNR flow, to reach the reactor inlet temperature which we had fixed at 400°C.

In the ideal case (no losses), both flows are equal. Due to the use of helium, an ideal gas, the recuperator temperature difference between the fluids was held constant at 15 K. Because of the losses, more mechanical power is needed by the heat pump for less thermal power. This slightly modifies the flow balance between the two parts of the cycle and thus the recuperator design. With two different flows, inlet and outlet recuperator temperatures evolve. A 15 K difference between pipes (1) and (11) leads to a 20.06°C difference between pipes (6) and (12).

4.5 Concentration of High Temperature Process Heat to a Narrow Temperature Span

The issue of thermochemical H₂ production is related to the narrow temperature window in which process heat can be delivered to the thermochemical processes. In case of a VHTR with RIT/ROT = 400/1000°C, and process heat supply between 1000°C and 950°C, only 8.3% of the nuclear power would be used for H₂ production. This fraction can be enhanced using recompression: once the coolant exits the IHX, it can be recompressed several times to attain again the required 1000°C, as shown on Fig. 4.10. The effect on the heat/electricity ratio and overall efficiency is listed in Table 4.6.

A “low-tech” approach for high temperature process heat production (e.g. for large-scale H₂ generation) was investigated: Based on AGR technology [150] and the recompression heat pump, it is possible to satisfy the requirements of a VHTR as proposed within GIF with less stringent conditions on fuel, materials and components.

A 600 MWth HTR (pebble bed or hexagonal block type) was assumed as the primary heat source with a primary top cycle temperature of 640°C (same as AGR).

At this temperature, the primary He coolant may be replaced by less expensive CO₂. This would avoid He leakage issues, enable the use of AGR technology with positive effects on feasibility and cost of components. This circuit was then coupled to a secondary reverse Brayton cycle for high temperature process heat generation and completed by a bottoming cycle for efficiency maximization.

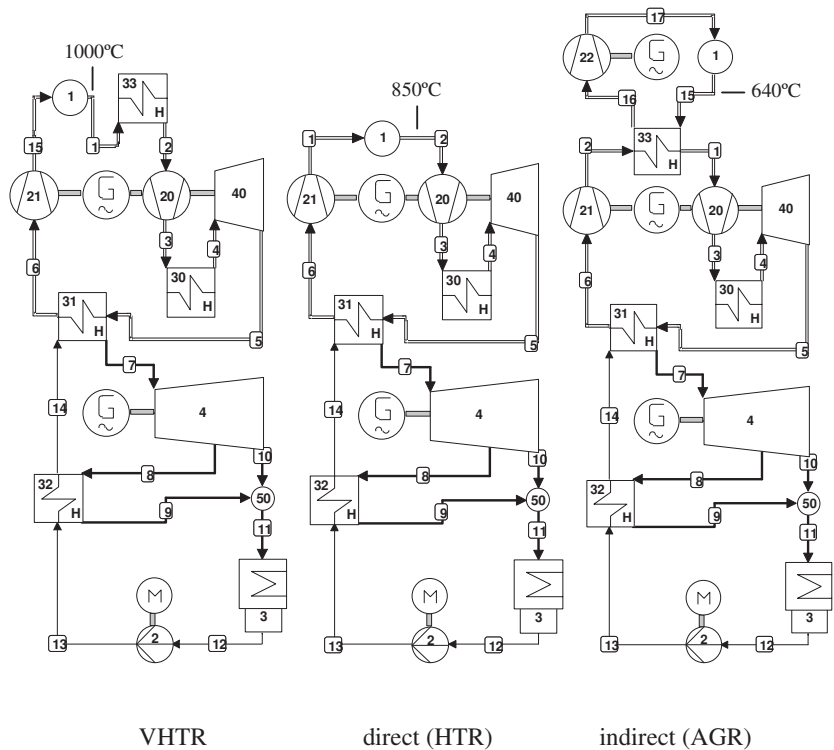


Fig. 4.10: VHTR with single recompression, Direct (HTR) / indirect (AGR) Brayton cycle with single recompression and bottoming Rankine cycle.

Table 4.6: Effect of recompression.

Recompressions/ no of IHX	High Temperature Heat [MWth]	Electricity [MWe]	Energy [MW]	Efficiency [%]
0 / 0	0	360.0	360.0	60.0
0 / 1	50	323.9	373.9	62.3
1 / 2	100	282.8	382.8	63.8
2 / 3	150	242.2	392.2	65.3
3 / 4	200	201.9	401.9	67.0
4 / 5	250	162.0	412.0	68.7
5 / 6	300	122.6	422.6	70.4

For comparison purposes we first present the results for a typical HTR with a He outlet temperature of 850°C. The first compression step is used to raise the reactor outlet temperature to the desired process heat temperature (of 1000°C) as shown in Fig. 4.10. The effect of recompression on efficiency is shown in Table 4.7.

Table 4.7: *Effect of recompression on an HTR with 850°C reactor outlet temperature.*

Recompressions/ no of IHX	High temperature heat [MWth]	Electricity [MWe]	Energy [MW]	Efficiency [%]
0 / 0	0	332.8	332.8	55.5
1 / 1	66.7	271.7	338.4	56.4
2 / 2	133.3	218.7	352	58.7
3 / 3	200.0	166.2	366.2	61.0
4 / 4	266.6	114.3	380.9	63.5
5 / 5	333.3	63.0	396.3	66.0
6 / 6	400	11.2	411.2	68.5

An AGR with 640°C reactor outlet temperature would achieve the performance and effect of recompression on efficiency as shown in Table 4.8. Between 3 and 4 recompressions, the system turns into a net electricity consumer.

Table 4.8: *Effect of recompression on an AGR with 640°C reactor outlet temperature.*

Recompressions/ no of IHX	High Temperature Heat [MWth]	Electricity [MWe]	Energy [MW]	Efficiency [%]
0 / 0	0	295.9	295.9	49.3
1 / 1	87.72	190.5	278.2	46.4
2 / 2	175.42	118.3	293.7	48.9
3 / 3	263.13	46.5	309.6	51.6
4 / 4	350.84	-24.7 (consumption)	326.1	54.3

Fig. 4.11, Fig. 4.12 and Fig. 4.13 summarize process heat and electricity production as well as overall efficiency of VHTR, HTR and AGR cycles depending on the number of Intermediate Heat Exchanger.

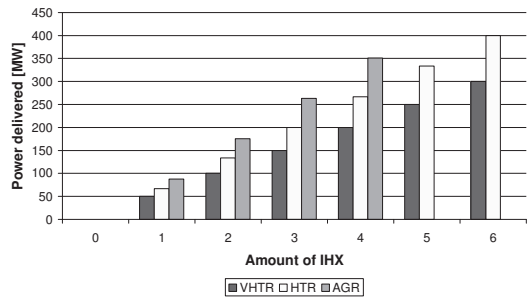


Fig. 4.11: High temperature process heat production.

Fig. 4.11 illustrates that an AGR with three IHX produces more high temperature process heat than a VHTR with five. This is paid by a significant overall efficiency penalty (from 68.7% to 51.6%) and can be explained by the primary coolant flow-rates: due to different reactor inlet and outlet temperatures of the three compared heat sources, the flows are not the same in all computations. As illustrated in Table 4.9, a higher reactor inlet temperature requires higher coolant flow-rates to remove the heat from the reactor thus increasing the flow through IHX and compressors which then require more compression work.

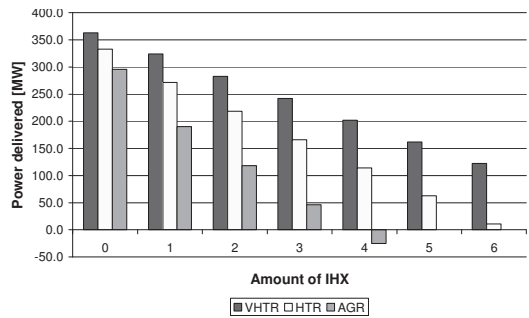


Fig. 4.12: Electricity production.

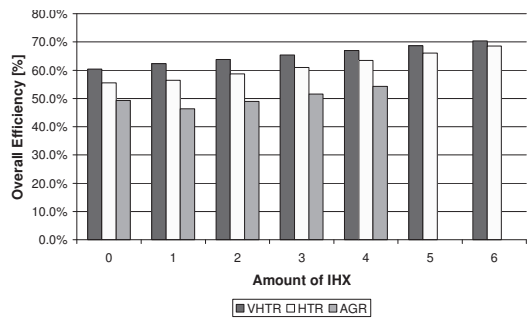


Fig. 4.13: Overall efficiencies.

Table 4.9: Influence of primary coolant heat-up span on process heat and compression work.

Reactor	Coolant heat-up [K]	Mass Flow [kg/s]	Process Heat & Compression Work per IHX [MW]
VHTR	600	192.6	50
HTR	450	256.8	66.7
AGR	342	337.9	87.7

For comparison purposes, a VHTR with five IHX was simulated with HTR and AGR flow. This was done by increasing the reactor inlet temperature RIT to 550°C so as to match the coolant heat-up in an HTR, and to 658°C for an AGR (cf. Table 4.10):

Table 4.10: RIT Influence on the production (VHTR case).

RIT	400	550	658	[°C]
Reactor Flow	192.6	256.8	337.9	[kg/s]
HTPH Production	250.0	333.3	438.6	[MW]
Electricity Prod.	162.0	93.2	6.4	[MW]
Overall Efficiency	68.7%	71.1%	74.2%	[%]

Furthermore, an HTR with four IHX was simulated with AGR flow. This was done by raising the RIT to 508°C to match AGR conditions (cf Table 4.11).

Table 4.11: RIT Influence on production (HTR case).

RIT	400	508	[°C]
Reactor Flow	256.8	337.8	[kg/s]
HTPH Prod.	266.6	350.8	[MW]
Electricity Prod.	114.3	40.5	[MW]
Overall Efficiency	63.5%	65.2%	[%]

From this, the following dependencies can be derived:

$$\uparrow RIT \Leftrightarrow \uparrow Process_Heat \ \& \ \downarrow Electricity$$

Owing to this observation, tuning of heat and electricity supply to various customer needs can be achieved, very roughly first by the number of recompressions and Intermediate Heat Exchangers, then finely through variation of reactor inlet temperature. Limits to this approach are materials (e.g. graphite and reactor pressure vessel) and throughput limits in reactor and IHX (pressure drop) and turbo-machinery (size).

Table 4.12 shows the influence of RIT on the required mass and volume flow-rates as well as on process heat and electricity production for a reactor with 640°C outlet

temperature and indirect co-generation of heat and electricity using three IHX and a recompression circuit with He. It can be seen that the variation of the mass flow-rate and thus RIT is a flexible means to adapt the ratio of delivered process heat and electricity. The highest RIT value selected (357°C) enables full conversion to process heat while a further increase would require importing electricity. A moderate flow-rate increase from 320.5 to 407.8 kg/s (+27%) would enable the variation of electricity output from 63.5 to 0.2 MWe.

Table 4.12: *RIT Influence on the production (AGR case).*

RIT	280	298	357	[°C]
CO ₂ /He HX Outlet Mass Flow-Rate	320.5	337.4	407.8	[kg/s]
CO ₂ /He HX Outlet Volume Flow-Rate	86.1	90.6	109.4	[m ³ /s]
HTPH Prod.	249.7	262.8	317.6	[MW]
Electricity Prod.	63.5	51.4	0.2	[MW]
Overall Efficiency	52.2%	52.4%	53.0%	[%]

These volume flow-rates could be significantly reduced by using Ar or other noble gases instead of He in the secondary recompression circuit.

We have not investigated whether the variation of RIT would enable limited load-following with this system, but the resulting thermal transients will certainly negatively impact the lifetime of fuel and heat exchangers.

4.6 Reverse Brayton Cycle for Combined Cooling and Desalination

Arid regions are in demand for both seawater desalination and cooling systems both requiring significant power. Reverse Brayton have the capability to simultaneously respond to this dual demand.

In [151], several desalination systems are reviewed. Among them, distillation/evaporation requires the highest temperature (between 110°C and 130°C). For large air conditioning systems, a temperature of 15°C might be foreseen with a counter flow heat exchanger. This is why we assume here delivery of cold at 15°C and delivery of heat at 130°C.

The layout shown in Fig. 4.6 is only an idealized situation, whereas in reality one has to account for entropy increase in turbomachinery. This increases turbine outlet temperature which is further raised by entropy increases in compressors. (By decreasing the high pressure required to match the targeted 130°C leading to a lower expansion in the turbine). Raising turbine outlet temperature (or Cold Exchanger Low Temperature) increases the required mass flow and thus compression work.

Two solutions are then possible: Either decreasing the hot exchanger low temperature below 110°C or using recompression to produce more heat for

desalination and enable the temperature match of the cold exchanger. This option is shown in Table 4.13.

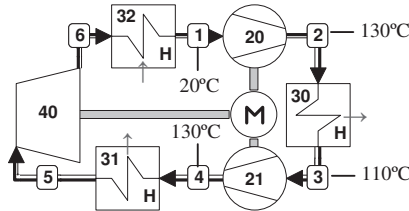


Fig. 4.14: RB2C1ENR cycle with recompression for combined cooling and desalination applications.

Table 4.13: Parameters of the cooling and desalination RB2C1ENR cycle.

Parameter	Value	Unit
Air Conditioning Power	1.00	MWth
Compression Work	-20.87	MWm
Desalination Power	6.18	MWth
Expansion Work	15.69	MWm
COP	-1.39	
Cold Exchanger Low Temperature	282.23	K

Due to the assumption that a mass flow increase would lead to a heat exchanger size increase, the pressure drop calculation is not depending on mass flow. According to this assumption and in the conditions described above, the pressure drops in heat exchangers can be calculated. In the order of 8E-2 bar, they do not significantly influence results including turbomachinery entropy, as shown in Table 4.13.

The small temperature windows in heat exchangers lead to a high coolant mass flow, which increases the required compression work. Therefore more recompressions and expansions might be used, as suggested on Fig. 4.15. Effect on the Coefficient of performance is available in Table 4.14:

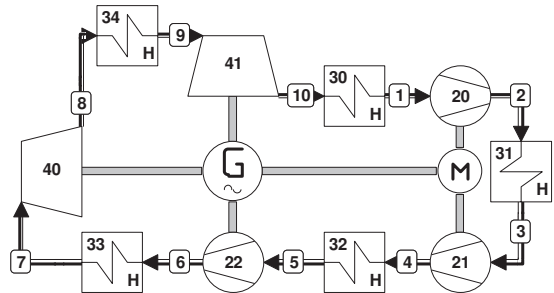


Fig. 4.15: RB3C2ENR cycle with recompression for combined cooling and desalination.

Table 4.14: *Parameters of the cooling and desalination RB3C2ENR cycle.*

Parameter	Value	Unit
Air Conditioning Power	2.00	MWth
Compression Work	-17.31	MWm
Desalination Power	6.70	MWth
Expansion Power	12.61	MWm
COP	-1.85	
Cold Exchanger Low Temperature	279.74	K

Coefficient of Performance can be further raised by adding extra compressions and expansions. An economic assessment will determine the optimum number of recompressions.

4.7 Future Work

4.7.1 Other Power Conversion Cycles

The possibility to use a lower temperature reactor for high temperature process heat generation enables the use of various power conversion cycles for the required mechanical power generation.

SCW-Bottoming Cycle

The supercritical water reactor (SCWR, Fig. 4.16) uses supercritical water (25 MPa and a reactor outlet temperature of 550°C) as the working fluid [77] in a direct power conversion cycle. Higher temperatures improve economics, while operating above the critical pressure keeps the coolant in single-phase. Components handling the phase change in LWRs can be eliminated reducing construction costs.

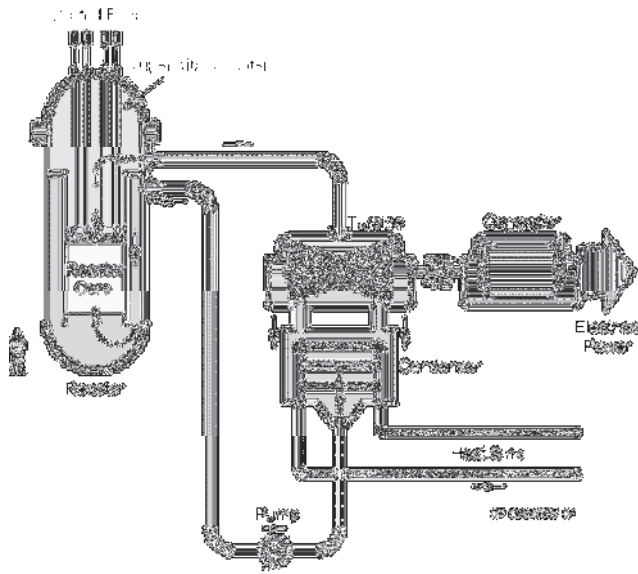


Fig. 4.16: SCWR cycle.

SCWRs are expected to yield a high thermal efficiency (approx. 45% as opposed to 33% for current LWRs) and considerable plant simplification. Major issues are in-core materials resisting against stress corrosion cracking and the coupled neutronics/thermal-hydraulics stability of the system. In this configuration (cf. Fig. 4.17) heat from a high temperature reactor is pumped up to the desired high temperature level in a reverse Brayton cycle. The waste heat from this reverse Brayton cycle is then used in a supercritical bottoming cycle for electricity generation.

With the reverse Brayton cycle between the reactor cooling system, the bottoming cycle avoids water ingress into the HTR core and enables the use of a fluid other than He in the heat pump cycle.

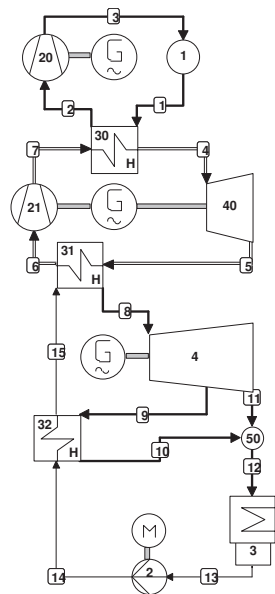


Fig. 4.17: CC_IRB1CNR_SCW.

Supercritical CO₂ Bottoming Cycle

A supercritical CO₂ cooled reactor was proposed at the MIT. Several power conversion units for such a reactor were investigated. Among them the recompression cycle seems most promising [152] because it would yield the highest efficiency while still retaining simplicity. With a conservative turbine inlet temperature of 550°C and a compressor outlet pressure of 20 MPa, the direct cycle achieves a thermal efficiency above 45%. A supercritical CO₂ cycle is well suited to any type of nuclear reactor with a core outlet temperature above 500°C in either direct or indirect configuration. By taking advantage of the abrupt property changes near the critical point of CO₂ (CO₂ is no ideal gas) the compression work can be reduced, which results in a significant efficiency improvement. However, a real gas cycle requires much more careful optimization than an ideal gas Brayton cycle.

Radiolysis of CO₂ can cause graphite corrosion, and CO₂ can carburize metals. Future high temperature materials, resistant to these issues might allow pushing turbine inlet temperatures to 700°C. This high performance design would achieve a thermal efficiency approaching 53%.

The configuration proposed in Fig. 4.18 uses a supercritical CO₂ cycle as the bottoming cycle for the generation of electricity. To avoid issues related to CO₂ at high temperature, the reverse Brayton cycle will be using a fluid other than CO₂, e.g. argon, thus circumventing CO₂ or nitrogen related issues.

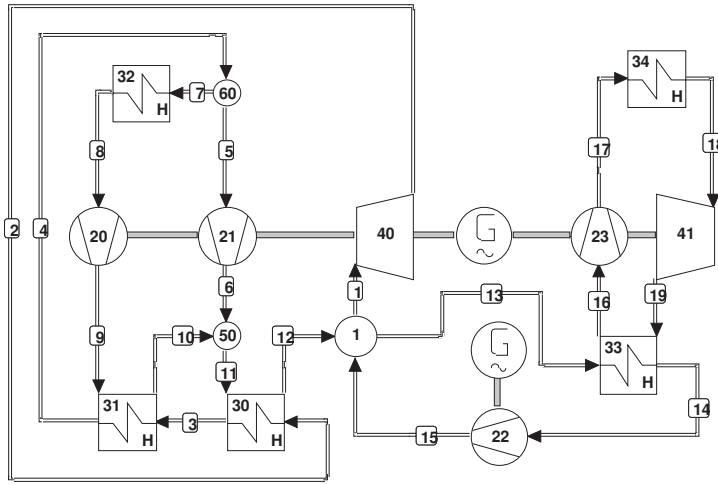


Fig. 4.18: CC_SCO₂_RIBCNR.

Organic Rankine Bottoming Cycles

Organic Rankine cycles (ORC) run on propane, butane, toluene or other organic compounds or even mixtures of water and 20% ammonia (“Kalina cycle”). They are used today to convert low temperature heat ($>80^{\circ}\text{C}$) e.g. from geothermal water to electricity. Machines for these cycles are produced by several companies worldwide and reach a heat-to-electricity efficiency of $< 23\%$ for capacities < 1 MWe.

Once higher capacities have become feasible, an ORC can be used as a final bottoming cycle to further raise efficiency. This would require the main power cycle to reject its heat at a higher temperature than normal thus decreasing its efficiency but making large amounts of heat available for further electricity generation. In the case of a classical steam cycle, steam is rejected to the condenser at approx. $30\text{--}40^{\circ}\text{C}$ depending on the temperature of the heat sink. To use an ORC, steam could be bled from the low pressure turbine at about 150°C instead and directed to the ORC steam generator.

In this case, a supercritical steam cycle would decrease from 50% efficiency to approx. 39%, but the overall efficiency would increase to 53%.

4.7.2 Use of Other Reactors as the Heat Source

So far, only High Temperature Reactors were considered as the heat source. As shown in section IV.B, a CC_B2CR_RB1CNR based on an HTR with an outlet temperature of 550°C would still achieve a thermal efficiency above 75%. Therefore, all Generation IV International Forum concepts [77] may actually be used as the primary heat source in combination with a heat pump cycle to produce high temperature process heat, e.g. for hydrogen production, although at different efficiencies. This would further enable reducing the temperature requirements on a VHTR to values that are feasible in the nearer term.

Table 4.15: *Primary coolant outlet temperatures of GIF concepts.*

GIF system	Coolant outlet temperature
VHTR	1000°C
GFR	850°C
LFR	$550 - 800^{\circ}\text{C}$
MSR	$> 700^{\circ}\text{C}$
SFR	550°C
SCWR	550°C

Fig. 4.19 and Fig. 4.20 show possible layouts for various GIF concepts in view of co-generation of high temperature process heat and electricity.

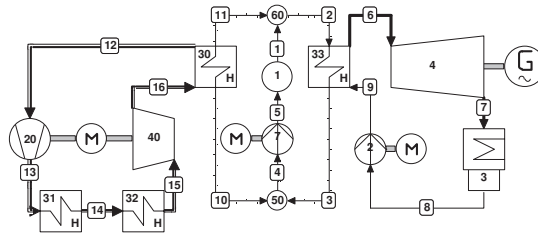


Fig. 4.19: Possible LFR, MSR, SFR or SWCR power conversion cycle: CC_SCW_RIBCNR.

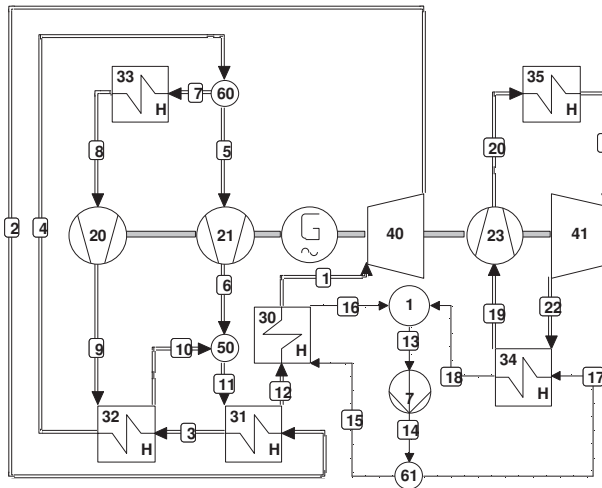


Fig. 4.20: Possible LFR, MSR, SFR or SWCR power conversion cycle: CC_SCO₂_RIBCNR.

4.8 Conclusions

This chapter discussed the use of the reverse Brayton cycle as a heat pump to reach VHTR process heat and efficiency objectives. This opens opportunities to design innovative, flexible and efficient power conversion cycles that can be adapted to virtually all Generation IV International Forum reactor concepts as well as to existing or near-term reactor designs such as the Advanced Gas Cooled Reactor (AGR), HTR or other heat sources. While so far only HTR technology was investigated as the primary heat source, it is planned to pursue efforts towards other concepts and to enable feasible configurations with significantly less stringent technology requirements, in particular for the VHTR.

Based on this enabling technology and the expectation that switching to a hydrogen or methanol economy would require much more high temperature process heat than

produced by current VHTR designs, innovative layouts were developed enabling delivery of high temperature process heat in the required narrow temperature window.

This study showed the feasibility of nearer term hydrogen production and other high temperature process heat applications while avoiding costly and time consuming R&D of VHTR. The induced penalty for replacing VHTR by AGR is approx. 17% points of overall efficiency with the resulting efficiency still exceeding 50%.

Finally, a short feasibility study for combined cooling and desalination based on the technology developed in the previous objectives was performed. For these combined applications, a coefficient of performance significantly larger than unity was calculated. This figure can be further raised but complicates the cycle layout.

In all three objectives, an economical study is required to assess whether these technical achievements make economical sense.

4.9 Legend

Index	
1	Reactor
2	Water pump
3	Condenser
4	Steam turbine
5	Pre-heater
6	Process-heat source
7	circulator (Process-heat or primary coolant)
8	Process-heat sink
2X	Helium compressor
3X	Heat exchanger
4X	Helium turbine
5X	Mixer
6X	Splitter

5 Conclusions and discussion

Since Carnot's law has been formulated, technical developments (among others new materials and power conversion units) have been engineered to further raise temperature and thus efficiency, aiming at better economics, reduced resource consumption and emissions. A more recent trend also tends to justify higher temperatures: Process heat applications, and in particular the thermo-chemical production of bulk hydrogen which at first glance seemed to require reactor outlet temperatures of the order of 1000°C.

However, higher temperatures introduce challenges that then jeopardise the safety of the nuclear reactor (lower temperature margin before fuel failure) and unnecessarily delay the deployment of this reactor concept. The main objective of this thesis is therefore to improve reactor performances, while preserving its key safety features.

The objective of **Chapter 2** was to study and qualify fuels under stringent irradiation conditions. This chapter has shown that the particle technology, although developed in the 1970s, is mature enough to fulfil today's expectations in term of integrity at high temperature up to elevated burn-ups.

Chapter 2 also analyses graphite contamination with heavy metals as a source of parasitic fission gas release. If high fuel quality indeed prevents release of fission products from the particles, the large volume of structural and functional graphite in an HTR core contributes to the radioactivity source term. This needs to be assessed and eventually corrected. A possible way to solve this issue would be to recycle irradiated graphite. The FP7 project CARBOWASTE (www.carbowaste.eu) currently investigates techniques for graphite decontamination and recycling which could also reduce stockpiles of irradiated graphite and preserve resources.

If HRF-EU1 experiment proved successful, previous experiments have shown that both high burn-up and high temperature tend to weaken the coatings while increasing gas pressure build-up inside the particle, potentially leading to particle failure. Through this multidisciplinary thesis, two different options were therefore investigated to alleviate the temperature constraints:

1. Wallpaper fuels have been scrutinized in **Chapter 3** by means of neutronic calculations. By placing particles farer away from the pebble center, one can reduce particle temperature, which positively impacts pressure build-up and particle failure.

Due to manufacturing issues, wallpaper fuel exhibited bad irradiation performance and fell into oblivion. In parallel, a modification of the production process brought regular HTR fuel to its current high quality. It is expected that this newer production process could easily be adapted to Wallpaper fuel, solving production issues. This newly produced fuel would then need to be qualified against existing fuel under irradiation.

Furthermore, by selecting variant 2 of this fuel type, one can extend the burn-up by 5%, while maintaining the reactor critical. As demonstrated in Chapter 3, this improves economics by reducing either the need for fresh fuel supply or the required enrichment.

In addition, by extending fuel burn-up, by reducing the conversion ratio and by reducing the temperatures (which then decrease neutron absorption by ^{238}U) the minor actinide production is significantly reduced.

Finally, Chapter 3 started to investigate how burn-up could be increased by decreasing the core temperature. Lower temperatures lead to higher reactivity that can be used for extending the burn-up, which in the end might produce more energy. This thesis recommends completing this study with PANTHERMIX simulations for finding the optimal temperature vs. burn-up operating conditions for the reactor. Such a study would a) define new targets for future fuel irradiations (Chapter 2), b) impact the particle failure fraction (Chapter 3) and c) potentially require the use of reverse Brayton cycle (Chapter 4) to achieve higher process heat temperatures.

2. **Chapter 4** presents the concept of reverse Brayton cycle which, like a heat pump, transforms low temperature into higher exergy. The main interest of this technology would be to operate the nuclear reactor at lower temperature, while restraining high temperature to few components in the conventional part of the power conversion system. Operating the reactor at lower temperature would improve the safety features, while one of the key assets of HTR design (capability to deliver process heat at very high temperature) would be preserved.

Chapter 4 further investigates the concept of reverse Brayton cycle in view of concentrating process heat production to high temperatures: Current designs aim at a process heat production comprised between reactor inlet and reactor outlet temperatures. Thanks to heat pumps the output temperature of the reactor can be first raised and then concentrated in a secondary cycle above the reactor outlet temperature for use in specific applications. Besides raising the reactor overall efficiency, this very flexible power conversion system can be adapted to the needs of a large variety of high temperature processes, including those only operating at high temperature.

Test reactors, based on HTR technology, have accumulated a significant experience. However no full-scale industrial demonstrator has been build so far, which can be traced back to excessive ambitions for such demonstrator. In parallel, the current demonstration projects HTR-PM (in China) and NGNP (in the US) are likely to be successful as they apply a “low-tech fast track” approach, remain at conventional reactor temperatures and produce steam.

For maximum robustness, Chapter 4 suggests to couple a reverse Brayton cycle with a reactor of proven technology, such as for instance AGR. This would serve as a validation experiment for large components, while reducing development risks, costs and delays. However the economical viability of the different reactor products (electricity, process heat or both) is yet to be assessed.

If technically feasible, one needs to balance the economical gains of simplicity and low-cost materials, higher efficiency against a more complex power conversion system.

All in all, this thesis demonstrates the versatility of this (SMR)-type of reactor, which can operate with different fuel designs and deliver both electricity and/or process heat, following customer's expectations. Coupled to a potential economy of scale, this versatility would then turn into better economics: "Qui peut le plus, peut le moins".

This thesis suggests by several approaches to render the technology of HTR credible and robust in view of a short-term demonstration.

- On the fuel side, it was shown that the fuel of current HTR is fully satisfying for short-term applications but that there is still potential for further improvements by relatively minor modifications of the design.
- On the power conversion side, a new process was proposed which opens an even wider range of applications for HTR than before, while keeping the reactor itself at very conservative operating conditions.

Appendix A: Particle temperature in a Wallpaper fuel

A.1 Temperature profile

This chapter presents the equations for the temperature profile across a wallpaper fuel element. The following parameters are introduced:

r : radial coordinate in the pebble geometry [cm]

R_c : radius of the central fuel free zone of the pebble 2.20 cm

R_i : radius of the fuel zone of the pebble 2.5 cm

R_o : radius of the pebble 3.0 cm

$TCZ(r)$: Temperature in the central fuel free zone ($0 < r < R_c$) [K]

$TFZ(r)$: Temperature in the fuel zone ($R_c < r < R_i$) [K]

$TSh(r)$: Temperature in the pebble shell ($R_i < r < R_o$) [K]

T_o : Temperature at the surface of the pebble [K]

T_c : Temperature at the centre of the pebble [K]

P : Power generated by the pebble [W/pebble]

λ : Thermal conductivity coefficient for graphite [W/cm/K]

λ_{fz} : Thermal conductivity coefficient for the fuel zone [W/cm/K]

The stationary heat equations (in radial coordinates) for fuel zone and pebble shell are available in [10]. These read

For the Fuel Zone:
$$\frac{1}{r^2} \frac{d}{dr} \left(r^2 \lambda_{fz} \frac{dT_{fz}}{dr} \right) = - \frac{P}{\frac{4}{3} \pi (R_i^3 - R_c^3)}$$

For the Shell (and CFFZ since no power is produced there):
$$\frac{1}{r^2} \frac{d}{dr} \left(r^2 \lambda \frac{dT_{CZ/Sh}}{dr} \right) = 0$$

with the boundary conditions:

$r = 0 : \frac{dT_{CZ}}{dr} = 0$	$r = R_c : \frac{dT_{CZ}}{dr} = \frac{dT_{fz}}{dr} = 0$ and $T_{CZ} = T_{fz}$
$r = R_i : T_{fz} = T_{sh}$	$r = R_o : T_{sh} = T_o$

Solving the differential equations in combination with the boundary conditions results in:

$$T_{Sh}(r) = T_0 + \frac{P}{4\pi\lambda} \left(\frac{1}{r} - \frac{1}{R_0} \right)$$

$$T_{FZ}(r) = T_0 + \frac{P}{4\pi\lambda} \left(\frac{1}{Ri} - \frac{1}{R_0} \right) + \frac{P}{4\pi\lambda_{FZ}(Ri^3 - Rc^3)} \left(\frac{Ri^2 - r^2}{2} + \frac{Rc^3}{Ri} - \frac{Rc^3}{r} \right)$$

$$T_{CZ}(r) = T_0 + \frac{P}{4\pi\lambda} \left(\frac{1}{Ri} - \frac{1}{R_0} \right) + \frac{P}{4\pi\lambda_{FZ}(Ri^3 - Rc^3)} \left(\frac{Ri^2 - Rc^2}{2} + \frac{Rc^3}{Ri} - \frac{Rc^3}{Rc} \right)$$

This shows that the temperature is constant in the central fuel free zone and decreases through the fuel free zone and the shell. The maximal temperature reads:

$$T_0 + \frac{P}{4\pi\lambda} \left(\frac{1}{Ri} - \frac{1}{R_0} \right) + \frac{P}{4\pi\lambda_{FZ}(Ri^3 - Rc^3)} \left(\frac{Ri^2 - Rc^2}{2} + \frac{Rc^3}{Ri} - \frac{Rc^3}{Rc} \right)$$

The temperature differences across the three zones (and the pebble) read

$$\Delta T_{CZ} = 0$$

$$\Delta T_{FZ} = \frac{P}{4\pi\lambda_{FZ}(Ri^3 - Rc^3)} \left(\frac{Ri^2 - Rc^2}{2} + \frac{Rc^3}{Ri} - \frac{Rc^3}{Rc} \right)$$

$$\Delta T_{Sh} = \frac{P}{4\pi\lambda} \left(\frac{1}{Ri} - \frac{1}{R_0} \right)$$

$$\Delta T = \frac{P}{4\pi\lambda} \left(\frac{1}{Ri} - \frac{1}{R_0} \right) + \frac{P}{4\pi\lambda_{FZ}(Ri^3 - Rc^3)} \left(\frac{Ri^2 - Rc^2}{2} + \frac{Rc^3}{Ri} - \frac{Rc^3}{Rc} \right)$$

For a pebble bed with an overall power of 400 MW filled with 450.000 fuel elements, the power per pebble is equal to $P=889$ W. If we assume a heat conductivity coefficient of $\lambda=26$ W/m/K [125] for the graphite and the fuel zone, the maximal temperature difference over the pebble becomes $\Delta T = 24.75K$, to be compared with $\Delta T = 72.55K$ for a conventional fuel.

A.2 Average temperatures

With constant temperature in the central fuel free zone, the average temperature equals the temperature.

The average temperature in the fuel zone becomes:

$$T_{FZ}^{ave} = \frac{\int_{R_c}^{R_i} T_{FZ}(r) 4\pi r^2 dr}{\int_{R_c}^{R_i} 4\pi r^2 dr} = \frac{\int_{R_c}^{R_i} T_{FZ}(r) r^2 dr}{\int_{R_c}^{R_i} r^2 dr}$$

$$T_{FZ}^{ave} = T_0 + \frac{P}{4\pi\lambda} \left(\frac{1}{R_i} - \frac{1}{R_0} \right) + \frac{P}{4\pi\lambda_{FZ}(R_i^3 - R_c^3)} \left\{ \frac{R_i^2}{2} + \frac{R_c^3}{R_i} - \frac{3}{(R_i^3 - R_c^3)} \left\{ \frac{R_i^5 - 6R_c^5 + 5R_c^3 R_i^2}{10} \right\} \right\}$$

The average temperature in the pebble shell becomes:

$$T_{Sh}^{ave} = \frac{\int_{R_i}^{R_0} T_{Sh}(r) 4\pi r^2 dr}{\int_{R_i}^{R_0} 4\pi r^2 dr} = T_0 + \frac{P}{4\pi\lambda} \left\{ \frac{3}{2} \frac{R_0^2 - R_i^2}{R_0^3 - R_i^3} - \frac{1}{R_0} \right\}$$

Since the wallpaper fuel enables graphite density to be raised in the Central Fuel Free Zone, the graphite temperature, averaged over the entire pebble, is equal to the graphite mass weighted average of the average temperatures of the central fuel free zone, the fuel zone and pebble shell, and hence reads

$$T_{Peb}^{ave} = \frac{M_{GCF} T_{CF}^{ave} + M_{GFZ} T_{FZ}^{ave} + M_{GSh} T_{Sh}^{ave}}{M_{GCF} + M_{GFZ} + M_{GSh}}$$

A.3 Temperature increase vs. particle packing fraction

In this section, influence of particle packing fraction on the temperature increase in a wallpaper fuel is investigated.

According to A.1, $\Delta T = \frac{P}{4\pi\lambda} \left(\frac{1}{R_i} - \frac{1}{R_0} \right) + \frac{P}{4\pi\lambda_{FZ}(R_i^3 - R_c^3)} \left(\frac{R_i^2 - R_c^2}{2} + \frac{R_c^3}{R_i} - \frac{R_c^3}{R_c} \right)$

According to [3], $\lambda_f = \lambda^* \frac{1 - PPF}{1 + 0.5 * PPF}$. This leads to $R_c = \left(R_i^3 - Np * \frac{Rp^3}{PPF} \right)^{\frac{1}{3}}$ with

PPF particle packing fraction, Np and Rp number and radius of particles.

$$\Delta T = \frac{P}{4\pi\lambda} \left[\frac{1}{R_i} - \frac{1}{R_o} + \frac{(1 + 0.5 * PPF)}{(1 - PPF) * \left(\frac{Np}{PPF} * Rp^3 \right)} \left(\frac{3}{2} R_i - \frac{Np}{PPF} * \frac{Rp^3}{R_i} - \frac{3}{2} \left(R_i^3 - \frac{Np}{PPF} * Rp^3 \right)^{\frac{2}{3}} \right) \right]$$

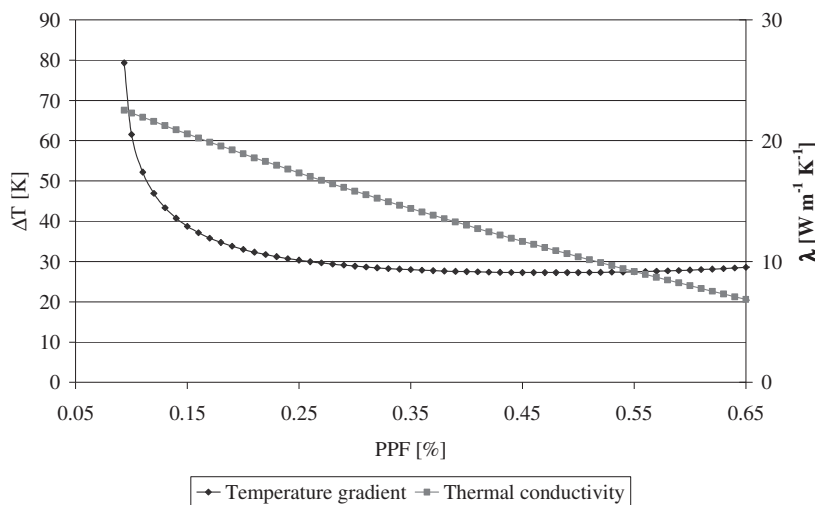


Fig. A.1: *Temperature gradient as a function of particle packing fraction.*

Fig. A.1 shows that, for low particle packing fraction, the temperature gradient decreases although the thermal conductivity is also decreasing. It reaches a minimum around 48% in particle packing fraction and then increases back.

Appendix B: Influence of particle packing fraction on fuel zone thermal conductivity

B.1 Introduction

The point here is to verify Kania [136] assumption concerning graphite thermal conductivity to accommodate for the presence of particles in the fuel zone: Since the fuel zone contains coated particles, its thermal conductivity differs from pure graphite. A suggestion was made to correct the fuel zone thermal conductivity by multiplying with the following factor:

$$Fp = \frac{1 - PPF}{1 + 0.5 * PPF}, \text{ where PPF stands for particle packing fraction}$$

B.2 Modelling

In HTR fuel, particles are mixed with graphite matrix inside the fuel zone. Heat produced by particles is conducted via the graphite from the warm places to the cold ones. In steady state operations, this means that heat is conducted from the center to the surface of the pebble. Therefore particles see a polarized heat flux. A TRISO particle is composed of a UO_2 kernel coated by four different layers. This particle is embedded in a graphite matrix, whose geometry deserves special attention. In this appendix, thermal conductivity is assumed constant for each material (i.e. not temperature dependant).

B.2.1 Particle thermal conductivity by integration method

The method described here consists of two distinct steps:

- 1- The particle is divided in radial direction according to the number of materials.
- 2- For each radial zone, material thicknesses are determined as a function of radius.
- 3- For each radial zone, thermal conductivity at the radius r is the averaged thermal conductivity (determined by serie smearing) of the different materials present at radius r .
- 4- The radial zone equivalent thermal conductivity is determined as the integration of the thermal conductivity over the radius r within the radial zone.
- 5- The particle equivalent thermal conductivity is determined by the parallel smearing of the different radial zone according to there projected surface.

In other words and as shown in Fig. B.1 with M being the number of materials; V_μ being the volume of the M materials within the radial zone defined by $r \in [r_{\mu-1}; r_\mu]$ and S_μ being the section of the radial zone defined by $r \in [r_{\mu-1}; r_\mu]$.

1- Radial zones are determined by the outer radius of the coatings r_μ .

2- The thickness H_μ of material μ is determined by:

For $0 < r < r_{\mu-1}$:

For $r_{\mu-1} < r < r_\mu$:

$$H_\mu(r) = 2\left(\sqrt{r_\mu^2 - r^2} - \sqrt{r_{\mu-1}^2 - r^2}\right)$$

$$H_\mu(r) = 2\sqrt{r_\mu^2 - r^2}$$

3- The thermal conductivity at radius r $\lambda_\mu(r)$ of all $M-\mu+1$ materials, for $r \in [r_{\mu-1}; r_\mu]$, is determined by:

$$\lambda_\mu(r) = \sum_{i=\mu}^M H_i(r) / \sum_{i=\mu}^M \frac{H_i(r)}{\lambda_i}$$

4- The equivalent thermal conductivity (radial averaged) $\lambda_{\mu_{av}}$ of all $M-\mu+1$ materials, for $r \in [r_{\mu-1}; r_\mu]$, is determined by:

$$\lambda_{\mu_{av}} = \frac{2\pi \int_{r_{\mu-1}}^{r_\mu} \lambda_\mu^2(r) dr}{V_\mu}$$

$$= \frac{2\pi}{V_\mu} \int_{r_{\mu-1}}^{r_\mu} \left(\frac{\sum_{i=\mu}^M H_i(r)}{\sum_{i=\mu}^M \frac{H_i(r)}{\lambda_i}} \right)^2 dr$$

$$= \frac{2\pi}{V_\mu} \int_{r_{\mu-1}}^{r_\mu} \left(\frac{H_M(r)}{\sum_{i=\mu}^M \frac{H_i(r)}{\lambda_i}} \right)^2 dr$$

5- Particle equivalent thermal conductivity λ_{Eq} is determined by:

$$\lambda_{Eq} = \frac{\sum_{\mu=1}^{\mu=M} \lambda_{\mu_{av}} * S_\mu}{\sum_{\mu=1}^{\mu=M} S_\mu}$$

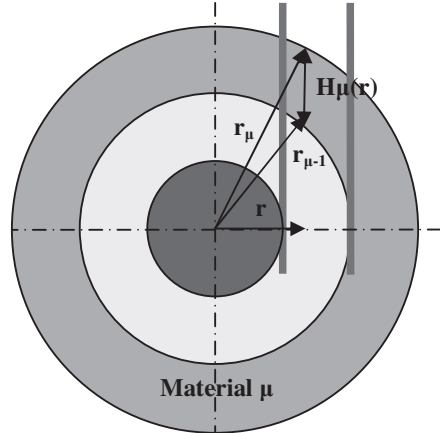


Fig. B.1: Material thickness determination.

B.2.2 Particle thermal conductivity by mean chord length conservation method

The spherical geometry of the TRISO particle, coupled to a unidirectional power flow, makes it difficult to model the thermal conductivity as such. Therefore, mean chord length and volume conservation method were used to model the couple TRISO/Matrix in a more practical way, namely cylinders. The method consists of different steps, as shown on Fig. B.2:

- 1- Transformation from spherical to cylindrical geometry
- 2- Axial (serie) smearing of the particle
- 3- Radial (parallel) smearing of the particle

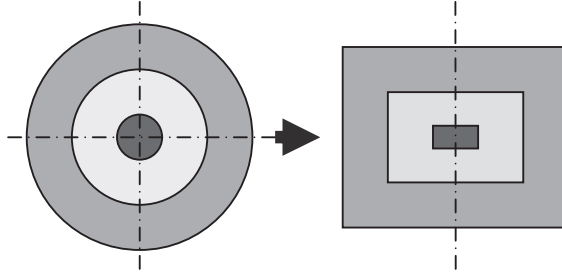


Fig. B.2: Mean chord length conservation method.

For a convex body, mean chord length is given in [125] and [153] as $\langle R \rangle = 4V/S$, where V is the volume of the body and S the outer surface.

For a sphere, mean chord length is $\langle R_s \rangle = 4R_s/3$ and the volume $V_s = 4\pi R_s^3/3$.

For a cylinder of radius R_c and length H_c , the mean chord length is $\langle R_c \rangle = 2(R_c H_c)/(R_c + H_c)$ and the volume is $V_c = \pi H_c R_c^2$.

However, the conservation of mean chord lengths and the volumes, as defined above, does not provide any results. Therefore a second approximation is considered: The cylinder is assumed being of infinite dimensions along its axis, leading to a mean chord length of $\langle R_a \rangle = 2R_c$. Hence $R_c = 2r/3$ and $H_c = 3r$.

In comparison with the correct mean chord length equation, this leads to an error of $\frac{\langle R_c \rangle - \langle R_a \rangle}{\langle R_c \rangle} = -\frac{R_c}{H_c} = -\frac{2}{9} \approx -22.22\%$ on the mean chord length, but none on the volumes.

B.2.3 Graphite matrix geometries

Variation of particle packing fraction leads to variation of the matrix graphite to be considered. The geometry of this graphite is important (It is however assumed that thermal conductivities do not depend on temperature and fluence). Therefore three geometries will be considered, as shown in Fig. B.3:

- 1- Particles are embedded in a cube of graphite matrix, whose dimension is tuned to accommodate PPF.
- 2- Particles are embedded in a tight cylinder of graphite matrix. The matrix leftover is considered as an added cylinder.
- 3- Particles are embedded in a shell of graphite matrix, whose dimension is tuned to accommodate PPF. Only this approach is considered for particle thermal conductivity determined by mean chord length conservation method.

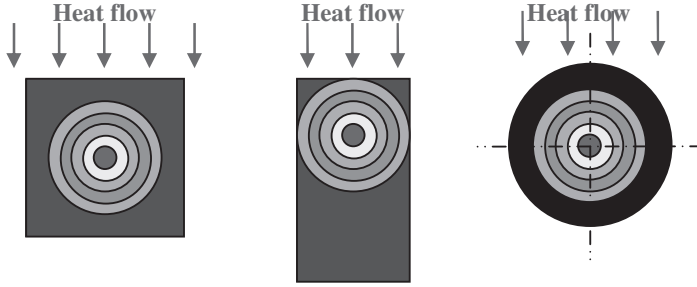


Fig. B.3: *Different graphite matrix geometry.*

B.3 Thermal conductivity calculation

Depending on the method for the determination of particle thermal conductivity, numerical solutions can be achieved by two different means:

- 1- The integration method does not allow the determination of analytical solutions. Therefore a Monte-Carlo method was developed below for numerical solutions.
- 2- The approximated mean chord length method transform spherical into cylindrical geometry. Based on these simple geometries and rules laid down below, analytical solutions can be retrieved.

B.3.1 Numerical determination: Monte-Carlo method

Since the radial averaged equivalent thermal conductivity $\lambda_{\mu_{av}}$ cannot be solved numerically by the integration method, one can develop a Monte-Carlo method to determine statistically the value of the particle thermal conductivity:

- 1- An axial position s is randomly generated between 0 and r^2 .
 - 2- $H_\mu(r = \sqrt{s})$ are determined thanks to the integration method equations, leading to $\lambda_\mu(r)$.
 - 3- Previous steps are repeated 10^5 times to determine average thermal conductivity.
- To achieve a correct statistical error, 10^5 positions were sampled. This figure has been determined by the number of positions required to achieve convergence of the thermal conductivity of one particle, as displayed in Fig. B.4.

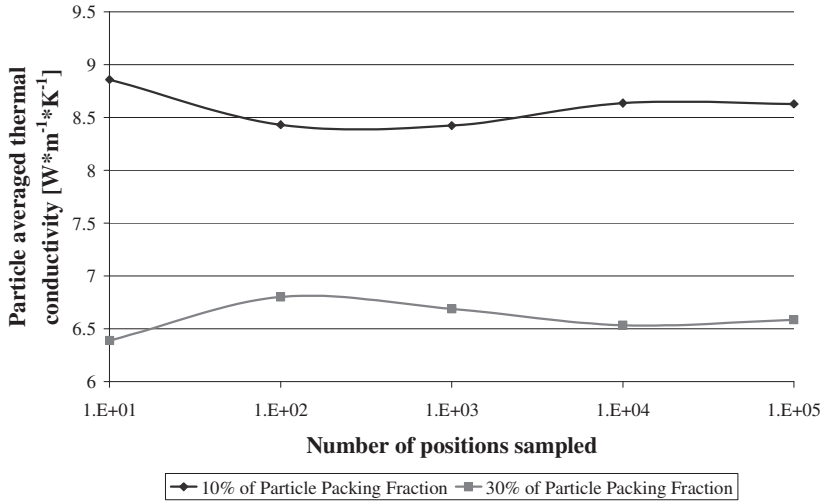


Fig. B.4: Thermal conductivity vs. number of data sampled.

B.3.2 Rules for equivalent thermal conductivity determination

When several materials of the same section but different thermal conductivity and length are placed in serie, the equivalent thermal conductivity value is determined by the following formula, where l_i and λ_i are the length and thermal conductivity of material i :

$$\lambda_{Eq} = \frac{\sum \Delta l_i}{\sum \frac{\Delta l_i}{\lambda_i}}$$

When several materials of the same length but different thermal conductivity and section are placed in parallel, the equivalent thermal conductivity value is determined by the following formula, where S_i and λ_i are the surface and thermal conductivity of material i :

$$\lambda_{Eq} = \frac{\sum S_i * \lambda_i}{\sum S_i}$$

B.4 PBMR fuel as an example

Table B.1 displays PBMR particle characteristics. With approx. 15000 particles of .46 mm radius for a 25 mm fuel zone, the particle packing fraction is around 9.34%.

Table B.1: *PBMR fuel geometry.*

Kernel radius [μm]	250	
Thickness of coatings [μm]		Outer radius [μm]
Buffer	95	345
IPyC	40	385
SiC	35	420
OPyC	40	460
Particle packing fraction [-]	PPF	9.34%

Table B.2 displays thermal conductivity values, taken from [155].

Table B.2: *Thermal conductivity values.*

Material	Thermal conductivity [W/m/K]
Kernel	3.46
Buffer	1
IPyC	4
SiC	18.3
OPyC	4
Matrix	25

Integration method with Monte-Carlo solution is used to determine the thermal conductivity values for the three graphite geometries, as shown in Table B.4.

For the determination of λ by mean chord length method, the equivalent cylinder dimensions, as displayed in Table B.3, are required.

Table B.3: *Equivalent cylinder dimensions [mm].*

Material	Radius	Cylinder length for r				
		<rKernel	<rBuffer	<rIPyC	<rSiC	<rOPyC
Kernel	0.167	2.22E-01				
Buffer	0.230	5.24E-01	6.67E-02			
IPyC	0.257	6.79E-01	1.32E-01	2.72E-02		
SiC	0.280	8.30E-01	1.95E-01	7.86E-02	2.37E-02	
OPyC	0.307	1.02E+00	2.74E-01	1.43E-01	8.20E-02	2.71E-02

Using thermal conductivity values of Table B.2, one can determine the particle equivalent thermal conductivity, which can then be ponderated with the matrix one according to the same method:

Matrix radius is particle packing fraction dependant: $R_m = R_p / PPF^{\frac{1}{3}}$

Hence its equivalent cylinder radius: $R_{cm} = 2R_p / 3PPF^{\frac{1}{3}}$

And length: $H_{cm} = 3R_p / PPF^{\frac{1}{3}}$

Table B.4 and Fig. B.5 represent graphite matrix thermal conductivity as function of particle packing fraction and geometry.

Table B.4: *Thermal conductivity values.*

Method	Kania	Monte-Carlo	M-C	M-C	MCL
PPF	Overcoating in cube		Overcoating in cylinder	Overcoating in sphere	Overcoating in sphere
0	25.00	25.00	25.00	25.00	25.00
5%	23.17	22.37	20.59	22.94	22.66
10%	21.43	20.56	17.87	21.49	21.07
15%	19.77	18.97	15.97	20.14	19.71
20%	18.18	17.55	14.55	19.00	18.47
25%	16.67	16.19	13.44	17.82	17.31
30%	15.22	14.90	12.51	16.71	16.22
35%	13.83	13.71	11.72	15.77	15.19
40%	12.50	12.55	11.04	14.69	14.20
45%	11.22	11.42	10.46	13.69	13.24
50%	10.00	10.34	9.93	12.72	12.31
55%	8.82		9.48	11.81	11.41
60%	7.69		9.08	10.86	10.54
65%	6.60		8.73	9.95	9.68
70%	5.56		8.39	9.00	8.85

One should first notice that particle modelling method impacts thermal conductivity: The difference between Monte-Carlo and mean chord length method (both with spherical overcoating) reaches up to 3.6%. This difference can be partly explained by the approximation made on the equivalent cylinder geometry: The infinite cylinder is thinner and longer, therefore (as explained below) its equivalent thermal conductivity is lower. The mean chord length method is therefore less accurate than the integration method.

When considering the Monte-Carlo method, thermal conductivity can differ by up to 34% depending on the matrix graphite overcoating geometry. This is a result of the

heat flux polarisation, where long models are more impacted than compact ones: When switching from spherical overcoating to cubic and to cylindrical, the heat fraction crossing the particle increases. The particle serves more and more as an isolation layer and therefore reduces the effective thermal conductivity.

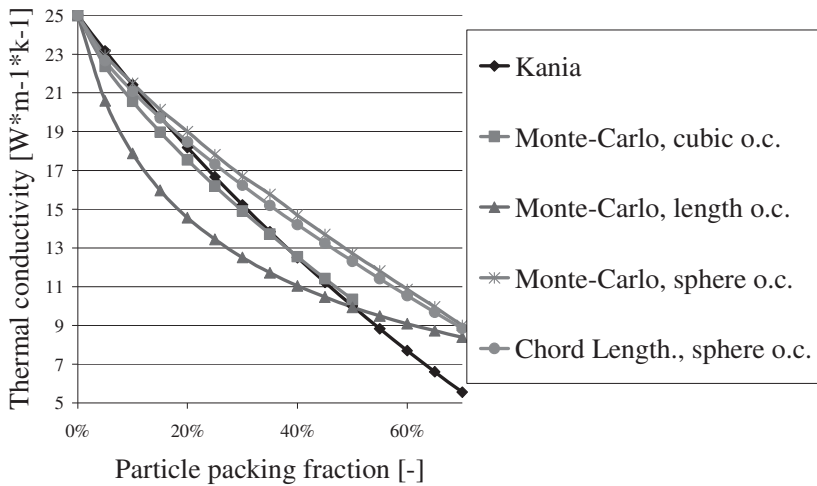


Fig. B.5: *Different graphite matrix geometry.*

It should be noted that the real matrix geometry is dependant on the production process and therefore undefined.

In comparison with the Kania model, the best method is the Monte-Carlo one with cubic overcoating geometry.

Although the Kania model does not consider particle materials, the results of this model lay within the range of values achieved by the integration method with the different geometries. If this seems surprising, one should however consider that this model might have been defined experimentally, implicitly using the thermal conductivity value of the different materials.

Nomenclature

Abbreviations

AGR	Advanced Gas Cooled Reactor
ANE	Averaged Neutron Energy
ATBR	A Thorium Breeder Reactor
ATR	Advanced Test Reactor
AVR	Arbeitsgemeinschaft Versuchsreaktor
B1CNR	Brayton cycle with one Compressor and no Recuperator
B2CR	Brayton cycle with two Compressors and Recuperator
BISO	Bi-Isotropic
BOI	Beginning Of Irradiation
CC	Combined Cycle
CCCTF	Core Conduction Cooldown Test Facility
CR	Conversion Ratio
CRYSTAL	Code foR analYsis of STress in coAted particLes
DLOCA	Depressurized Loss of forced Cooling Accident
EFPD	Effective Full Power Day
EOI	End Of Irradiation
FGR	Fission Gas Release
FP	Fission Product
GIF	Generation IV International Forum
HEU	High Enriched Uranium
HFR	High Flux Reactor
HP	Heat Pump or RB1CNR
HPHT	High Process Heat Temperature
LPHT	Low Process Heat Temperature
HTGR	High Temperature Gas-cooled Reactor
HTR	High Temperature Reactor
HTR-TN	European High Temperature Reactor Technology Network
HTSE	High Temperature Steam Electrolysis

HTTR	High Temperature Engineering Test Reactor
IHX	Intermediate Heat Exchanger
INET	Institute of Nuclear and New Energy Technology
INL	Idaho National Laboratory
IPyC	Inner Pyrolytic Carbon
IS	Iodine-Sulfur process for H ₂ production
JAEA	Japan Atomic Energy Agency
JAERI	Japan Atomic Energy Research Institute
JEFF	Joint Evaluated Fission and Fusion File
JHR	Jules Horowitz Reactor
JMTR	Japan Materials Testing Reactor
JRC-IE	Institute for Energy of the European Commission
JRC-ITU	Inst. for Transuranium elements of the European Commission
KÜFA	Kühlfinger Apparat
LEU	Low Enriched Uranium
LFR	Lead-Cooled Fast Reactor
LWR	Light Water Reactor
MA	Minor Actinide
MCB	Monte-Carlo Continuous Energy Burnup Code
MCNP	Monte Carlo N-Particle Transport Code
MINATOM	Russian Atomic Ministry
MSR	Molten Salt Reactor
MTR	Material Test Reactor
NPP	Nuclear Power Plant
OPyC	Outer Pyrolytic Carbon
ORC	Organic Rankine Cycle
PBMR	Pebble Bed Modular Reactor
pcm	Per Cent Mil
PIE	Post Irradiation Examination
PPF	Particle Packing Fraction

RB1CNR	Reverse Brayton cycle with one Compressor and no Recuperator
RIT	Reactor Inlet Temperature
RMWR	Reduced-Moderation Water Reactor
ROT	Reactor Outlet Temperature
SAGD	Steam Assisted Gravity Drainage
S-CO ₂	Supercritical Carbon Dioxide
SFR	Sodium-Cooled Fast Reactor
SiC	Silicon Carbide
SLF	Sweep Loop Facility
SMR	Steam Methane Reforming
SWCR	Supercritical-Water-Cooled Reactor
THTR	Thorium High Temperature Reactor
TRISO	Tri-Isotropic
TRUs	Transuranics
TTA	Transmutation Trajectory Analysis code
VHTR	Very High Temperature Reactor

Symbols

$\langle R \rangle$	Mean Chord Length
p_{FNL}	Probability that a fast neutron will not leak out of the system.
p_{TNL}	Probability that a thermal neutron will not leak out of the system
$\langle R_{\text{c}} \rangle$	Mean Chord Length of a cylinder of infinite dimensions along its axis
$\langle R_{\text{C}} \rangle$	Mean Chord Length of a cylinder of radius R_{C} , length H_{C} and volume V_{C}
$\langle R_{\text{S}} \rangle$	Mean Chord Length of a sphere of radius R_{S} and volume V_{S}
CT_{F}	Fuel temperature coefficient of reactivity
CT_{FG}	Combined fuel and graphite temperature coefficient of reactivity
CT_{G}	Graphite temperature coefficient of reactivity
ΔT	Temperature differences across the pebble
ΔT_{CZ}	Temperature differences across the central fuel free zone
ΔT_{FZ}	Temperature differences across the fuel zone
ΔT_{Sh}	Temperature differences across the shell

Nomenclature

ϵ	Fast fission factor
f	Thermal utilization of the reactor
F_p	Correction factor the fuel zone thermal conductivity
η	Reproduction factor
H_μ	Thickness of material μ
λ	Thermal conductivity coefficient for graphite
λ_{Eq}	Particle equivalent thermal conductivity
λ_{FZ}	Thermal conductivity coefficient for the fuel zone
λ_μ	Thermal conductivity at radius r of all $M-\mu+1$ materials, for $r \in [r_{\mu-1}; r_\mu]$
$\lambda_{\mu av}$	Equivalent thermal conductivity (radial averaged) of all $M-\mu+1$ materials, for $r \in [r_{\mu-1}; r_\mu]$
M	Number of materials in a particle
M_{GCZ}	Graphite mass in the central fuel free zone
M_{GFZ}	Graphite mass in the fuel zone
M_{GSh}	Graphite mass in the shell
N_p	Number of particles
P	Power generated by the pebble
p	Resonance escape probability,
r	Radial coordinate in the pebble geometry
R_c	Radius of the central fuel free zone of the pebble
R_i	Radius of the fuel zone of the pebble
R_o	Radius of the pebble
R_p	Radius of particles
r_μ	Outer radius of material M
$r_{\mu-1}$	Inner radius of material M
σ	Standard deviation
S_μ	Section of the radial zone defined by $r \in [r_{\mu-1}; r_\mu]$
T_{CZ}^{ave}	Average temperature in the central fuel free zone
T_{FZ}^{ave}	Average temperature in the fuel zone
T_{Peb}^{ave}	Average temperature in the pebble
T_{Sh}^{ave}	Average temperature in the shell

T_c	Temperature at the centre of the pebble
$TCZ(r)$	Temperature in the central fuel free zone ($0 < r < R_c$)
$TFZ(r)$	Temperature in the fuel zone ($R_c < r < R_i$)
T_o	Temperature at the surface of the pebble
$TSh(r)$	Temperature in the pebble shell ($R_i < r < R_o$)
V_μ	Volume of the M materials within the radial zone defined by $r \in [r_{\mu-1}; r_\mu]$

Bibliography

- [1] International Energy Agency. Energy Technology perspectives; Scenarios & Strategies to 2050. Technical report, OECD/IEA, France, 2008.
- [2] International Atomic Energy Agency. Nuclear Power Reactors in the World. Technical Report IAEA-RDS-2/28, Vienna, Austria, July 2008. ISBN 978-92-0-107708-0.
- [3] International Energy Agency, World Energy Outlook 2010, ISBN 978-92-64-08624-1.
- [4] G. Melese, R. Katz, Thermal and flow design of helium cooled reactors. American Nuclear Society, 1984. ISBN 0-89448-027-8.
- [5] C.A. Rennie, Achievements of the Dragon project, Annals of Nuclear Energy, Volume 5, Issues 8-10, 1978, Pages 305-320.
- [6] J.L. Everett, E. Kohler, Peach Bottom Unit No. 1: A High-Performance Helium-Cooled Nuclear Power Plant. Annals of Nuclear Energy, 5(321), 1978.
- [7] R. Bäumer, et al., AVR: experimental high temperature reactor; 21 years of successful operation for a future energy technology, Association of German engineers (VDI) – Düsseldorf: VDI-Verl., 1990, ISBN 3-18-401015-5.
- [8] A. Habush, A. Harris, 330-MW(e) Fort-St. Vrain High-Temperature Gas-Cooled Reactor. Nuclear Engineering and Design, 7 (312), 1968.
- [9] Das 300 MW Thorium-Hochtemperatur-Kernkraftwerk THTR. Atomwirtschaft, May 1971.
- [10] K. Kugeler, R. Schulten, Hochtemperaturreaktortechnik. Springer 1989.
- [11] H. Reutler, G.H. Lohnert, The Modular High-Temperature Reactor. Nuclear Technology, 62 (22), July 1983.
- [12] G. Brinkmann, J. Pirson, S. Ehster, M.T. Dominguez, L. Mansani, I. Coe, R. Moormann, W. Van der Mheen and HTR-L project partners, Important viewpoints proposed for a safety approach of HTGR reactors in Europe: Final results of the EC-funded HTR-L project, Nuclear Engineering and Design, Volume 236, Issues 5-6, March 2006, Pages 463-474.
- [13] P. von der Hardt, H. Röttger, Handbook of material testing reactors and associated hot laboratories in the European community, D. Reidel Publishing Company, ISBN 90-277-1347-2, 1981.
- [14] M. T. Simnad, The early history of high-temperature helium gas-cooled nuclear power reactors, Energy, Volume 16, Issues 1-2, January-February 1991, Pages 25-32.

- [15] G. Ivens, M. Wimmers, The AVR as a test bed for fuel elements, AVR: experimental high temperature reactor; 21 years of successful operation for a future energy technology, ISBN 3-18-401015-5, 1990.
- [16] M. Wimmers, Das Verhalten kugelförmiger HTR-Brennelemente bei der Massenerprobung im AVR-Reaktor, AVR Report, Arbeitsgemeinschaft Versuchs-Reaktor, Düsseldorf, Germany (1977).
- [17] M. Hrovat, H. Nickel, K. Koizlik, Über die Entwicklung eines Matrixmaterials zur Herstellung gespresster Brennelemente für Hochtemperatur-Reaktoren. Juel-969-DW, 1973.
- [18] C. Tang, Y. Tang, J. Zhu, Y. Zou, J. Li, X. Ni, Design and manufacture of the fuel element for the 10 MW high temperature gas-cooled reactor, Nuclear Engineering and Design, Volume 218, Issues 1-3, October 2002, Pages 91-102.
- [19] K. Sawa, S. Ueta, Research and development on HTGR fuel in the HTTR project, Nuclear Engineering and Design, Volume 233, Issues 1-3, October 2004, Pages 163-172.
- [20] W. Schenk, K. Verfondern, H. Nabielek, E. H. Toscano, Limits of LEU TRISO Particle Performance, Proceedings International HTR Fuel Seminar, Brussels, Belgium, February 1-2, 2001.
- [21] H. Nickel, H. Nabielek, G. Pott, A. W. Mehner, Long Time Experience with the Development of HTR Fuel Elements in Germany, Nuclear Engineering and Design 217 (2002) 141–151.
- [22] H. Kostecka, J. Ejton, W. de Weerd, E.H. Toscano, Post-irradiation testing of HTR fuel elements under accident conditions, Proc. HTR 2004, Beijing, China, 22-24 September 2004.
- [23] S. Shiozawa, S. Fujikawa, T. Iyoku, K. Kunitomi, Y. Tachibana, Overview of HTTR design features, Nuclear Engineering and Design, Volume 233, Issues 1-3, October 2004, Pages 11-21.
- [24] N. Nojiri, S. Shimakawa, N. Fujimoto, M. Goto, Characteristic test of initial HTTR core, Nuclear Engineering and Design, Volume 233, Issues 1-3, October 2004, Pages 283-290.
- [25] W. Steinwarz, XU Yuanhui, Status of design of the HTR test module China, Nuclear Engineering and Design, Volume 121, Issue 2, 2 July 1990, Pages 317-324.
- [26] Y. Xu, K. Zuo, Overview of the 10 MW high temperature gas cooled reactor—test module project, Nuclear Engineering and Design, Volume 218, Issues 1-3, October 2002, Pages 13-23.
- [27] S. Ueta, J. Sumita, K. Emori, M. Takahashi, K. Sawa, Fuel and Fission Gas Behavior during Rise-to-Power Test of the High Temperature Engineering Test Reactor (HTTR), J. of Nuclear Science and Technology, Vol 40, p. 679-686, 2003.

-
- [28] S. Ueta, M. Umeda, K. Sawa, S. Sozawa, M. Shimizu, Y. Ishigaki, H. Obata, Preliminary Test Results for Post Irradiation Examination on the HTTR Fuel, *Journal of Nuclear Science and Technology*, Vol. 44 (2007) No. 8, pp.1081-1088.
- [29] S. Sato, A. Kurumada, K. Kawamata, N. Suzuki, M. Kaneko, K. Fukuda, Fracture mechanical properties and neutron irradiation effects of fuel compacts for the HTTR, *Nuclear Engineering and Design*, Volume 141, Issue 3, 1 July 1993, Pages 395-408.
- [30] K. Fukuda, S. Kashimura, T. Tobita, T. Kikuchi, Irradiation behavior of HTGR coated particle fuel at abnormally high temperature, *Nuclear Engineering and Design*, Volume 157, Issues 1-2, 1 July 1995, Pages 221-230.
- [31] K. Minato, T. Ogawa, K. Fukuda, H. Sekino, I. Kitagawa, N. Mita, Fission product release from ZrC-coated fuel particles during post-irradiation heating at 1800 and 2000°C, *Journal of Nuclear Materials*, Volume 249, Issues 2-3, October 1997, Pages 142-149.
- [32] K. Minato, T. Ogawa, T. Koya, H. Sekino, T. Tomita, Retention of fission product caesium in ZrC-coated fuel particles for high-temperature gas-cooled reactors, *Journal of Nuclear Materials*, Volume 279, Issues 2-3, June 2000, Pages 181-188.
- [33] C. Tang, X. Fu, J. Zhu, T. Liang, K. N. Koshcheyev, A. V. Kozlov, O. G. Karlov, Y. G. Degaltsev, V. I. Vasiliev, Fuel irradiation of the first batches produced for the Chinese HTR-10, *Nuclear Engineering and Design*, Volume 236, Issue 1, January 2006, Pages 107-113.
- [34] T.X. Liang, H.S. Zhao, C.H. Tang, K. Verfondern, Irradiation performance and modeling of HTR-10 coated fuel particles, *Nuclear Engineering and Design*, Volume 236, Issue 18, September 2006, Pages 1922-1927.
- [35] X. Luo, S. Yu, X. Sheng, S. He, Temperature effect on IG-11 graphite wear performance, *Nuclear Engineering and Design*, Volume 235, Issue 21, October 2005, Pages 2261-2274.
- [36] J. T. Maki, D. A. Petti, D. L. Knudson, G. K. Miller, The challenges associated with high burnup, high temperature and accelerated irradiation for TRISO-coated particle fuel *Journal of Nuclear Materials*, Volume 371, Issues 1-3, 15 September 2007, Pages 270-280.
- [37] J. Ahlf, R. Conrad, G.P. Tartaglia, G. Tsotridis, The HFR Petten as a test bed for fusion materials and components, *Journal of Nuclear Materials*, Volumes 212-215, Part 2, September 1994, Pages 1635-1639.
- [38] M. A. Fütterer, E. D'Agata, M. Laurie, A. Marmier, F. Scaffidi-Argentina, P. Raison, K. Bakker, S. de Groot, F. Klaassen, Next generation fuel irradiation capability in the High Flux Reactor Petten, *Journal of Nuclear Materials*, Volume 392, Issue 2, 15 July 2009, Pages 184-191.

- [39] J.A. Vreeling, O. Wouters, J.G. van der Laan, Graphite irradiation testing for HTR technology at the High Flux Reactor in Petten, *Journal of Nuclear Materials*, Volume 381, Issues 1-2, 31 October 2008, Pages 68-75.
- [40] D.K.L. Tsang, B.J. Marsden, J.A. Vreeling, J. van der Laan, Analyses of a restrained growth graphite irradiation creep experiment, *Nuclear Engineering and Design*, Volume 238, Issue 11, November 2008, Pages 3026-3030.
- [41] M. A. Fütterer, G. Berg, A. Marmier, E. Toscano, D. Freis, K. Bakker, S. de Groot, Results of AVR fuel pebble irradiation at increased temperature and burn-up in the HFR Petten, *Nuclear Engineering and Design*, Volume 238, Issue 11, November 2008, Pages 2877-2885
- [42] M. A. Fütterer, A. Marmier, J. Morand, L. Metten, A. van de Sande, Feasibility of Weak Irradiation in the HFR as a Tool for Pre-Irradiation Qualification of HTR Fuel, Technical Memorandum HFR/06/4823, D(06)26164, January 2007.
- [43] S. B. Grover, The Advanced Test Reactor irradiation capabilities available as a national scientific user facility, *International Conference on the Physics of Reactors Nuclear Power: A Sustainable Resource*, Interlaken, Switzerland, September 14-19, 2008.
- [44] D. Petti, G. Bell, AGR Team, The DOE Advanced Gas Reactor (AGR) Fuel Development And Qualification Program, *Proc. ICAPP'05*, Seoul, Korea, May 15-19, 2005.
- [45] S. B. Grover, Final Assembly and Initial Irradiation of the First Advanced Gas Reactor Fuel Development and Qualification Experiment in the Advanced Test Reactor, *Proceedings of ICAPP'07*, Nice, France, May 13-18, 2007.
- [46] D. A. Petti, S. B. Grover, J. T. Maki, Status of the first advanced gas reactor fuel irradiation experiment in the advanced test reactor, *Proc. HTR 2008*, Washington, USA, 28 September – 1 October 2008.
- [47] R. N. Morris, An assessment of ORNL PIE capabilities for the AGR program capsule post irradiation examination, *ORNL/TM-2006/526*, September 2006.
- [48] D. Iracane, P. Chaix, A. Alamo, Jules Horowitz Reactor: a high performance material testing reactor, *Comptes Rendus Physique*, Volume 9, Issues 3-4, April-May 2008, Pages 445-456.
- [49] The Oklo Phenomenon, Report on International Symposium on the Oklo Phenomenon, Libreville, Gabon, June 1975.
- [50] E. Fermi, L. Szilard, 'Neutronic Reactor', US Patent 2,708,656, 1955.
- [51] Von Halban, H. H., Joliot, J.-F., Kowarsky, L., Improvement in and relating to the liberation of atomic energy, United Kingdom Patent GB633,339, 12 December 1949.
- [52] L. Massimo, *Physics of High Temperature Reactors*, ISBN 0-08-019616-0, U.K.A.E.A., 1976

- [53] H. von Halban, F. J. Joliot, L. Kowarsky, Improvements in and relating to the production of energy through nuclear fission of uranium, GB patent 641213, 1951.
- [54] J. J. Duderstadt, L. J. Hamilton, Nuclear Reactor Analysis, John Wiley & Sons, Inc. ISBN 0-471-22363-8, 1976.
- [55] E. Merz, H. Brücher, St. Halaszovich, 1993. Lösung der Entsorgungsfrage beim Hochtemperaturreaktor. In: Kugeler, K., Neis, H., Ballensiefen, G. (Eds.), Fortschritte in der Energietechnik. Monographien des Forschungszentrums Jülich, Bd 8, pp. 336–348.
- [56] M. A. Fütterer, H. Bluhm, P. Hoppé, J. Singer, Head-End Process for the Reprocessing of Reactor Core Material, International Patent WO/2006/087360, European Patent EP1849164, publication date 24.08.2006.
- [57] M. Masson, S. Grandjean, J. Lacquement, S. Bourg, J. M. Delauzun, J. Lacombe, Block-type HTGR spent fuel processing: CEA investigation program and initial results, Nuclear Engineering and Design, Volume 236, Issues 5-6, March 2006, Pages 516-525.
- [58] T. Tsukada, K. Takahashi, N. Yoshiki, Behavior of Uranium in the Partitioning Process of PUREX Reprocessing Journal of Nuclear Science and Technology, Vol. 45 (2008) No. 2 pp.179-194.
- [59] D. L. Moses, Nuclear safeguards considerations for pebble bed reactors (PBRs), Nuclear Engineering and Design (2011), doi:10.1016/j.nucengdes.2011.10.043.
- [60] C. Rodriguez, A. Baxter, D. McEachern, M. Fikani, F. Venneri, 2003. Deep-burn: making nuclear waste transmutation practical. Nuclear Engineering and Design 222, 299.
- [61] PUMA, Integrated Project nr. 30194 of the 6th Framework Program of the European Commission, <http://www.puma-project.eu/>
- [62] D. W. McEachern et al., Deep-Burn Modular Helium Reactor Fuel Development Plan, September 2002 ORNL/TM-2002/135.
- [63] N. Kodochigov, Yu. Sukharev, E. Marova, N. Ponomarev-Stepnoy, E. Glushkov, P. Fomichenko, Neutronic features of the GT-MHR reactor, Nuclear Engineering and Design, Volume 222, Issues 2-3, June 2003, Pages 161-171.
- [64] H. J. Rütten, K. A. Haas, Research on the incineration of plutonium in a modular HTR using thorium-based fuel, Nuclear Engineering and Design, Volume 195, Issue 3, 2 February 2000, Pages 353-360.
- [65] H. J. Rütten, C. E. Lee, E. Teuchert, The Pebble-Bed HTR as a Net-Breeding Reactor System, KFA Jülich report Jül-1521, July 1978, ISSN 0336-0885.
- [66] H. Chang, Y. Yang, X. Jing, Y. Xu, Thorium-Based Fuel Cycles in the Modular High Temperature Reactor, Tsinghua Science & Technology, Volume 11, Issue 6, December 2006, Pages 731-738.

- [67] Thorium based fuel options for the generation of electricity: Developments in the 1990s, International Atomic Energy Agency, Vienna (Austria), IAEA-TECDOC—1155.
- [68] Thorium fuel utilization: Options and trends, Proceedings of three IAEA meetings held in Vienna in 1997, 1998 and 1999, International Atomic Energy Agency, Vienna (Austria), IAEA-TECDOC—1319.
- [69] Thorium fuel cycle — Potential benefits and challenges, International Atomic Energy Agency, Vienna (Austria), IAEA-TECDOC—1450.
- [70] D. B. Trauger, Thorium utilisation, *Annals of Nuclear Energy*, Vol. 5, pp. 375-403, 1978.
- [71] S. Permana, N. Takaki, H. Sekimoto, Power density effect on feasibility of water cooled thorium breeder reactor, *Progress in Nuclear Energy*, Volume 50, Issues 2-6, March-August 2008, Pages 308-313.
- [72] S. Permana, N. Takaki, H. Sekimoto, Preliminary study on feasibility of large and small water cooled thorium breeder reactor in equilibrium states, *Progress in Nuclear Energy*, Volume 50, Issues 2-6, March-August 2008, Pages 320-324.
- [73] S. Şahin, K. Yıldız, H. M. Şahin, A. Acır, Investigation of CANDU reactors as a thorium burner, *Energy Conversion and Management*, Volume 47, Issues 13-14, August 2006, Pages 1661-1675.
- [74] V. Jagannathan, Usha Pal, Towards an intrinsically safe and economic thorium breeder reactor, *Energy Conversion and Management*, Volume 47, Issue 17, October 2006, Pages 2781-2793.
- [75] S. Permana, N. Takari, H. Sekimoto, Breeding Capability and Void Reactivity Analysis of Heavy-Water-Cooled Thorium Reactor, *Journal of Nuclear Science and Technology*, Vol. 45 (2008) No. 7, pp.589-600.
- [76] A. Nuttin, D. Heuer, A. Billebaud, R. Brissot, C. Le Brun, E. Liatard, J.-M. Loiseaux, L. Mathieu, O. Meplan, E. Merle-Lucotte, H. Nifenecker, F. Perdu, S. David, Potential of thorium molten salt reactors, detailed calculations and concept evolution with a view to large scale energy production, *Progress in Nuclear Energy*, Volume 46, Issue 1, 2005, Pages 77-99.
- [77] Generation IV International Forum (2002), A Technology Roadmap for Generation IV Nuclear Energy Systems, Report GIF-002-00, December 2002, <http://gif.inel.gov/roadmap>.
- [78] L. Mathieu, D. Heuer, R. Brissot, C. Garzenne, C. Le Brun, D. Lecarpentier, E. Liatard, J.-M. Loiseaux, O. Méplan, E. Merle-Lucotte, A. Nuttin, E. Walle, J. Wilson, The thorium molten salt reactor: Moving on from the MSBR, *Progress in Nuclear Energy*, Volume 48, Issue 7, September 2006, Pages 664-679.
- [79] E. S. Bettis, R. C. Robertson (1970), The Design and Performance Features of a Single-Fluid Molten-Salt Breeder Reactor, *Nucl. App. and Tech.* 8, 190-207.

-
- [80] F. Venneri, Y. Kim, D. McEachern, C. M. Persson, C. K. Jo, The Analysis of the Thorium-Fueled Modular Helium-Cooled Reactor, Proc. HTR 2008, Washington, USA, 28 September – 1 October 2008.
- [81] A. Ramanujam, Purex and Thorex Processes (Aqueous Reprocessing), Encyclopedia of Materials: Science and Technology, 2008, Pages 7918-7924.
- [82] K. Anantharaman, V. Shivakumar, D. Saha, Utilisation of thorium in reactors, Journal of Nuclear Materials, Volume 383, Issues 1-2, 15 December 2008, Pages 119-121.
- [83] A. Borella, K. Volev, A. Brusegan, P. Schillebeeckx, and F. Corvi, Determination of the $^{232}\text{Th}(n,g)$ Cross Section from 4 to 140 keV at GELINA, Nuclear Science and Engineering: 152, 1–14, 2006.
- [84] T. Kim and T. J. Downar, Thorium fuel performance in a tight-pitch light water reactor lattice, Nuclear Technology Vol. 138, April 2002.
- [85] R. Bäumer, I. Kalinowski, E. Röhler, J. Schöning, W. Wachholz, Construction and operating experience with the 300-MW THTR nuclear power plant, Nuclear Engineering and Design, Volume 121, Issue 2, 2 July 1990, Pages 155-166.
- [86] W. M. Stacey. Nuclear Reactor Physics. John Wiley & Sons, Inc. 2001. ISBN 0-471-39127-1.
- [87] R. Bäumer, I. Kalinowski, THTR commissioning and operating experience, Energy, Volume 16, Issues 1-2, January-February 1991, Pages 59-70.
- [88] S. Brandes, H. Daoud, U. Schmid, V. Drüke, Core Physics of Thorium High Temperature Reactor Pebble Bed Core at Zero Power, Nuclear Science and Engineering, Vol. 97, pp 89-95, 1987.
- [89] D. Schwarz, R. Bäumer, THTR operating experience, Nuclear Engineering and Design, Volume 109, Issues 1-2, September-October 1988, Pages 199-205.
- [90] C.H. Forsberg, Hydrogen, nuclear energy and the advanced high-temperature reactor. International Journal of Hydrogen Energy, 28, 2003.
- [91] International Energy Agency. Prospects for hydrogen and fuel cells, December 2005. OECD/IEA.
- [92] IAEA-TECDOC-1085, Hydrogen as an energy carrier and its production by nuclear power, May 1999.
- [93] J. L. McCormick, High Temperature Reactor: Driving Force to Convert CO₂ to Fuel, Proc. HTR 2008, Washington, USA, 28 September – 1 October 2008.
- [94] C. W. Forsberg, Use of High-Temperature Reactor Heat in Refineries, Underground Refining, and Biorefineries for Liquid Fuels Production, Proc. HTR 2008, Washington, USA, 28 September – 1 October 2008.
- [95] A. Morris, R. Kuhr, J. McKinnell, The Pebble Bed Modular Reactor (PBMR) as a Source of High Quality Process Heat for Sustainable Oil Sands Expansion, Proc. HTR 2008, Washington, USA, 28 September – 1 October 2008.

- [96] B.M. Misra, Seawater desalination using nuclear heat/electricity — Prospects and challenges, *Desalination* 205 (2007) 269–278.
- [97] S. Nisan, S. Dardour, Economic evaluation of nuclear desalination systems, *Desalination* 205 (2007) 231–242.
- [98] M. Phélip et al., High Temperature Reactor Fuel Technology in the HTR-F1 and RAPHAEL European Projects, *Proc. HTR 2006*, Johannesburg, South Africa, 1-4 October 2006.
- [99] M. A. Fütterer et al., RAPHAEL: The European Union's (Very) High Temperature Reactor Technology Project, *Proc. ICAPP'06*, Reno, NV, USA, 4-8 June 2006.
- [100] IAEA TECDOC-978, Fuel performance and fission product behaviour in gas cooled reactors, ISSN 1011-4289, November 1997.
- [101] J. H. Venter, H. Nabelek, Performance envelope of modern HTR TRISO fuel, *Proc. HTR 2006*, Johannesburg, South Africa, 1-4 October 2006.
- [102] R. Conrad, A. W. Mehner, G. Pott, Bestrahlungserprobung und Auswertung von Daten für HTR-LEU Referenzbrennelemente im HFR Petten, *Jahrestagung Kerntechnik*, Berlin, (1983).
- [103] A. W. Mehner, W. Heit, K. Röllig, K. Ragoss, H. Müller, Spherical fuel elements for advanced HTR manufacture and qualification by irradiation testing, *J. Nucl. Mater.* 171 (1990) 9-18.
- [104] J. Ahlf, R. Conrad, M. Cundy, H. Scheurer, Irradiation experiments on High Temperature Gas-Cooled Reactor fuels and graphites at the High Flux Reactor Petten, *J. Nucl. Mater.* 171 (1991) 31-36.
- [105] J. Ahlf, A. Zurita, (Eds.), 1993. High Flux Materials Testing Reactor, HFR Petten. Characteristics of Facilities and Standard Irradiation Devices. EUR 15151EN.
- [106] S. C. van der Marck, et al., HFR-EU1 (337-01) Nuclear Analysis, 2.2068/07.83318/C, Oct. 2007.
- [107] J. Oppe, J.C. Kuijper, OCTOPUS_TNG Reference guide, 20748/03.54103/C, NRG, Petten, 26 November 2004.
- [108] J. F. Briesmeister, MCNP-A General Monte Carlo N-Particle Transport Code, LA-13709-M, version 4C, 18.12.2000.
- [109] R.A. Forrest, FISPACT-2001: User manual (issue 1), UKAEA FUS 450, AKAEA Fusion Association, Abingdon UK (2001).
- [110] A. van Heek, HTR Pebble Burnup Experimental Benchmark, *Proc. HTR 2008*, Washington, October 2008.
- [111] J. Cetnar, W. Gudowski, J. Wallenius, User Manual for Monte-Carlo Continuous Energy Burnup (MCB) Code, Version 1C.

-
- [112] H. Van der Merwe, J. Venter, A method to evaluate fission gas release during irradiation testing of spherical fuel, Proc. HTR 2008, Washington, USA, September 28-October 1, 2008.
- [113] Personal communications with SGL Carbon, emails from 23/03/2009.
- [114] K. Röllig, Release of rare fission gases from spherical elements with coated particles, Nuclear Technology, 35, pp 516-523, 1977.
- [115] S. de Groot et al., Fission-Product Behaviour during Irradiation of TRISO Coated Particles in the HFR-EU1bis Experiment, Proc. HTR 2008, Washington, USA, 28 September – 1 October 2008.
- [116] A. Marmier, M.A. Fütterer, K. Tuček, J.B.M. de Haas, J.C. Kuijper, J.L. Kloosterman, Revisiting the concept of Wallpaper fuel, Nuclear Engineering and Design, Volume 240, Issue 10, October 2010, Pages 2485-2492.
- [117] A. Marmier, M.A. Fütterer, K. Tuček, J. Jonnet, J.C. Kuijper, J. Oppe, B. Petrov, J.L. Kloosterman, B. Boer, Fuel cycle investigation for the wallpaper type of fuel, submitted to Nuclear Technology.
- [118] E. Teuchert, H.J. Rütten, Core physics and fuel cycles of the pebble bed reactor, Nucl. Eng. Des. 34 (1975) 109-118.
- [119] K. Sawa, S. Suzuki, S. Shiozawa, Safety criteria and quality control of HTTR fuel, Nuclear Engineering and Design 208 (2001) 305–313.
- [120] Clarence L. Hoenig, (Livermore, CA), United States Patent, 5336520.
- [121] J.B.M. de Haas, J.C. Kuiper J. Oppe, core physics and transient analyses by the Panthermix code system, MC proceedings, Avignon, France, September 12-15, 2005.
- [122] WIMS - A Modular System for Neutronic calculations - User Guide for Version 8, Report ANSWERS/WIMS(99)9, Serco Assurance, ANSWERS Software Service, Winfrith, U.K.
- [123] P.K. Hutt et al., “The UK Core Performance Package”, Nucl. Energy, 30, No. 5, p. 291 (1991).
- [124] S. Struth, THERMIX-DIREKT: ein Rechenprogramm zur instationären, zweidimensionalen Simulation thermohydraulischer Transienten, ISR-KFA Juelich, Germany, August 1994 (private communication).
- [125] F. Reitsma, et. al, The OECD/NEA/NSC PBMR Coupled Neutronic/Thermal Hydraulics Transient Benchmark: The PBMR-400 Core Design, Proceedings PHYSOR-2006, Vancouver Canada, 10-14 September 2006.
- [126] B. Boer, A.M. Ougouag, J.L. Kloosterman, G.K. Miller, Stress Analysis of Coated Particle Fuel in Graphite of High Temperature Reactors. Nuclear Technology, 162, Pages 276-292.

- [127] J. Jonnet, J.L. Kloosterman, B. Boer, Performance of TRISO particles fuelled with plutonium and Minor Actinide in a PBMR-400 core design, *Nuclear Engineering and Design*, Volume 240, Issue 6, June 2010, Pages 1320-1331.
- [128] J.L. Kloosterman, A.M. Ougouag, Comparison and Extension of Dancoff Factors for Pebble-Bed Reactors, *Nuclear Science and Engineering*, 157:16-29, 2007.
- [129] S. Hu, R. Wang, Z. Gao, Transients tests on blower trip and rod removal at the HTR-10, *Nuclear Engineering and Design* 236 (2006) 677–680.
- [130] T. Kindt, H. Haque, Recriticality of the HTR-Module Power Reactor after hypothetical accidents, *Nuclear Engineering and Design*, Volume 137, Issue 1, September 1992, Pages 107-114.
- [131] B. Boer, J.L. Kloosterman, D. Lathouwers, T.H.J.J. van der Hagen, In-core fuel management optimization of pebble-bed reactors, *Annals of Nuclear Energy*, Volume 36, Issue 8, August 2009, Pages 1049-1058.
- [132] J. Jonnet, J.L. Kloosterman, B. Boer, Development of a stress analysis code for TRISO particles in HTRs, *PHYSOR-2008*, Interlaken, Switzerland (September 14-19 2008).
- [133] R.G. Cochran, N. Tsoulfanidis, *The nuclear fuel cycle: Analysis and management*, American Nuclear Society (ANS) – La Grange Park, Illinois 60525, 1990, ISBN 0-89448-451-6.
- [134] S. de Groot, et al., Modeling of the HFR-EU1BIS experiment and thermomechanical evaluation, *Nuclear Engineering and Design*, Volume 238, Issue 11, November 2008, Pages 3114-3120.
- [135] E.E. Bende, *Plutonium Burning in a Pebble-Bed Type High Temperature Nuclear Reactor*, Ph.D. Thesis, Delft University of Technology, ISBN 90-9013168, 1999.
- [136] M.J. Kania, H. Nickel, 1980, Performance assessment of the (Th,U)O₂ HTI-BISO coated particle under PNP/HHT irradiation conditions, KFA Jülich report Jül-1685, ISSN 0366- 0885.
- [137] D.A. Petti, J. Buongiorno, J.T Maki, R.R. Hobbins, G.K. Miller, Key differences in the fabrication, irradiation and high temperature accident testing of US and German TRISO-coated particle fuel, *Nuclear Engineering and Design* 222 (2003) 281–297.
- [138] H. Nickel, HTR coated particles and fuel elements, *High Temperature Reactor School CEA Cadarache*, France (November 4-8, 2002).
- [139] D. Matzner, W. Kriel, M. Correia, R. Greyvenstein, 2006, Cycle configuration for a PBMR Steam and Electricity Production Plant, *Proc. ICAPP 2006*, Reno, NV, USA, June 4-8, 2006.

-
- [140] J. Buggea, S. Kjæra, R. Blum, High-efficiency coal-fired power plants development and perspectives, *Energy*, Volume 31, Issues 10-11, August 2006, Pages 1437-1445.
- [141] N. Woudstra, Cycle-Tempo release 5.0, Delft University of Technology, 2006. www.cycle-tempo.nl
- [142] B. Yildiz, M. S. Kazimi, 2006, Efficiency of hydrogen production systems using alternative nuclear energy technologies, *Int. J. of Hydrogen Energy*, Volume 31, Issue 1, January 2006.
- [143] B. Yildiz, K. J. Hohnholt, M. S. Kazimi, 2005, Hydrogen production Using High-Temperature Steam Electrolysis Supported by Advanced Gas Reactor with Supercritical CO₂ Cycles, *Nuclear Technology*, Vol. 155, July 2005.
- [144] V. Fujiwara, et AL., Hydrogen production by high temperature electrolysis with nuclear reactor, *Progress in Nuclear Energy*, Volume 50, Issues 2-6, March-August 2008, Pages 422-426
- [145] X. Vitart, A. Le Duigou, P. Carles, 2006, Hydrogen Production using the Sulfur-Iodine cycle coupled to a VHTR: An Overview, *Energy Conversion and Management*, Volume 47, Issue 17, p. 2740-2747, October 2006.
- [146] N. Sakaba, S. Kasahara, K. Onuki, K. Kunitomi, Conceptual design of hydrogen production system with thermochemical water-splitting iodine-sulphur process utilizing heat from the high-temperature gas-cooled reactor HTTR, *International Journal of Hydrogen Energy* 32 (2007) 4160 – 4169
- [147] Y.H. Jeong, M.S. Kazimi, K.J. Hohnholt, B. Yildiz, 2005, Optimization of the Hybrid Sulfur Cycle for Hydrogen production, *Nuclear Energy and Sustainability Program*, Massachusetts Institute of Technology Technical Report MIT-NES-TR-004, May 2005.
- [148] X. Li, R. Le Pierres, S. D. Dewson, 2006, Heat Exchangers for the Next Generation of Nuclear Reactors, *Proc. ICAPP'06*, Reno, NV, USA, June 4-8, 2006.
- [149] G. Angelino, C. Invernizzi, 1994, Supercritical heat pump cycles *International Journal of Refrigeration*, Volume 17, Issue 8, 1994, Pages 543-554
- [150] D. E. Shropshire, 2004, Lessons learned from Gen I carbon-dioxide cooled reactors, *Proc. ICONE-12*, Arlington, VA, USA, 25-29 April 2004.
- [151] IAEA-TECDOC-1444, 2005, Optimization of the coupling of nuclear reactors and desalination systems, Final report of a coordinated research project, 1999–2003, June 2005.
- [152] V. Dostal, P. Hejzlar, M. J. Driscoll, 2006, High Performance Supercritical Carbon Dioxide Cycle for Next-Generation Nuclear Reactors, *Nuclear Technology*, 154, 265 (2006).
- [153] J.M. Noh, K.-S. Kim, Y. Kim, H. C. Lee, Development of a computer code system for the analysis of prism and pebble type VHTR cores, *Annals of Nuclear Energy* 35 (2008), pp 1919-1928.

Bibliography

- [154] W. J. M. de Kruijf, J.L. Kloosterman, 2003, On the average chord length in reactor physics, *Ann. Nucl. Energy* 30 (2003), pp. 549–553.
- [155] N. Z. Cho, H. Yu, J. W. Kim, Two-temperature homogenized model for steady-state and transient thermal analyses of a pebble with distributed fuel particles, *Annals of Nuclear Energy*, Volume 36, Issue 4, 1 May 2009, Pages 448-457.

List of publications

A. Marmier, M.A. Fütterer, K. Tuček, J. Jonnet, J.C. Kuijper, J. Oppe, B. Petrov, J.L. Kloosterman, B. Boer, Fuel cycle investigation for the wallpaper type of fuel, submitted to Nuclear Technology.

M. Laurie, A. Marmier, G. Berg, J.M. Lapetite, M. A. Fütterer, C. Tang, Results of the HFR-EU1 fuel irradiation of INET and AVR pebbles in the HFR Petten, Nuclear Engineering and Design, Available online 6 December 2011, ISSN 0029-5493, 10.1016/j.nucengdes.2011.10.063.

M. Laurie, M.A. Fütterer, K.H. Appelman, J.M. Lapetite, A. Marmier, G. Berg, JRC's on-line fission gas release monitoring system in the high flux reactor Petten, Nuclear Engineering and Design, Available online 22 October 2011, ISSN 0029-5493, 10.1016/j.nucengdes.2011.09.062.

A. Marmier, M.A. Fütterer, K. Tuček, J.B.M. de Haas, J.C. Kuijper, J.L. Kloosterman, Revisiting the concept of Wallpaper fuel, Nuclear Engineering and Design, Volume 240, Issue 10, October 2010, Pages 2485-2492.

D. Haas, M. Fuetterer, M. Laurie, A. Marmier, V. Rondinella, J. Somers, JRC Research on High Temperature Reactor Fuels. In Conference Proceedings: ENS, editor. Proceedings of the ENC 2010, ISBN: 978-92-95064-09-6. Brussels (Belgium): European Nuclear Society; 2010. p. 1-7. JRC54324.

M. Laurie, A. Marmier, G. Berg, J. Lapetite, M. Fuetterer, C. Tang, Results of the HFR-EU1 Fuel Irradiation of INET and AVR Pebbles in the HFR Petten. In Conference Proceedings: Proceedings of HTR 2010. Prague (Czech Republic): TERIS; 2010. JRC58319.

M. Laurie, M. Fuetterer, K. Appelman, J. Lapetite, A. Marmier, G. Berg, JRC's On-Line Fission Gas Release Monitoring System in the High Flux Reactor Petten . In Conference Proceedings: Proceedings of HTR 2010. PRAGUE (Czech Republic): TERIS; 2010. p. Paper 122 (1-6). JRC59303.

M. A. Fütterer, E. D'Agata, M. Laurie, A. Marmier, F. Scaffidi-Argentina, P. Raison, K. Bakker, S. de Groot, F. Klaassen, Next Generation Fuel Irradiation Capability in the High Flux Reactor Petten, Journal of Nuclear Materials (2009), doi: 10.1016/j.jnucmat.2009.03.030.

M. A. Fütterer, G. Berg, A. Marmier, E. Toscano, D. Freis, K. Bakker, S. de Groot, Irradiation results of AVR fuel pebbles, at increased temperature and burn-up in the HFR Petten, Nuclear Engineering and Design 238 (2008) 2877–2885.

A. Marmier, M. A. Fütterer, Nuclear Powered Heat Pumps for Near Term Process Heat Applications, Nuclear Engineering and Design 238 (2008) 2272–2284.

A. Marmier, M. A. Fütterer, K. Tuček, H. de Haas, J. C. Kuijper, J. L. Kloosterman, Revisiting the concept of wallpaper fuel, HTR2008-58114, Proceedings of HTR2008, Washington, USA, October 2008.

A. Marmier, M. A. Fütterer, M. Laurie, C. Tang, Preliminary results of the HFR-EU1 fuel irradiation of INET and AVR pebbles in the HFR Petten, HTR2008-58049, Proceedings of HTR2008, Washington, USA, October 2008.

M. A. Fütterer, E. D'Agata, M. Laurie, A. Marmier, F. Scaffidi-Argentina, P. Raison, K. Bakker, S. de Groot, F. Klaassen, Next Generation Fuel Irradiation Capability in the High Flux Reactor Petten, NFSM 2008, Anaheim, USA, June 2008.

M. Laurie, A. Marmier, G. Berg, M. A. Fütterer, Design of the on-line fission gas release analysis system in the High Flux Reactor Petten, Technical Meeting on Fuel Rod instrumentation and In-Pile Measurement Techniques, Halden, Norway, September 2007.

A. Marmier, M. A. Fütterer, HTR with downgraded specifications for high temperature process heat applications, Proceedings of ICAPP'07, Nice, France, May 2007.

A. Marmier, M. A. Fütterer, Nuclear Cogeneration of High Temperature Process Heat and Electricity with Heat Pump Driven Superheating, Proceedings of ICAPP'07, Nice, France, May 2007.

A. Marmier, M. A. Fütterer, High Temperature Process Heat Generation with Medium Temperature Heat Source, IAEA-CN-152-71, Proceedings of the International Conference on Non-Electric Applications of Nuclear Power: Seawater Desalination, Hydrogen Production and other Industrial Applications, Oarai, Japan, April 2007.

M. A. Fütterer, G. Berg, A. Marmier, E. Toscano, K. Bakker, Irradiation results of AVR fuel pebbles, at increased temperature and burn-up in the HFR Petten, Proceedings HTR2006, Johannesburg, South Africa, October 2006.

M. A. Fütterer, H. Lohner, A. Marmier, S. de Groot, C. M. Sciolla, Preliminary Results from an AVR Fuel Pebble Irradiation at Increased Temperature and Burn-Up in the HFR Petten, Proceedings of ICAPP'05, Seoul, Korea, May 2005.

Summary

The work presented in this thesis covers three fundamental aspects of High Temperature Reactor (HTR) performance, namely fuel testing under irradiation for maximized safety and sustainability, fuel architecture for improved economy and sustainability, and a novel Balance of Plant concept to enable future high-tech process heat applications with minimized R&D.

The development of HTR started in the 1950s as a graphite moderated and helium cooled reactor. This concept featured important inherent and passive safety characteristics, namely: high thermal inertia and good thermal conductivity of the core; a negative Doppler coefficient; high quality of fuel elements and low power density. All together, these features keep the core temperature within safe boundaries and minimise fission product release, even in case of severe accidents.

The Very High Temperature Reactor (VHTR) was selected by the Generation IV International Forum as one of the six most promising nuclear reactor concepts for the future based on the following criteria: sustainability, economy, safety and reliability, proliferation resistance and physical protection. The VHTR is based on the same safety concept as the initial HTR. However, it aims at offering better economy with a higher reactor outlet temperature (and thus efficiency) and a high fuel discharge burn-up (and thus better sustainability). The inherent safety features of HTR have been demonstrated in small pebble-bed reactors in practice, but have to be replicated for reactors with industrially relevant size and power. While an increase of the power density (in order to increase the helium coolant outlet temperature) would be attractive with regard to efficiency and possible process heat applications, it leads to higher fuel temperatures and therefore higher fuel failure probability.

The core of a pebble-bed reactor consists of 6 cm diameter spheres (pebbles) that form a randomly packed porous bed, which is cooled by high pressure helium. These pebbles contain thousands of 1 mm diameter fuel particles baked into a graphite matrix. These fuel particles, in turn, consist of a fuel kernel with successive coatings of pyrocarbon and silicon carbide layers. The coating layers are designed to contain the fission products that build up during operation of the reactor. Like for most nuclear energy sources, the feasibility and performance of the fuel is key to future improvements and requires experimental verification in view of fuel qualification and licensing. For HTR fuel, the required test string comprises amongst others high temperature irradiation to high burn-ups with fission gas release measurements.

To this end, the HFR-EU1 fuel irradiation in the High Flux Reactor Petten (2006-2010) explored the potential for high performance and high burn-up of existing German fuel (3 pebbles produced for the AVR reactor at the German research centre Jülich) and newly produced Chinese fuel (2 pebbles produced by INET for use in the HTR-10 test reactor in China). These five pebbles were irradiated for 445 days in

separately controlled capsules, while the fission gas release was monitored by gamma spectrometry thus enabling evaluation of the characteristic release over birth fraction, indicative for the health of the fuel. In none of the pebbles, abnormally increased fission gas release was observed indicating that all of the approx. 45,000 coated particles in the pebbles had remained intact. The results presented in this thesis cover the first 332 days of irradiation.

While HFR-EU1 was dedicated to a particularly high burn-up, HFR-EU1bis, performed between 2004 and 2005, investigated extremely high temperature for steady-state conditions. The comparison of both experiments confirms that temperature plays a decisive part in fuel performance and integrity.

The peak fuel temperature in pebbles can be lowered with the so-called “wallpaper fuel”, in which the coated fuel particles are arranged in a spherical shell within a pebble. This wallpaper concept also enhances neutronic performance through improved neutron economy, resulting in reduced fissile material and/or enrichment needs or providing the potential to achieve higher burn-up. To quantify these improvements, calculations were performed using the Monte Carlo neutron transport and depletion codes MCNP/MCB (to assess conversion ratio, temperature coefficient of reactivity and neutron multiplication) and PANTHERMIX (for fuel cycle in steady state conditions and loss of coolant accident calculations). Based on PANTHERMIX steady-state conditions, both particle failure fractions (with the CRYSTAL code) and the fissile material cost were determined: Wallpaper type of fuel impacts positively on the fuel cycle and reduces both the need for fissile material and the production of minor actinides, facilitating fuel reprocessing and reducing fuel cost. Safety is also improved with particle temperature being reduced during steady-state operation. In parallel, this reduces the expected particle failure fraction by up to 85% over its in-core lifetime, and, concomitantly also the fission product release.

In the long term, the very high temperature version VHTR is believed to be the most suitable concept for co-generation of process heat. Its high coolant exergy would enable large-scale hydrogen production and other process heat applications: It was meant to supply heat ($> 850^{\circ}\text{C}$) to large-scale thermochemical hydrogen production processes. Although the need for hydrogen has by far not disappeared, in recent years the tendency in international projects goes back to lower reactor outlet temperatures (“HTR” instead of “VHTR”) mainly for three reasons. The first is that two of the main driver countries of the VHTR have dropped thermochemical hydrogen production from their high priority list, due to expected economic and material corrosion issues. The second is that the extremely high reactor outlet temperatures of $> 950^{\circ}\text{C}$ would require totally new materials and construction standards thus delaying the effective use of this reactor concept very far into the future. The third reason is that market research has shown that the existing process heat market (steam $< 600^{\circ}\text{C}$) is already so big that investment into longer term concepts receives lower priority. In addition, the high temperature operation would tend to increase particle failure fraction and fission product release.

In order to reach the VHTR objectives of high temperature and power conversion efficiency much earlier, a novel approach was developed: The nuclear part of the power plant would run at acceptably low temperature and would power a compression heat pump system acting as a temperature booster. Thus, very high temperature operation could be limited to a section of a conventional external gas circuit, avoiding the constraints related to the combination of very high temperatures and irradiation. The separation of the high temperatures from the reactor would avoid massive R&D requirements on materials, components and fuel with uncertain outcome, which would unnecessarily delay introduction of this otherwise very attractive reactor concept. Additionally, this approach improves the HTR capability to deliver high temperature process heat in the narrow temperature window (50 – 100 K) typically required by thermochemical hydrogen production cycles or other specific end-user applications.

Petten, The Netherlands, December 2011

A. Marmier

Samenvatting

Dit proefschrift beschrijft een onderzoek aan drie fundamentele aspecten van de Hoge Temperatuur Reactor (High Temperature Reactor, HTR), namelijk: Experimenteel onderzoek aan het gedrag van brandstoffen om de veiligheid en duurzaamheid van de reactor te optimaliseren; de interne opbouw van de brandstof ter maximalisatie van de economische prestatie en duurzaamheid; en een nieuw Balance of Plant principe waarmee high-tech toepassingen van proceswarmte mogelijk worden met een minimale verdere ontwikkelingsinspanning.

De ontwikkeling van de HTR begon in de jaren 50 als een grafiet gemodereerde en helium gekoelde reactor. Dit reactorconcept kenmerkt zich door een aantal belangrijke inherente en passieve veiligheidskenmerken, namelijk: een hoge thermische inertie en een goede thermische capaciteit in de reactorkern; een negatieve Dopplercoëfficiënt; hoge kwaliteit van de splijtstofelementen en een lage vermogensdichtheid. De combinatie van deze eigenschappen zorgt ervoor dat de kerntemperatuur binnen veilige grenzen blijft met een minimale hoeveelheid vrijkomende splijtingsproducten, zelfs bij ernstige ongevallen.

De Zeer Hoge Temperatuur Reactor (Very High Temperature Reactor, VHTR) werd geselecteerd door het Generation IV International Forum als een van de zes meest veelbelovende toekomstige kernreactorconcepten op basis van de volgende criteria: duurzaamheid rendement; veiligheid en betrouwbaarheid; het tegengaan van proliferatie en fysieke bescherming. De VHTR is gebaseerd op hetzelfde veiligheidsconcept als de oorspronkelijke HTR. Echter, de VHTR richt zich op een betere rentabiliteit vanwege een hogere reactor-uitlaattemperatuur (en dus efficiëntie) en een verhoogd brandstofverbruik vanwege een verhoging van de opbrand en daarmee een betere duurzaamheid. De inherente veiligheidsvoorzieningen van HTR zijn in de praktijk aangetoond met kleine kogelbed (pebble-bed) reactoren, maar moeten worden opgeschaald naar reactoren met een industrieel relevante grootte en bijbehorend vermogen. Een toename van de vermogensdichtheid om de heliumkoelvloeistof-uitlaattemperatuur te verhogen is weliswaar aantrekkelijk met het oog op de efficiëntie en de mogelijke proceswarmte toepassingen, maar deze vermogensdichtheid leidt tot ook tot hogere brandstoftemperaturen en daarmee verhoogde faalkans van de brandstof.

De kern van een kogelbedreactor bestaat uit bollen of kogels met een doorsnede van 6 cm, die een willekeurig gepakt poreus bed vormen. Dit bed wordt gekoeld met Helium onder hoge druk. De bollen bevatten duizenden in een grafiet matrix gebakken brandstofdeeltjes met een diameter van ongeveer 1 mm. Deze brandstofdeeltjes bestaan op hun beurt weer uit een brandstofkern met opeenvolgende laagjes (coatings) van pyrolytische carbon en siliciumcarbide. De laagjes zijn ontworpen voor de retentie van de splijtingsproducten die tijdens reactorbedrijf worden gevormd. Net zoals voor de meeste andere kernenergiebronnen, zijn de toepasbaarheid en het gedrag van de brandstof van cruciaal belang voor toekomstige verbeteringen. Deze eigenschappen moeten

experimenteel aangetoond worden voor brandstofkwalificatie en vergunningverlening. Voor de HTR brandstof, bestaan de vereiste kwalificatietesten onder andere uit hoge temperatuur bestraling tot aan hoge opbrand met meting van de vrijkomende splijtingsgassen.

De HFR-EU1 brandstof bestraling in de Hoge Flux Reactor Petten (2006-2010) onderzocht de mogelijkheden voor hoge prestaties en een hoge opbrand van bestaande Duitse brandstof (3 kogels geproduceerd voor de AVR reactor bij het Duitse onderzoekscentrum Jülich) en nieuw geproduceerde Chinese brandstof (2 kogels geproduceerd door INET voor gebruik in de HTR-10-test reactor in China). Deze vijf kogels werden gedurende 445 dagen in twee apart regelbare capsules bestraald, terwijl de vrijkomende splitsingsgassen werden gemeten met gamma-spectrometrie om de ontwikkeling van de ontgassing vanaf het begin te volgen als indicatie is voor de gesteldheid van de brandstof. In geen van de kogels werd een abnormale verhoging van de vrijgeving van splitsingsgassen gemeten, wat aangeeft dat alle ca. 45.000 gecoate deeltjes in de kogels intact waren gebleven. Dit proefschrift beschrijft de resultaten van de eerste 332 bestralingsdagen.

Terwijl het HFR-EU1 experiment was gericht op een bijzonder hoge opbrand, onderzocht het HFR-EU1bis experiment, dat uitgevoerd werd van 2004 tot 2005, de invloed van extreem hoge temperatuur bij normaal bedrijf. Een vergelijking van beide experimenten toont aan dat de temperatuur een beslissende rol speelt in de prestaties en integriteit van de brandstof.

De piek brandstoftemperatuur in de kogels kan worden verlaagd met zogenaamde "wallpaper brandstof", waarbij de gecoate brandstofdeeltjes verpakt worden in een bolvormige schil in de kogel. Dit wallpaper-concept verbetert ook de kernprestaties door een verbeterde neutronbalans, wat leidt tot een vermindering van de hoeveelheid splijtbaar materiaal en/of lagere verrijking of het biedt de mogelijkheid om een hogere opbrand te bereiken. Om deze verbeteringen te kwantificeren, werden de berekeningen uitgevoerd om de conversie ratio, temperatuurcoëfficiënt van reactiviteit en neutronenvermenigvuldiging te beoordelen met behulp van de Monte-Carlo neutron transport codes MCNP / MCB en voor berekeningen aan brandstof gedrag bij een normaal bedrijf of tijdens een ongeval, b.v. het verlies van actieve kernkoeling optreedt met de code PANTHERMIX. Op basis van berekeningen van normale bedrijfscondities met PANTHERMIX werd zowel de deeltjesfaalkans bepaald met de CRYSTAL code, als het verbruik aan splijtstof. Wallpaper brandstof heeft een positieve invloed op de splijtstofcyclus en vermindert zowel de noodzaak van splijtstof en als de productie van lagere actiniden, wat de opwerking vergemakkelijkt en de totale brandstofkosten vermindert. De veiligheid wordt ook verhoogd, omdat de deeltjestemperatuur bij normaalbedrijf lager worden. Tegelijkertijd vermindert daarmee ook de faalkans van deeltjes met maar liefst 85% tijdens de totale verblijfsduur van de kogels in de kern, en daarmee ook de ontgassing van de splijtingsproducten.

Op de lange termijn wordt de zeer hoge temperatuur versie VHTR beschouwd als de geschiktste reactor voor het gezamenlijk opwekken van proceswarmte en elektriciteit. De hoge koelstofexergie zou de productie van waterstof en andere toepassingen van warmte op grote schaal mogelijk maken: De VHTR was bedoeld om op grote schaal warmte ($> 850^{\circ}\text{C}$) voor de thermochemische splitsing van water te leveren. Hoewel de behoefte aan waterstof niet is verdwenen, is er een tendens in internationale projecten tijdens de afgelopen jaren om terug te gaan naar een lagere reactor uitlaattemperatuur ("HTR" in plaats van "VHTR") voornamelijk om drie redenen. De eerste reden is, dat twee van de belangrijkste sturende landen van de VHTR de thermochemische productie van waterstof uit hun hoge prioriteitenlijst hebben gehaald vanwege de verwachte economische en materiaalcorrosie problemen. De tweede reden is dat de extreem hoge reactor uitlaattemperatuur van meer dan 950°C totaal nieuwe materialen en constructienormen vereist, waardoor het effectieve gebruik van het reactorconcept heel ver in de toekomst ligt. De derde reden is dat marktonderzoek heeft aangetoond dat de bestaande markt voor proceswarmte (stoom $< 600^{\circ}\text{C}$) al zo groot is dat investeringen in langere termijnconcepten een lagere prioriteit krijgen. Daarnaast heeft het bedrijven van de reactor bij de hoge temperaturen de neiging om de deeltjesfaalkans en ontgassing van splitsingsproducten te vergroten.

Om de doelen van de VHTR, een hoge uitlaattemperatuur en een hoge vermogensomzettingsefficiëntie eerder te bereiken, is er een nieuwe aanpak ontwikkeld: Het nucleaire gedeelte van de reactor zou bij acceptabele lagere temperatuur draaien en vermogen leveren aan een compressie-warmtepompsysteem, dat als een temperatuur booster zou optreden. Zo kan het hoge temperatuurbedrijf beperkt worden tot een conventioneel extern gas-circuit en de beperkingen ten gevolge van de combinatie van zeer hoge temperaturen en bestraling vermeden worden. Door het scheiden van de hoge temperaturen en het reactorbedrijf bij lagere temperaturen, kunnen enorme R & D-inspanningen voor materialen, onderdelen en brandstof met een onzekere uitkomst vermeden worden, die de invoering van dit overigens zeer aantrekkelijke reactorconcept onnodig zouden vertragen. Bovendien verbetert deze oplossing de mogelijkheid van de HTR om de hoge-temperatuurproceswarmte te leveren binnen een zeer smalle temperatuurband van 50 - 100 K, die meestal nodig is voor thermochemische splitsing van water of andere specifieke eindgebruikertoepassingen.

Petten, Nederland, december 2011

A. Marmier

Acknowledgements

Six years! It took six years to complete this thesis... 50% more than normal Dutch thesis, twice the duration of French ones... But as one could say: “Tout est bien qui finit bien!”

This would not have been possible without the support of the JRC in general and Michael Fütterer in particular, who took me in as a trainee in November 2004 and opened a grantholder position in October 2005 for me to work on nuclear fuel irradiation. It has been a long challenging but stimulating activity which, through a fruitful learning process, transformed into this PhD thesis.

And what would a thesis be without an academic reference? In this regard, my deepest gratitude goes to Prof. van der Hagen and Prof. Verkooijen for their supervision, advice and guidance throughout all the regular HTR-NL meetings.

Finally a warm acknowledgement and appreciation to all the co-authors of papers, who have widened the scope of the research and thus of this thesis. Just to name a few of them:

Mathias Laurie for the experimental and Kamil Tuček for the analytical approaches; Jim Kuijper, Biser Petrov, Jerome Jonnet and other NRG colleagues, both from the reactor and the analytical groups, for their support and collaboration; Jan Leen Kloosterman for his persistence in pushing me to finish this thesis over the last months; Ynte Stockman, Dita Calero and Antoine Rivalan (<http://antoane.canalblog.com/>) for the last touch: “De laatste loodjes wegen het zwaarst”.

Acknowledgement is as tricky as working on the thesis! Obviously significantly more persons were involved, especially when it comes to nuclear experimentation or European projects. Please be assured that I have not forgotten you, nor your support.

Life does not stop after the thesis: Technically speaking, colleagues from the Infrastructure Dept., the Programme Office and even the broader Directorate of the Institute for Energy and Transport (as we now should name it) also understood over the last two years the need to finish this thesis even though it was long overdue: Many thanks to them as well.

And life does not stop after work either: Expatriation is quite an experience, which could turn into a nightmare if not properly prepared (so many came and left...). In my case, life has been eased by:

The friends scattered throughout Europe, especially the expatriate ones, sensitive to the “challenge” and those around Alkmaar, happily joined by some lucky Dutch...

Modern technology: No need to turn into a nerd to keep in touch!

And my family who, if they complained and challenged me, understood the concept.

Acknowledgements

Of course, the best support over this period came from Virginie, the little French girl I found in the bus on the way to Petten. I am glad that the thesis is over while she still is by my side.

All in all, I had my share of good spirits and memorable moments over the last 6 years, with the top one being the birth of my son Jules on 07/07/2011. He also deserves to be thanked for being so cool and letting daddy sleep! ;-)

Curriculum Vitae

Alain Marmier

E-mail: alain.marmier@ec.europa.eu

Date and place of birth: 28-12-1981; Montbéliard, France

Professional Experience

- 2010 – Assistant at the Programme Office of the Joint Research Center of the European Commission, Petten, The Netherlands
- 2009 – 2010 Assistant at the infrastructure department of the Joint Research Center of the European Commission, Petten, The Netherlands
- 2005 - ... Fellow in the Safety of Future Nuclear Reactor of the Joint Research Center of the European Commission, Petten, The Netherlands
- & PhD candidate at the Reactor Institute Delft, Delft University of Technology
- Thesis title: Sustainability and Efficiency Improvements of Gas-Cooled High Temperature Reactors*
- 2004 - 2005 Internship at the Joint Research Center of the European Commission, Petten, The Netherlands

Education

- 2003 – 2005 Diplom - Ingenieur from the Technical University of Karlsruhe, Germany
- Specialisation: Combustion engine design and nuclear energy.*
Thesis title: Feasibility study to model the HFR-EU1bis fuel irradiation experiment by means of the Monte-Carlo method
- 2001 – 2004 Diplôme d'ingénieur from the engineering school Ecole Nationale Supérieure d'Arts et Métiers, Paris, France
- 1999 – 2001 Classes préparatoires PTSI/PT at lycée R. Follereau, Belfort, France
- 1995 – 1999 Baccalauréat Scientifique at lycée G. Cuvier, Montbéliard, France

